Coupling between atmospheric CO_2 and temperature during the onset of the Little Ice Age

Thomas Bastiaan van Hoof

Laboratory of Palaeobotany and Palynology
Utrecht University
Budapestlaan 4
3584 CD Utrecht
The Netherlands

T.B.vanHoof@bio.uu.nl

Cover: *Quercus robur* leaves, design Leonard Bik

ISBN 90-9018774-X

NSG Publication No: 20040907

LPP CONTRIBUTIONS SERIES No. 18

Print: Febodruk BV, Enschede

Coupling between atmospheric CO_2 and temperature during the onset of the Little Ice Age

De relatie tussen atmosferisch CO_2 en temperatuur gedurende de beginfase van de Kleine IJstijd

(Met een samenvatting in het Nederlands)

Proefschrift

Ter verkrijging van de graad van doctor aan de Universiteit Utrecht
op gezag van de Rector Magnificus, Prof. Dr. W.H. Gispen
ingevolge het besluit van het College voor Promoties
in het openbaar te verdedigen op
maandag 6 december 2004 des middags te 16.15 uur

door

Thomas Bastiaan van Hoof

geboren op 10 Juni 1976 te Oosterhout

Promotor: Prof. Dr. H. Visscher
Faculteit Biologie, Universiteit Utrecht

Co-promotor: Dr. W.M. Kürschner
Faculteit Biologie, Universiteit Utrecht

The research in this thesis was carried out at the Laboratory of Palaeobotany and Palynology, Budapestlaan 4, 3584 CD Utrecht, the Netherlands. As a contribution to the CLIVARNET program this research was supported by the Netherlands Council for Earth and Life Sciences (ALW) with financial support from the Netherlands Organization for Scientific Research (NWO), project no. 835.230.02.

“**The knack of flying is learning how to throw yourself at the ground and miss**”

Douglas Adams

voor mijn ouders

Contents

Algemene Inleiding en Samenvatting

Inleiding

De Kleine IJstijd is de meest recente van een reeks terugkerende, honderdjarige afkoelingsfasen die de klimaatsgeschiedenis van de laatste 10.000 jaar (het Holoceen) kenmerken. De aanzet tot de Kleine IJstijd wordt gekenmerkt door een langdurige periode van klimaatsinstabiliteit die reeds in de 11de eeuw begon, toen de vrij warme en stabiele weersomstandigheden van het Middeleeuws Klimaat Optimum verslechterden. In West-Europa leidde deze stijgende instabiliteit tot een periode met een hogere frequentie van strenge winters vanaf het midden van de vijftiende tot het midden van de negentiende eeuw. Deze periode wordt vaak als de Kleine IJstijd sensu stricto beschouwd; zij eindigt met de mondiale temperatuursstijging aan het begin van de Industriële Revolutie.

Om de processen te begrijpen die hebben bijgedragen aan de klimaatsverandering die resulteerde in de Kleine Ijstijd, is gedetailleerde kennis van het oceaan-atmosfeer-klimaatssysteem tijdens de eerste helft van het afgelopen millennium noodzakelijk. Een belangrijke vraag is in welke mate de temperatuurveranderingen in deze periode samenhangen met veranderingen in de atmosferische concentratie van het broeikasgas CO_2.

De huidige mondiale temperatuurstijging wordt, zoals algemeen wordt aangenomen, hoofdzakelijk veroorzaakt door de verhoogde antropogene CO_2 emissie sinds het begin van de Industriële Revolutie. Studies van het atmosferisch CO_2-gehalte gemeten aan ingesloten luchtbellen in Antarctische ijskernen tonen aan dat de temperatuurveranderingen die samenvallen met de overgang van ijstijden (glacialen) naar warmere perioden (interglacialen), sterk gekoppeld zijn aan CO_2-fluctuaties. Echter, gedurende het Holoceen, de warme periode waarin wij ons nu bevinden, veronderstellen de ijskernmetingen stabiele CO_2-niveaus. Dit impliceert dat CO_2 niet gekoppeld is aan de kortdurende afkoelingsfasen tijdens het Holoceen, zoals b.v. de zogenaamde Preboreale Oscillatie (ca. 11.200 jaar geleden) en een kortdurende koele fase omstreeks 8.200 jaar geleden (het “8,2 Kyr event”).

Het is echter opmerkelijk dat er tijdens de laatste afkoelingsfase van het Holoceen, de Kleine IJstijd, wel kleinschalige veranderingen (tot 12 ppmv) in het CO_2-gehalte in de Antarctische ijskernen worden waargenomen. Maar in vergelijking met de potentiële gevolgen van veranderingen in zonneactiviteit en vulkanisme, wordt van dergelijke kleinschalige CO_2-schommelingen niet verondersteld dat zij een belangrijke bijdrage hebben geleverd aan de veranderingen in de luchttemperatuur tijdens de Kleine IJstijd.

Een alternatieve methode om het atmosferische CO_2-gehalte in het verleden te bepalen maakt gebruik van het verband tussen het aantal huidmondjes (stomata) op bladeren van landplanten en de CO_2-concentratie in de atmosfeer. CO_2 is de belangrijkste bouwstof voor een plant en wordt tijdens de fotosynthese samen met water omgezet in zuurstof en suikers. CO_2 wordt aan de atmosfeer onttrokken via de huidmondjes. Wanneer de

hoeveelheid CO_2 in de atmosfeer verandert, past de plant de huidmondjesdichtheid van de bladeren aan om waterverlies door verdamping via de huidmondjes te beperken. Dit verband is daarom omgekeerd evenredig: hoe hoger het gehalte aan CO_2, hoe lager het aantal huidmondjes. Het kwantificeren van dit verband kan worden bereikt door de huidmondjesdichtheid van bladeren van de afgelopen 150 jaar te analyseren en te vergelijken met de gemeten toename van het atmosferisch CO_2-gehalte sinds de Industriële Revolutie. De stomatafrequentie-analyse van bladresten uit veen- en meerafzettingen maakt het vervolgens mogelijk CO_2-veranderingen in het verleden op te sporen en te kwantificeren. Stomatafrequentie-analyses met betrekking tot de vroeg-Holocene afkoelingsfasen, zoals de eerder genoemde Preboreale Oscillatie en het "8.2 Kyr event", tonen aan dat de CO_2-ontwikkeling gedurende het Holoceen dynamischer was dan tot nu toe verondersteld werd op grond van studies aan ijskernen.

De aanwezigheid van een meer dynamisch CO_2-regime tijdens het afgelopen millennium wordt reeds gesteund door verschillende stomatafrequentiestudies. Onderzoek aan bladeren van een polaire wilgensoort (*Salix herbacea*) uit Zweden en aan naalden van de hemlockspar (*Tsuga heterophylla*) uit het noordwesten van de Verenigde Staten bevestigt de aanwezigheid van kortdurende CO_2-schommelingen, die wellicht gekoppeld zijn aan temperatuursveranderingen gedurende de Kleine IJstijd. De amplitude van deze schommelingen is aanzienlijk hoger dan de amplitude van de oscillaties die in Antarctische ijskernen wordt waargenomen. De meest prominente CO_2-veranderingen vonden plaats gedurende de periode tussen de elfde en de vijftiende eeuw, dus vóór het begin van de Kleine IJstijd sensu stricto. In dit proefschrift worden de laatstgenoemde CO_2-oscillaties met een hoge resolutie bestudeerd op basis van stomatafrequentie-analyses van bladresten van de zomereik (*Quercus robur*).

Een ononderbroken reeks van bladeren van de zomereik over de periode van 1000 tot 1500 AD werd verkregen uit sterk organische sedimenten afkomstig uit een afgesneden meander van de rivier de Roer bij Sint Odiliënberg in de provincie Limburg. De ouderdom van deze afzettingen werd nauwkeurig bepaald met behulp van de zogenaamde "^{14}C wiggle-matching" methode. Stomatafrequentie-analyses van deze eikenbladeren werden met een hoge resolutie uitgevoerd met als doel:
1. de omvang en de timing van de CO_2-fluctuaties te bepalen tijdens de overgang van het Middeleeuwse Klimaat Optimum naar de Kleine Ijstijd;
2. het effect van deze veranderende CO_2-gehaltes op de stralingsbalans te bepalen en de daaruit volgende potentiële invloed op de mondiale luchttemperatuur te kwantificeren;
3. de gereconstrueerde CO_2-trends en de daaruit volgende berekende veranderingen van de luchttemperatuur te vergelijken met temperatuurreconstructies van het oppervlaktewater van de Noord-Atlantische Oceaan en met de beschikbare mondiale reconstructies van de luchttemperatuur;
4. te bepalen welke rol CO_2 speelde in het oceaan-atmosfeer-klimaatsysteem gedurende de beginfase van de Kleine IJstijd;

5. te evalueren in welke mate koolstofopslag (in de vorm van bosopslag) op landbouwgronden, die tengevolge van de pestepidemieën gedurende de 14de en 15de eeuw op grote schaal verlaten werden, een bijdrage heeft kunnen leveren aan de afname van het atmosferisch CO_2-gehalte tijdens deze periode;
6. de tegenstrijdige resultaten van de op ijskernen gebaseerde en op bladonderzoek gebaseerde CO_2-reconstructies op te lossen;
7. de reproduceerbaarheid en de integriteit van de op bladonderzoek gebaseerde Holocene CO_2-reconstructies in te schatten.

Om de gevoeligheid van *Q. robur* voor veranderingen in het atmosferisch CO_2-gehalte te kwantificeren, wordt in Hoofdstuk 1 de verandering in de stomatafrequenties bestudeerd tijdens de CO_2-toename van de afgelopen 150 jaar. De SI-response (veranderingen in de Stomata Index, een maat voor het aantal huidmondjes) van *Q. robur* tijdens de industriële CO_2 toename vertoont een sigmoidaal karakter en lijkt sterk op die van de wintereik (*Q. petraea*). Beide soorten verschillen in hun responslimiet ten opzichte van de CO_2-stijging. Voor calibratiedoeleinden wordt echter alleen het lineaire interval van de sigmoidale SI-responscurve gebruikt. Deze aanpak zorgt er wel voor dat gereconstrueerde CO_2-gehaltes die buiten het responsinterval liggen, een onderschatting zijn van de werkelijke situatie.

In Hoofdstuk 2 worden met behulp van bladresten van *Q. robur* uit restgeulafzettingen van de Roer bij Sint Odiliënberg de atmosferische CO_2-gehaltes gedurende de periode van 1000 tot 1500 AD gereconstrueerd. De resultaten wijzen op een zeer dynamisch CO_2-regime tijdens de beginfase van de Kleine Ijstijd. Er bestaat een sterke gelijkenis met patronen in de oppervlaktewatertemperatuur van de Noord-Atlantische Oceaan. Deze overeenkomst veronderstelt een causaal verband tussen de verstoring van de thermohaline circulatie en de productie of opname van atmosferisch CO_2. Van de gereconstrueerde CO_2-veranderingen wordt verder het effect op de stralingsbalans en de daaruit volgende effecten op de luchttemperatuur berekend. Deze door CO_2 geforceerde, berekende veranderingen in luchttemperatuur liggen in dezelfde orde van grootte als de veranderingen gereconstrueerd door verschillende 'proxy records' voor luchttemperatuur tijdens deze periode. De effecten van veranderende zonneactiviteit en vulkanisme verhullen het directe verband tussen CO_2 en luchttemperatuur gedurende de beginfase van de Kleine IJstijd. Het effect van CO_2 op de stralingsbalans, en dus op de luchttemperatuur, is echter belangrijk genoeg om, naast zonneactiviteit en vulkanisme, ook CO_2-concentratie als klimaatsforceringsmechanisme in toekomstige klimaatmodelstudies op te nemen.

Om de effecten van de lokale omgevingsfactoren op de stomatafrequentie van de middeleeuwse bladeren van *Q. robur* uit Sint Odiliënberg te bestuderen, werden deze omgevingsfactoren gereconstrueerd. Hiertoe worden in Hoofdstuk 3 de boomringen van de in de restgeulafzettingen aangetroffen, ^{14}C-gedateerde middeleeuwse

eikenstammen vergeleken met boomringen van de thans op deze locatie levende eikenpopulatie. Een statistische vergelijking van de hedendaagse groeipatronen met neerslag- en temperatuurgegevens bevestigt een positief verband tussen de boomringdikte en de jaarlijkse neerslag. Langere perioden van groeidepressies afgeleid uit de middeleeuwse eikenstammen duiden op wortelbeschadiging door anoxische condities in de bodem als gevolg van overstromingen tijdens het groeiseizoen. Soortgelijke groeipatronen in *Q. robur* worden nu nog aangetroffen in een populatie eiken op een waterverzadigde standplaats in het landgoed Oostbroek (Utrecht). Om te testen of de stomatafrequentie wordt beïnvloed door anoxische bodemcondities werden de bladeren van drie populaties met een verschillende waterhuishouding anatomisch met elkaar vergeleken. Hierbij bleek geen statistisch significant verschil in stomatafrequentie tussen de drie populaties voor te komen, hetgeen impliceert dat de verlengde groeidepressies in de middeleeuwse eiken uit Sint Odiliënberg geen invloed hebben gehad op de CO_2-reconstructies die op stomata indices zijn gebaseerd.

Pollendiagrammen van de goed-gedateerde restgeulafzettingen bij Sint Odiliënberg, gepresenteerd in Hoofdstuk 4, leveren een gedetailleerde reconstructie van de vegetatie en het middeleeuwse landgebruik gedurende de periode van 1000 tot 1500 AD. Deze reconstructie wordt gebruikt om een recentelijk ontwikkelde hypothese te testen waarin een verband wordt gelegd tussen kortstondige, negatieve anomalieën in het atmosferisch CO_2-gehalte, gemeten in Antarctische ijskernen, en koolstofopslag door bosgroei op landbouwgronden die tengevolge van pestepidemieën gedurende de 14de en 15de eeuw werden verlaten. In het pollendiagram zijn de regionale effecten van de grote pestepidemie rond 1350 AD (de Zwarte Dood) terug te vinden als een periode van landbouwregressie tussen 1350 en 1440 AD. De diagrammen wijzen op een gelijktijdige, grootschalige hergroei van bossen. Dit bevestigt de opslag van koolstof in de terrestrische biosfeer. Trends in de regionale bosdichtheid tijdens de periode van de 13de tot de 15de eeuw komen overeen met algemene CO_2-trends, zoals die herkend zijn met behulp van stomatafrequentie-analyse. Het lijkt daarom mogelijk dat de door pestepidemieën veroorzaakte koolstofopslag een rol heeft gespeeld bij de afname van het atmosferisch CO_2-gehalte gedurende de 14de en 15de eeuw.

Om de kritiek te weerleggen dat de Holocene CO_2-fluctuaties afgeleid uit stomatafrequentie-analyses het resultaat zouden zijn van het effect van locale omgevingsfactoren of methodologische onnauwkeurigheden, wordt in Hoofdstuk 5 een vergelijking gemaakt tussen verschillende stomatafrequentiestudies van drie prominente, honderdjarige afkoelingsfases gedurende het Holoceen. Naast de Kleine Ijstijd, worden de Preboreale Oscillatie en het “8.2 kyr event” geëvalueerd. De op stomatafrequentie gebaseerde CO_2-reconstructies aan de hand van taxonomisch en ecologisch van elkaar verschillende loof- en naaldbomen uit Europa en Noord-Amerika, waarbij gebruik wordt gemaakt van verschillende calibratietechnieken, vertonen een hoge mate van overeenkomst. Dit wijst erop dat bladanatomisch onderzoek een integere methode is om CO_2-fluctuaties in het verleden te reconstrueren.

Zowel het onderzoek aan ijskernen als het bladonderzoek tonen sterke fluctuaties aan in atmosferische CO_2-concentraties gedurende de 13de eeuw. De resultaten van de twee onafhankelijke methoden verschillen echter significant in de amplitude van de geschatte CO_2-veranderingen: 10 ppmv bij onderzoek aan ijskernen versus 34 ppmv bij bladanalyses. Om het effect van gasdiffusie, dat plaatsvindt in de firnlaag tijdens de insluiting van de luchtbellen in het ijs, op de amplitude van de op ijs gebaseerde CO_2-reconstructies te onderzoeken, worden in Hoofdstuk 6 de op beide manieren verkregen gegevens met elkaar vergeleken met behulp van een firndiffusie model. Het grote verschil in amplitude van de 13de eeuwse CO_2-anomalie bij beide methoden verdwijnt, wanneer met behulp van een diffusiemodel het natuurlijke gasdiffusie-effect wordt geïncorporeerd in de op stomatafrequentie gebaseerde CO_2-reconstructie. Dit impliceert dat de verschillen tussen beide methodieken kleiner zijn dan tot nu toe werd aangenomen, maar dat de natuurlijke variatie van het CO_2-gehalte in de atmosfeer die door onderzoekers aan ijskernen wordt gepostuleerd, een onderschatting is van de werkelijkheid.

General Introduction and Synopsis

Introduction

The Little Ice Age (LIA) represents the most recent event in a series of recurrent, centennial-scale cooling pulses that punctuate Holocene climate history. Its onset is characterized by a prolonged episode of climatic instability, beginning already in the 11th century when relatively warm and stable weather conditions of the Medieval Climatic Optimum started to deteriorate. In western Europe, increasing instability culminated in frequent severe winters from the mid-15th through mid-19th centuries, a period often referred to as the Little Ice Age *sensu stricto*. This period ended with the rapid onset of the current period of global warming.

In order to understand the processes that have contributed to the LIA climatic deterioration, it is necessary to obtain detailed knowledge about the physical conditions of the ocean-atmosphere-climate system during the first half of the last millennium. A central issue concerns the question to what extent temperature changes in this period correlate with trends in atmospheric CO_2 concentration.

Current global warming is primarily related to the greenhouse effect resulting from increased anthropogenic CO_2 emission since the beginning of the industrial revolution. Ice-core records from Antarctica document a strong coupling between temperature and atmospheric CO_2, both on glacial-interglacial and millennial timescales. In marked contrast, ice-core data suggest stable CO_2 levels for the Holocene that do not reflect any of the earlier centennial-scale cooling events, such as the Preboreal Oscillation and the so-called 8.2 kyr BP event.

Intriguingly, because of approximate time-equivalence, negative CO_2 anomalies up to 12 ppmv in Antarctic ice-core records for the last millennium have been related to the LIA. Such modest and smoothed CO_2 fluctuations, however, are usually considered to represent an insignificant forcing mechanism for generating air-temperature changes, especially when compared with the potential effects of changes in solar radiation and volcanic activity.

An alternative methodology to obtain a proxy record of atmospheric CO_2 levels is based on the inverse relationship between the number of leaf stomata and atmospheric CO_2 concentration. Calibrated against modern training sets, stomatal frequency analysis of leaves buried in peat and lake deposits enables detection and quantification of Holocene CO_2 changes. Stomatal frequency data from time-intervals corresponding to the Preboreal Oscillation and 8.2 kyr BP event demonstrate that prominent centennial-scale CO_2 fluctuations have contributed to a much more dynamic CO_2 regime than suggested by ice-core measurements.

Also the presence of significant short-term CO_2 variability in the last millennium is already supported by stomatal frequency data. Records for *Salix herbacea* leaves from Sweden and *Tsuga heterophylla* needles from the northwestern USA confirm the

presence of centennial-scale CO_2 fluctuations that could correspond to the LIA. The amplitude of the reconstructed variability considerably exceeds CO_2 anomalies recognized in Antarctic ice-cores. Prominent CO_2 shifts notably occurred in the 11th through 15th centuries, well before the Little Ice Age *sensu stricto*. In this thesis, the latter shifts are studied in more detail on the basis of high-resolution stomatal frequency data for *Quercus robur* leaves.

In the southeastern part of The Netherlands, in the vicinity of Sint Odiliënberg (Province of Limburg), an organic-rich infill of an oxbow lake of the river Roer yielded a continuous record of *Quercus robur* leaves for the period between AD 1000 and 1500. Accurately dated by ^{14}C wiggle-match dating, this record is analyzed in order to:
(1) establish the magnitude and precise timing of CO_2 shifts during the transition between Medieval Climatic Optimum and the Little Ice Age *sensu stricto*,
(2) quantify the relative radiative forcing of CO_2 fluctuations and its potential effects on air temperature,
(3) compare reconstructed CO_2 trends and derived temperature changes with proxy records of changes in North Atlantic sea-surface temperature and global air-temperature,
(4) contribute to a general assessment of the role of CO_2 in the ocean-atmosphere-climate system during the onset of the LIA,
(5) evaluate to what extent widespread carbon sequestration on abandoned farmland could have been a contributing factor to atmospheric CO_2 decline during the 14th and 15th centuries,
(6) resolve the conflicting results of ice-based and leaf-based CO_2 reconstructions,
(7) appraise the reproducibility and integrity of leaf-based Holocene CO_2 quantification.

In order to quantify the CO_2 responsiveness of *Quercus robur* leaves, the stomatal frequency response of *Q. robur* to current anthropogenic CO_2 increase is studied in **Chapter 1**. Stomatal index (SI) measurements of buried, herbarium and modern leaf material show a significant inverse relation between SI and CO_2. The historical SI response rate recorded for *Q. robur* closely resembles that of *Q. petraea,* although the response limit of the two species to the rising CO_2 mixing ratios differs slightly. For calibration purposes, however, in the presented CO_2 response model only the linear phase of the sigmoidal response curve is taken into consideration, which allows confident combination of *Q. robur* and *Q. petraea*. The model is conservative in reconstructing past CO_2 mixing ratios outside the monitored response range. As a result of the observed SI response limit, the model predicts CO_2 levels below 320 ppmv with a mean error of +/- 10.25 ppmv, whereas higher CO_2 levels are underestimated.

In **Chapter 2** atmospheric CO_2 mixing ratios over the period between AD 1000 and 1500 are reconstructed on the basis of buried *Q. robur* leaves from 60 successive horizons of the oxbow-lake deposits near Sint Odiliënberg. In addition, the relative radiative forcing of reconstructed CO_2 fluctuations and its potential effects on air

temperatures is quantified. Results corroborate a highly dynamic CO_2 regime during the onset of the LIA. Pronounced CO_2 shifts show a strong correlation with North-Atlantic trends in sea-surface temperature, confirming causal relationship between disturbances of the North-Atlantic thermohaline circulation and the production or depletion of atmospheric CO_2. Calculated CO_2-induced changes in air temperature are in the range of short-term fluctuations recognized in proxy records of global air-temperature, but forcing effects of solar radiation and volcanism obscure the coupling between CO_2 and air temperature. Temporal correlation of CO_2 changes and air-temperature changes is only possible by combining the modeled radiative effect of CO_2 fluctuations with coeval effects of changing solar radiation and prominent volcanic eruptions.

The radial growth dynamics of buried and living swamp oaks are studied in **Chapter 3** in order to evaluate the effect of local environmental conditions on stomatal frequency. Climate-growth analysis of the living population at Sint Odiliënberg reveals a positive correlation of ring-width to the year-round precipitation signal. Unique features in the ring-width series of buried oaks from the same site reflect prolonged periods of depressed growth, probably due to root damage caused by anoxia during growth-season flooding. Similar growth patterns exist in a living population at a more intensively waterlogged stand. To test whether stomatal frequency is affected by water logging, the leaf epidermal anatomy of three *Q. robur* populations from contrasting stands is analyzed. The results indicate no significant difference in stomatal frequency between the three populations. This suggests that growth-season inundation does not affect the stomatal index proxy used for CO_2 reconstruction on the basis of buried *Q. robur* leaves.

A well-dated pollen record from the organic-rich infill of the oxbow lake near Sint Odiliënberg, presented in **Chapter 4**, provides a high-resolution reconstruction of vegetation and medieval land use for the period between AD 1000 and 1500. This reconstruction is used to test a recent hypothesis, which relates negative CO_2 anomalies in Antarctic ice cores to periodic carbon sequestration due to reforestation of abandoned farmland following pandemics of plague and other diseases. In the pollen record, regional effects of the mid-14th century plague pandemic, known as the Black Death, are reflected by a period of significant agricultural regression between AD 1350 and 1440. Concomitant regrowth of forest confirms widespread carbon sequestration. Trends in regional forest density of the 13th-15th centuries resemble coeval atmospheric CO_2 trends as reconstructed by means of stomatal frequency analysis. It is conceivable that plague-induced carbon sequestration could have been a contributing factor to atmospheric CO_2 decline during the 14th and 15th centuries.

To address the critique that prominent Holocene CO_2 fluctuations derived from stomatal frequency variations could be the result of local environmental change or methodological

insufficiencies, **Chapter 5** is dealing with a comparison of multiple stomatal frequency records for three centennial-scale cooling events. Apart from the Little Ice Age, also the Preboreal Oscillation and the 8.2 kyr BP event are reviewed. The highly similar fluctuations in the atmospheric CO_2 records, which were obtained from different continents (Europe and North America), and taxonomically and ecologically contrasting tree species (deciduous angiosperms and conifers) using varying calibration approaches, provide strong evidence for the integrity of leaf-based CO_2 quantification.

A period where both ice-based and leaf-based CO_2 records consistently provide evidence for natural CO_2 changes is the 13th century. The results of the two independent methods differ significantly in the amplitude of the estimated changes (10 ppmv ice *vs.* 34 ppmv stomatal frequency). In **Chapter 6**, stomatal-frequency and ice-core results are compared by using a firn-diffusion model, in order to assess the potential influence of smoothing during enclosure on the temporal resolution as well as the amplitude of the CO_2 changes. The seemingly large discrepancies between the amplitudes estimated by the contrasting methods diminish when effects of natural smoothing of the ice-core record is simulated for the raw data of the *Q. robur* stomatal frequency record. Results indicate that the differences derived by the two methods may be less significant than previously thought.

N.B. The chapters of this thesis are or will be published as separate papers in scientific journals. As a consequence, some repetition of statement could not be avoided.

Chapter 1

Stomatal index response of *Quercus robur* and *Quercus petraea* to the anthropogenic atmospheric CO_2 increase

The high abundance of leaf fossils of *Quercus robur* in natural environmental archives covering the past 11,500 years (i.e. the Holocene) makes this species potentially suitable for stomatal frequency based CO_2 reconstructions. In order to quantify the CO_2 response in fossil *Q. robur* leaves, the behavior of *Q. robur* stomata frequency during the current anthropogenic CO_2 increase has been studied. Stomatal index (SI) measurements of Dutch buried, herbarium and modern *Q. robur* leaf material show a significant inverse relationship between SI and CO_2. The historical SI response rate recorded in *Q. robur* closely resembles that of *Q. petraea,* although the timing of their SI response limitation to the rising CO_2 mixing ratios differs slightly. For calibration purposes, however, in the CO_2 response model presented, only the linear phase of the sigmoidal response curve is taken into consideration, which allows confident combination of *Q. robur* and *Q. petraea*. The model is conservative in reconstructing past CO_2 mixing ratios outside the range of monitored response. As a result of the observed SI response limit, the model predicts CO_2 levels below 320 ppmv with a mean error of 10.25 ppmv, whereas higher CO_2 levels are underestimated.

Chapter 1

Introduction

The inverse relationship between atmospheric CO_2 and stomatal frequency is increasingly used as a proxy to calculate atmospheric CO_2 mixing ratios on various geological time-scales (Van der Burgh et al.,1993; Kürschner et al., 1996; Wagner et al.,1999; Royer et al., 2001). Stomatal frequency analysis of durmast oak (*Quercus petraea*) has previously been used to reconstruct CO_2 changes on time-scales of millions of years (Van der Burgh et al., 1993; Kürschner et al.,1996). In natural environmental archives covering the past 11,500 years (i.e. the Holocene) such as peat and lake deposits, leaf remains of the closely related pendunculate oak (*Quercus robur*) occur more frequently. This is due to the ability of *Q. robur* to endure flooding and to flourish on wet soils, while *Q. petraea* generally prefers well-drained stands. The high abundance of *Q. robur* leaf remains throughout the Holocene makes it a valuable species to use for stomatal frequency-based atmospheric CO_2 reconstructions. An initial herbarium study of *Q. robur* revealed a distinct stomatal frequency response in this species to current anthropogenic atmospheric CO_2 increase (Beerling and Chaloner,1993). A much more detailed study on the stomatal frequency of the closely related and frequently hybridizing *Q. petraea* to current CO_2 increase, however suggested a limited response to elevated CO_2 (Kürschner et al., 1997). According to a sigmoidal model, the response rate reaches its upper limit at CO_2 levels of approximately 350 ppmv (Kürschner et al., 1997). For the application of stomatal frequency as a proxy for CO_2, the reliability of the calibration model based on modern leaf material is therefore of primary importance.

In order to obtain maximum prediction accuracy from buried leaf remains and define the CO_2 range in which a certain species will provide appropriate results, the gradual phenotypical response in stomatal frequency to the rising atmospheric CO_2 levels of the past two centuries has to be assessed. To increase the temporal resolution of a calibration data-set, herbarium studies can be supplemented with leaves derived from natural archives such as young peat deposits (Wagner et al., 1996; Kouwenberg et al., 2002). Herbarium data-sets generally consist of a restricted number of individuals from a wide geographical range, growing under different local environmental conditions. Leaf material accumulated in a single locality usually originates from small populations or even individual trees that grew under relatively stable conditions. By combining both approaches, problems symptomatic for studies of either herbarium or buried leaf material can be circumvented, thus improving the accuracy of the calibration model.

Furthermore, the stomatal frequency response to CO_2 is often species specific as was illustrated for e.g. *Salix herbacea* and *Salix polaris* where the different responses required different modern training sets (Rundgren and Björk, 2003). In contrast, a study on European birch trees (*Betula pendula* and *B. pubescens*) demonstrates that closely related species can have highly similar stomatal frequency response characteristics and can, therefore, be combined for calibration purposes (Wagner et al., 2000). The

advantages of combining closely related hybridizing species into a single calibration data-set are that determination to species or hybrid level is not necessary for buried leaf material and that the amount of material available to develop a calibration model is substantially increased.

To assess whether the rich Holocene *Quercus robur* leaf record can be used to reconstruct Holocene atmospheric CO_2 levels, stomatal frequency analysis was been performed on herbarium material in combination with a study of buried leaf material covering the anthropogenic CO_2 rise. In order to test the similarity of the *Q. robur* and *Q. petraea* SI response to CO_2, the response characteristics of *Q. robur* are compared to *Q. petraea* data from earlier studies. Based on these results, an interspecific calibration data-set for CO_2 estimates from buried oak leaves was been developed.

Material and Methods

Twenty-five herbarium specimens of *Quercus robur,* from the collections of the Nationaal Herbarium Nederland, Units Utrecht and Leiden have been analyzed. The material originates from the Netherlands and adjacent regions in Belgium and Germany and was collected between AD 1892 and 1994. Forty-eight leaves from a leaf litter profile preserved in the Mariapeel reserve (the Netherlands) have been analyzed. The 25 centimeter leaf accumulation covers the period from AD 1900 to1994 (age-assessment by Wagner et al.,1996). Modern leaf material (2003) was obtained from three different *Quercus robur* populations in the Netherlands (Oostbroek, Mariapeel, and Sint Odiliënberg), where ten leaves per locality were analyzed. The oak population at the Oostbroek locality is known to suffer from severely stressed growth conditions due to an increased groundwater-table.

For microscopic analysis leaf fragments of 0.5 x 0.5 cm were bleached in a 4% sodiumhypochlorid solution to remove the mesophyll. The remaining cuticles were stained with safranin and mounted in glycerin jelly on microscopic slides. Computer aided stomatal frequency analysis was performed with the image analysis software analySIS 3.0 (Soft Imaging System GmbH, Germany). Counting areas were restricted to stomata bearing alveoles. Seven digital images per leaf with a field area of 0.03 mm^2 were analyzed. Parameters measured were epidermal cell density (ED [n/mm^2]) and stomatal density (SD [n/mm^2]). From SD and ED the area independent stomatal index (Salisbury, 1927) was calculated as :

$$SI\ [\%] = (SD) / (SD + ED) \times 100 \qquad (1)$$

where SI (%) represents the stomatal index, SD the stomatal density per unit leaf area and ED the epidermal cell density per unit leaf area. Global atmospheric CO_2 mixing ratios are annual means as measured on Mauna Loa since 1952 (Keeling and Whorf,

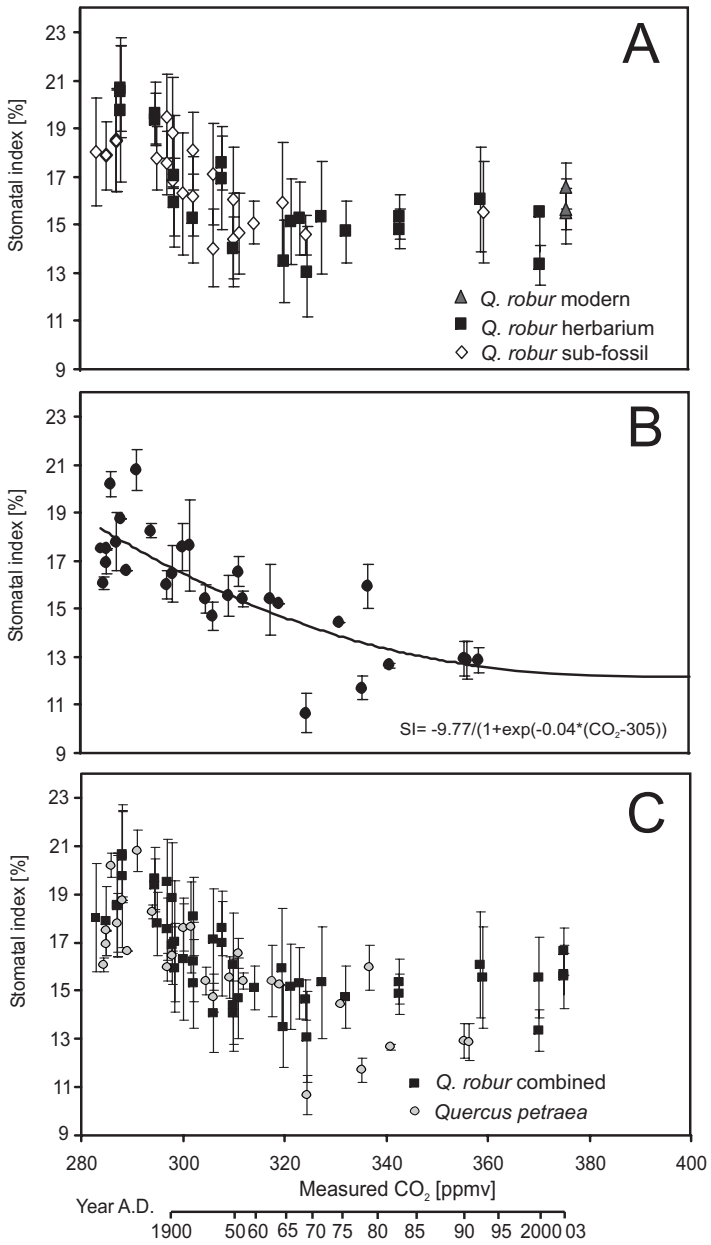

Figure 1.1 : Mean SI values (+/- 1 stdev) of herbarium, buried and modern *Q. robur* leaves (**A**) and herbarium *Q. petraea* leaves (**B**) of a previous study (Kürschner et al., 1997). CO_2 mixing ratios are annual means measured at Mauna Loa, Hawaii (Keeling and Whorf, 2002, http://cdiac.esd.ornl.gov/ndps/ndp001.html) supplemented with ice-core CO_2 measurements from Siple Dome, Antarctica (Neftel et al., 1985). **B** shows the sigmoidal response model previously developed for *Q. petraea* (Kürschner et al., 1997). **C** shows the combined data of Quercus robur (A) and the Quercus patraea data (**B**) plotted together.

2002), supplemented with CO_2 measurements from shallow Antarctic ice cores (Siple station, Neftel et al., 1985).

Results

Figure 1.1 A shows the mean SI values of the *Q. robur* herbarium, buried and modern leaf samples. Figure 1.1 B shows the *Q. petraea* herbarium data-set (Kürschner, 1996), whereas Figure 1.1 C shows the combined *Q. robur* and *Q. petraea* data-sets. All data are plotted against historical atmospheric CO_2 mixing ratios corresponding to the sample age.

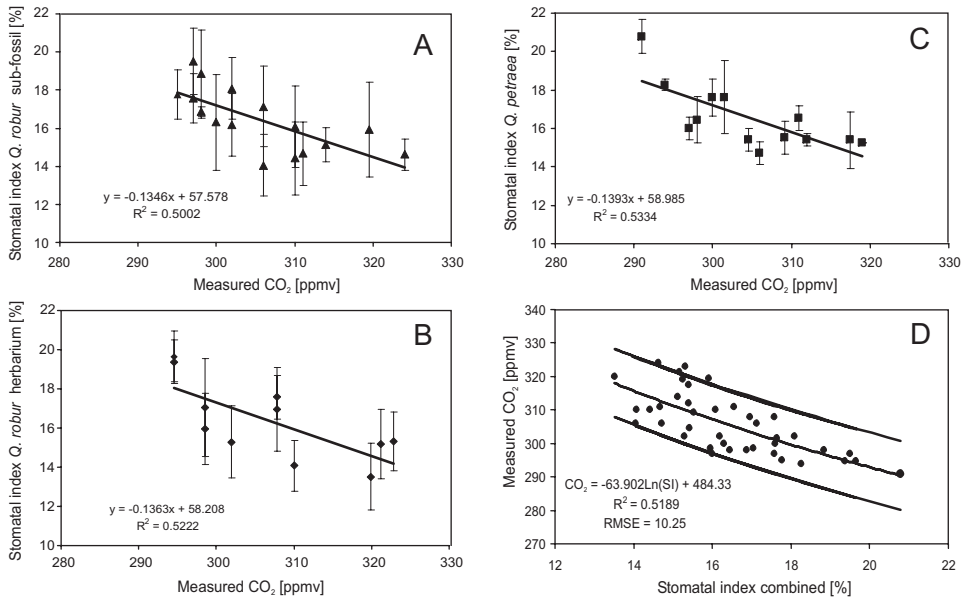

Figure 1.2 : **A, B** and **C** represent linear regressions through the *Q. robur* buried, the *Q. robur* herbarium and the *Q. petraea* herbarium data-sets over the 290-325 ppmv CO_2 linear response interval. **D** : Calibration model based on the combination of the three data-sets (**A**, **B** and **C**). Log-transformation was applied before fitting a linear response curve through the data-set. Error margins represent 95 % confidence intervals.

The original sigmoidal response model is plotted within the *Q. petraea* data, illustrating that the response limit of this species is reached around 350 ppmv (Kürschner et al., 1997).

$$SI = (A_1 - A_2) / (1+\exp(\alpha \bullet (C-C_0)) + A_2 \quad (2)$$

where SI [%] is the mean stomatal index, α is the slope at the symmetry point of the linear part of the curve, A_1 and A_2 (%) are the asymptotic values of SI [%] for, minimum and maximum CO_2 mixing ratios, respectively, C (ppmv) is the CO_2 mixing ratio of the ambient atmosphere and C_0 is the CO_2 mixing ratio of the ambient atmosphere at the symmetry point.

Figure 1.2 A, B and C show the SI decrease observed in the three different data-sets (*Q. petraea* herbarium, *Q. robur* buried, *Q. robur* herbarium, respectively) over the 290 to 325 ppmv CO_2 interval representing the linear part of the sigmoidal response function. Linear regression shows highly similar response characteristics for the three data-sets during the 35 ppmv CO_2 decrease.

The *Q. petraea* herbarium data-set reveals a response rate of 1.4 SI [%] decrease per 10 ppmv CO_2 increase with a coefficient of determination (r^2) of 0.53. The *Q. robur* data-set reveals a response rate of 1.3 SI [%] decrease per 10 ppmv CO_2 increase ($r^2 = 0.5$) and the *Q. robur* herbarium data-set a response rate of 1.4 SI [%] decrease per 10 ppmv CO_2 increase ($r^2 = 0.52$). Based on these results, the common response is defined as the linear interval of the sigmoidal model developed for *Q. petraea*.

The highly comparable response rates in the linear interval common to both *Quercus* species allow the combination of all data into one composite calibration curve (Fig. 1.2D). In order to further reduce the uncertainties in the data-set due to outliers in the data, both SI data and the historical CO_2 values were log-transformed before fitting a linear response curve. This resulted in a relationship of $CO_2 = 10^{2.7389} -(0.2091*\log(SI))$ with an r^2 of 0.52 between measured CO_2 and SI values and a root mean square error (RMSE) of 10.25 ppmv CO_2 (Figure 1.2 D).

Discussion

Leaves of *Q. robur* naturally grown under rising atmospheric CO_2 conditions of the last two centuries obtained from herbaria and a leaf-litter profile show a comparable SI response to the anthropogenic CO_2 increase. The close comparability between both records proves that site-specific environmental factors present in the geographically scattered herbarium data-set (e.g. local temperature and local hydrology) did not effect the SI response of *Q. robur*. This is illustrated by the similarity of the SI of the four

modern populations. At the site Oostbroek the population of *Q. robur* suffers substantially from an artificially increased groundwater-table during the past decade, with lethal consequences for a large number of trees. However, no significant difference in SI of these trees was observed compared to the other populations (Fig. 1.1 A).

The combined *Q. robur* records (Fig. 1.1 A) show a highly similar response to rising atmospheric CO_2 mixing ratios from 295 to 325 ppmv compared to the *Q. petraea* response curve of Kürschner et al. (1997) (Fig. 1.1 B, C). Although the response curves of *Q. petraea* and *Q. robur* are highly comparable within the linear phase of the sigmoid, a divergent pattern between both species is observed when they approach their lower response limits. In *Q. robur* the lower response limit is reached at 320 ppmv with SI stabilizing around 15 SI [%], whereas *Q. petraea* levels off around 350 ppmv at 13 SI [%].

The highly comparable response rate within the linear phase allows the combination of both species into one interspecific calibration curve. Such close comparability of SI response between two species has until now only been observed in *Betula pendula* and *Betula pubescens* (Wagner et al., 1996). Possible differentiation in response limitation of two closely related species as shown in this study for *Quercus*, could not be observed in the *Betula* study as *B. pubescens* and *B. pendula* have not approached their SI response limit yet (Wagner et al., 1996, Kürschner et al., 1997).The observed differentiation in the phenotypical response range of SI to CO_2 between *Q. robur* and *Q. petraea* could be an adaptation to the contrasting habitats preferred by these two species. The preference of *Q. petraea* for well-drained stands makes it more likely to encounter drought stress, whereas *Q. robu*r is adjusted to generally wetter soil conditions. This could have led to the development of a more plastic SI in *Q. petraea*.

A decreasing CO_2 sensitivity of SI above 350 ppmv has been observed in other species (*e.g*. *Metasequoia glyptostroboides* and *Ginkgo biloba*; Royer et al., 2001; Beerling and Royer, 2002), however it is argued that the response rate of SI to CO_2 is not limited above ambient CO_2 levels but rather decreased (Royer et al, 2001, Beerling and Royer, 2002). In order to test the behavior of the *Q. robur and Q. petraea* SI at elevated CO_2 levels, experimental setups, however, are required.

The comparability of the linear interval (290-325 ppmv) of the sigmoid shaped response curves of the three data-sets (*Q. robur* herb., *Q. robur* buried and *Q. petraea* herb.) allows the safe combination of all three data-sets into one calibration data-set. The calibration model based on log-linear transformation of the linear component of the sigmoidal shaped calibration curves (Fig. 1.2 D) tends to underestimate CO_2 approaching the response limit of 320 ppmv.Therefore, this model is a conservative approach to reconstruct CO_2 at the edges of the observed CO_2 gradient compared to any non-

linear calibration approach. Due to the limitation of the *Q. robur* stomatal index, values above 320 ppmv cannot be detected. However, below 320 ppmv the model provides an accurate but conservative base for estimating past CO_2 levels from SI measurements from buried *Quercus robur* and *Quercus petraea* leaves.

Conclusions

Stomata index measurements of buried, herbarium, and modern *Q. robur* leaf material demonstrate a highly similar inverse relationship between SI and the current anthropogenic CO_2 increase. This similar response illustrates that *Q.robur* herbarium data-sets can safely be supplemented with buried leaves in order to increase the resolution and the accuracy of the calibration data-set. The combined herbarium (modern) and buried *Q. robur* leaf record shows a highly similar SI response to anthropogenic CO_2 increase as was been previously demonstrated for the closely related species *Q. petraea* (Kürschner et al., 1997). However, between both species a differentiation in response limitation to the CO_2 increase is observed which is likely to be related to the contrasting habitat preferences. Despite the divergent response limitations the linear intervals of the sigmoid shaped response curves of both species are similar. This similarity in response rate characteristics over the interval from 290 to 320 ppmv CO_2 allows the combination of both data-sets into a single interspecific calibration curve for West European oak. The model presented is rather conservative at the edges of the CO_2 response interval. Due to the observed response limitation of *Q. robur* SI at a CO_2 level of 320 ppmv, atmospheric CO_2 values higher than 320 ppmv cannot be detected. As Holocene CO_2 levels have most likely been lower then 320 ppmv, buried leaf remains of *Q. robur* are highly suitable for stomatal index based atmospheric CO_2 reconstructions throughout the Holocene.

Chapter 2

The atmospheric CO_2 regime during the onset of the Little Ice Age

The onset of the Little Ice Age (LIA) is characterized by a prolonged period of climatic instability, beginning already in the 11th century. In order to understand the processes that contributed to LIA climatic deterioration, a central issue concerns the question to what extent there was a coupling between atmospheric CO_2 concentration and temperature trends. Because pre-industrial Antarctic ice-core records for the last millennium consistently reveal modest and smoothed CO_2 fluctuations, an alternative CO_2 reconstruction for the period between AD 1000 and 1500 is based on high-resolution stomatal frequency analysis of a continuous record of buried *Quercus robur* leaves from fluvio-lacustrine deposits in The Netherlands.

Introduction

The pre-industrial climate history of the last millennium is largely determined by the transition from a relatively warm phase, known as the 'Medieval Warm Period' or 'Medieval Climatic Optimum' (MCO), to the cooler conditions of the Little Ice Age (LIA). In a long-term Holocene perspective, the LIA is considered to represent the most recent event in a series of recurrent climate fluctuations, displaying a quasi-periodic, ~1500 year pattern of cold and dry events that are notably apparent in the North Atlantic realm (Bond et al., 1997).

It is generally agreed that the LIA lasted until the mid-19th century AD when the current period of global warming began. The beginning of the LIA, however, is less clearly defined. For western Europe, documentary records describe evidence of frequent severe winters from the mid-15th through mid-19th centuries AD (e.g. Lamb, 1977; Grove, 1988), a period often referred to as the Little Ice Age *sensu stricto*. On the other hand, the relatively warm, and especially stable weather conditions of the MCO ended well before the 16th century AD. In large parts of western Europe a trend towards a more unstable cooler climate started already by the end of the 12th century AD (Lamb, 1977; Grove, 2001). During the 13th and 14th centuries AD, documented instability is mainly expressed by mild but extremely wet winter conditions, rather than regular low-temperature anomalies (Buisman, 1995; Fagan, 2000).

Time-series data on environmental proxies obtained from tree rings (e.g. Esper et al., 2002), the Greenland ice sheet (e.g. Stuiver et al.,1997) and sediments (e.g. DeMenocal et al., 2000) consistently confirm a prolonged, irregularly declining temperature, beginning in the 11th century AD. Quantification attempts of Northern-Hemisphere and global air-temperature trends reveal anomalies in the range of 0.2 to 1°C (Mann et al., 1998; Briffa et al., 2000; Esper et al., 2002; Mann and Jones, 2003), whereas estimated anomalies in North Atlantic sea-surface temperature are considerably larger (DeMenocal et al., 2000).

It appears that the onset of the LIA is characterized by a prolonged transitional phase separating the MCO and the Little Ice Age *sensu stricto*. More detailed knowledge about the physical conditions of the ocean-atmosphere-climate system during this period is necessary in order to understand the processes causing the LIA climatic deterioration. A central issue concerns the question to what extent temperature changes correlate with global trends in atmospheric CO_2 concentration.

Several records of CO_2 mixing ratios measured in Antarctic ice-cores show variations of up to 12 ppmv for the last millennium (e.g. Siegenthaler et al., 1988; Barnola et al., 1995; Etheridge et al., 1997; Indermühle et al., 1999). Data from different coring localities are not in agreement with respect to amplitude and timing of CO_2 changes, but there is

little evidence of fluctuations in the 17th and 18th centuries AD. The modest CO_2 fluctuations are often considered to represent an insignificant forcing mechanism for air-temperature changes (Bauer et al., 2003), especially when compared with the potential effects of changes in solar radiation (e.g. Bard et al., 2000) and volcanic eruptions (e.g. Crowley et al., 2000). Yet, because of approximate time-equivalence, negative CO_2 anomalies have been related to the Little Ice Age *sensu stricto* (Indermühle et al., 1999; Ruddiman, 2003). Moreover, the magnitude of CO_2 changes in ice-core records may be underestimated because of diffusion of air in the firn before air bubbles are enclosed. This natural smoothing dampens the amplitude of CO_2 fluctuations recorded in ice (Schwander, 1996; Trudinger et al., 2003).

An alternative proxy for detecting and quantifying past CO_2 fluctuations is provided by stomatal frequency analysis of leaves buried in peat and lake deposits. In a wide variety of tree species the number of leaf stomata is directly determined by the ambient CO_2 concentration (e.g. Woodward, 1987; Wagner et al., 1996; Royer, 2001; Lake et al., 2001). Calibrated against modern training sets, Holocene stomatal frequency data demonstrate that centennial-scale CO_2 fluctuations have contributed to a much more dynamic CO_2 evolution than suggested by ice-core measurements (Wagner et al., 1999; Rundgren and Beerling, 1999; McElwain et al., 2002; Wagner et al., 2002; Rundgren and Björck, 2003; Chapter 5).

The presence of significant short-term CO_2 variability in the last millennium is supported by stomatal frequency records of *Salix herbacea* leaves from Sweden (Rundgren and Beerling, 1999) and *Tsuga heterophylla* needles from the northwestern USA (Kouwenberg, 2004). Stomatal frequency data confirm the presence of centennial-scale CO_2 fluctuations that may broadly correspond to marine and terrestrial temperature oscillations during the last millennium (Kouwenberg, 2004). The amplitude of the reconstructed variability considerably exceeds CO_2 anomalies in Antarctic ice-cores. Prominent changes occurred already between AD 1000 and 1400, well before the Little Ice Age *sensu stricto*. A reconstructed initial decrease of 50 ppmv, resulting in a CO_2 minimum around AD 1150, is followed by an increase of 60 ppmv, resulting in a CO_2 maximum around AD 1300 (Kouwenberg, 2004).

In the southeastern part of The Netherlands, young fluvio-lacustrine deposits often contain rich assemblages of buried leaf remains that are suitable for high-resolution stomatal frequency studies. In the vicinity of Sint Odiliënberg (Province of Limburg) we cored an organic-rich infill of an oxbow lake of the river Roer yielding a continuous record of *Quercus robur* leaves for the period between 1000 and 1500 AD. Accurately dated by AMS ^{14}C wiggle-match dating, in the present paper this record is analyzed in order (1) to corroborate the magnitude and timing of CO_2 changes during the transition between MCO and Little Ice Age *sensu stricto*, (2) to quantify the relative radiative forcing of CO_2 fluctuations and its potential effects on Northern-Hemisphere and global

air temperatures, (3) to compare reconstructed CO_2 trends and derived temperature changes with proxy records of changes in the North Atlantic sea-surface temperature and global air-temperature, and (4) to contribute to assess the role of CO_2 in the ocean-atmosphere-climate system during the onset of the LIA.

Material and Methods

A sediment core was taken in a former river channel of the river Roer in the vicinity of Sint Odilliënberg (southeastern Netherlands, 51.08°N, 6.00°E; Fig.2.1 A), which is completely filled with organic-rich clayey gyttja deposits and covered at the top by a peat layer. From this locality four meters of partly laminated, organic-rich sediments were recovered using a Livingston piston corer. Leaf-bearing layers contain abundant remains of leaves of *Quercus robur*, *Quercus petraea* and *Salix cinerea s.l.* Before the core was cut into 0.5 cm slices a correction for core compression was applied to calculate the actual depth for each sample.

Eleven samples were selected for ^{14}C dating at the AMS facility of the R.J. van de Graaff Laboratory (Utrecht University). From each interval thoroughly cleaned plant remains were used for the AMS ^{14}C analysis. Conversion of the ^{14}C dates into calendar ages AD with a 1σ-probability has been performed with the calibration program CALIB 4.4 (Stuiver et al., 1998; Tab. 2.1). In order to lower uncertainty levels, the ^{14}C dates were wiggle-matched to the INTCAL98 ^{14}C calibration curve (Stuiver et al., 1998).

The leaf-bearing part of the core is restricted to the interval between 60 cm and 360 cm depth. Fragments of *Quercus robur* leaves from 60 successive samples were used for stomatal frequency analysis. From each sample up to five leaves were analyzed. Adhering minerogenic matter was removed from the interior of the leaf remains by adding a 20% HF solution for 20 minutes. For light-microscopic analysis, leaf fragments of 0.5 x 0.5 cm were bleached in a 4% sodiumhypochlorid solution to remove the mesophyll. The remaining cuticle was stained with safranin. Stomatal frequency counts were made on the basis of digitized images, obtained with the image analysis software analySIS 3.0 (Soft Imaging System GmbH, Germany). Counting areas were restricted to stomata-bearing alveoles. Seven digital images per leaf with a field area of 0.03 mm^2 were analyzed. Parameters measured were (mean) epidermal cell density (ED [n/mm^2]) and (mean) stomatal density (SD [n/mm^2]). From SD and ED the area-independent (mean) stomatal index (SI) (Salisbury, 1927) was calculated as:

$$SI\ [\%] = (SD) / (SD + ED) \times 100 \qquad (1)$$

In order to infer atmospheric CO_2 mixing ratios from the calculated SI values for buried leaves, a calibration model based on the historical responsiveness of both *Q. robur* and *Q. petraea* SI to industrial CO_2 increase was used (Fig. 2.2 B; Chapter 1). This

model is rather conservative at the edges of the response interval and due to a response limitation of *Q. robur* SI at a CO_2 level of 320 ppmv, atmospheric CO_2 values higher than 320 ppmv cannot be inferred (Chapter 1). Because CO_2 reconstructions based on stomatal frequency analysis generally show higher mean pre-industrial CO_2 levels than coeval Antarctic ice-core records, normalized data are used for comparisons with ice-based CO_2 data and for calculating changes CO_2 in radiative forcing.

To calculate the amount of radiative forcing induced by the reconstructed CO_2 levels, two different approaches were used. The first one is based on Shi (1992), who expressed the radiative forcing as:

$$dF = \alpha \cdot \mathrm{Ln}(C/CO) + \beta \times (\sqrt{CO}) \quad (2)$$

where dF represents the radiative forcing (W/m^2), C represents the CO_2 mixing ratio (ppmv), CO represents the unperturbed CO_2 mixing ratio (ppmv), α = 4.841 and β = 0.906. The second approach is based on Myhre et al. (1998) who expressed the radiative forcing as:

$$dF = \alpha \cdot \mathrm{Ln}(C/CO) \quad (3)$$

where dF represents the radiative forcing (W/m^2), C represents the CO_2 mixing ratio (ppmv), CO represents the unperturbed CO_2 mixing ratio (ppmv) and α = 5.35.

As recommended by the IPCC (2001), radiative forcing calculations of CO_2 perturbations generally use a pre-industrial CO_2 level of 278 ppmv as a reference. To calculate changes in radiative forcing induced by the reconstructed CO_2 changes, normalized stomata-derived CO_2 data were therefore superimposed on this 278 ppmv base level.

To assess the effects of the calculated CO_2-induced radiative forcing changes on Northern-Hemisphere and global air temperatures, calculations with the coupled ECBILT-CLIO model were conducted on a low and high CO_2 sensitivity mode. ECBILT: a spectral T21, 3-level quasi-geostrophic atmospheric model (Opsteegh et al., 1998); CLIO: a coarse resolution sea-ice ocean general circulation model (Goosse and Fichefet, 1999).

Results

Age model

Results of the AMS ^{14}C measurements are summarized in Table 2.1 and Figure 2.1 B,C. The calibration with CALIB 4.4 provides an age-depth relationship with uncertainty levels of 100-200 years. In order to lower these uncertainties, the ^{14}C dates were wiggle-matched to the INTCAL98 ^{14}C calibration curve (Stuiver et al., 1998). Non wiggle-matched dates show that sedimentation rates are not constant throughout the core. Therefore

Depth (cm)	Composition	^{14}C age (BP±1sigma)	UTC nr
76.25	*Salix* twigs	351±40	11730
94.54	*Salix* and *Quercus* leaves	355±45	12058
111.25	*Salix* and *Quercus* leaves	369±41	11731
141.25	*Salix* and *Quercus* leaves	454±37	11732
174.84	*Salix* and *Quercus* leaves	713±32	12111
197.25	*Salix* and *Quercus* leaves	544±47	11736
210.79	*Salix* and *Quercus* leaves	783±35	12060
230.13	*Salix* and *Quercus* leaves	861±30	12059
276.4	*Salix* and *Quercus* leaves	1003±39	11733
315.8	*Salix* and *Quercus* leaves	961±36	11734
368.85	*Salix* and *Quercus* leaves	368±85	11735

Table 2.1: Radiocarbon AMS ^{14}C dating results given in years BP (1950) with a 1 sigma confidence interval

the wiggle-match was performed with three different sub-sets, of which each sedimentation rate was assumed to be linear. Results of wiggle-matching are shown in Fig. 2.1 B. The lower part (368-276 cm) and the upper part (111-76 cm) of the core section show significant higher sedimentation rates (1.17 and 1.04 cm/yr, respectively), compared to the middle part (276-111 cm; 0.29 cm/yr). The wiggle-matched dates provide an age-depth model for the period of AD 1000-1500, which consists of three linear components (Figure 2.1 C). Separated by a considerable hiatus, the clays and peat deposits of the top 75 cm of the core section were formed after AD 1800 (Bunnik, pers. com.).

Atmospheric CO_2 reconstruction

The mean SI per horizon as measured on buried *Q. robur* is plotted in Figure 2.2 A. Application of the *Q. robur/Q. petraea* calibration model developed in Chapter 1 (Fig. 2.2 B) enables quantification of the recorded SI changes in terms of atmospheric CO_2 mixing ratios (Fig. 2.2 C). Only the multi-decadal trends in the SI record are interpreted as a CO_2 signal. Short-term CO_2 fluctuations that are smaller than the standard deviation of an individual sample are regarded as insignificant. Abrupt (near-annual) SI fluctuations are considered to represent noise related to intrinsic stomatal frequency variation in leaves (Kürschner et al., 1997).

The reconstructed atmospheric CO_2 record indicates an average decrease of 0.23 ppmv/year from 310 ppmv at AD 1000 to a minimum value of 285 ppmv around AD 1200. A rapid increase of 0.3 ppmv/year during the 13th century results in levels of up to 320 ppmv around AD 1300. Subsequently, CO_2 gradually decreases with a rate of

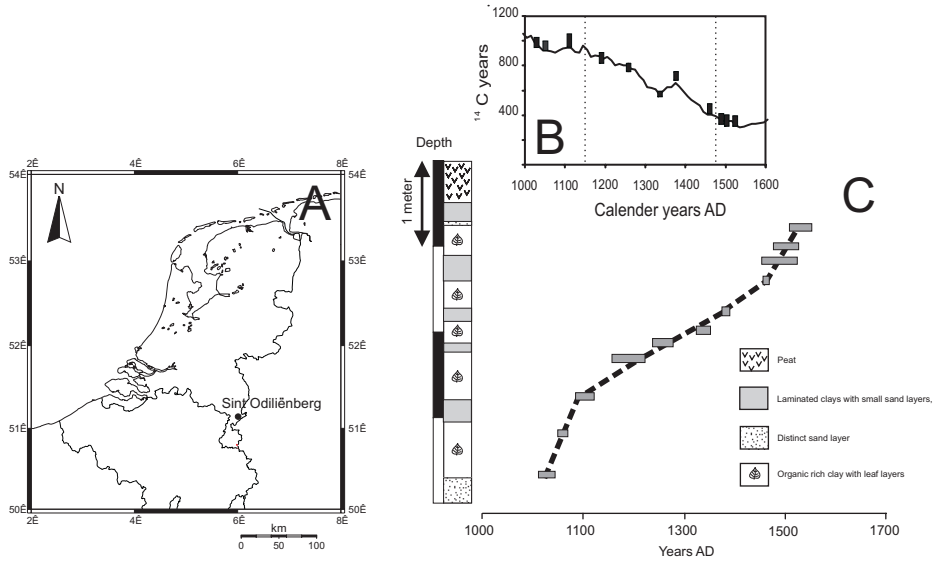

Figure 2.1: **A**: Location map of the core site, **B**: Radiocarbon versus calender ages of eleven AMS ^{14}C dates wiggle matched to the INTcal98 calibration curve of Stuiver et al. (1998). **C** : Age-depth model of the studied core based on wiggle matching of 11 AMS ^{14}C dates.

0.075 ppmv/yr to values of 300 ppmv around AD 1500. Short-lived CO_2 shifts are imprinted upon this general trend around AD 1025 (a decrease of 0.8 ppmv/yr), AD 1100 (an increase of 0.3 ppmv/yr), AD 1150 (a decrease of 0.4 ppmv/yr), and AD 1480 (a decrease of 0.75 ppmv/year).

CO_2 radiative forcing and modeled global temperature response

Figure 2.3 illustrates the effects of the reconstructed fluctuations on the CO_2 radiative forcing and its global temperature response. The two models (equations 2 and 3) produce essentially the same results, therefore the results based on the most recent model (equation 3; Myhre et al., 1998) were chosen to be used for further calculation. The radiative forcing shows a declining trend from AD 1000 until AD 1200 by 0.5 W/m^2, interrupted by a temporary increase of 0.2 W/m^2 around AD 1100 (Fig. 2.3 A). The modeled temperature response indicates a cooling by 0.25ºC and 0.15ºC at the high sensitivity and the low sensitivity run of the climate model, respectively (Fig. 2.3 B). This declining trend is followed by a prominent increase of 0.7 W/m^2 that occurs between AD 1200 and 1300 as a result of a 34 ppmv CO_2 rise. The corresponding temperature response is a warming by 0.25ºC and 0.12ºC at high sensitivity and low sensitivity, respectively. After AD 1300 the CO_2 forcing continuously declines by 0.4 W/m^2, which results in a cooling by 0.15ºC.

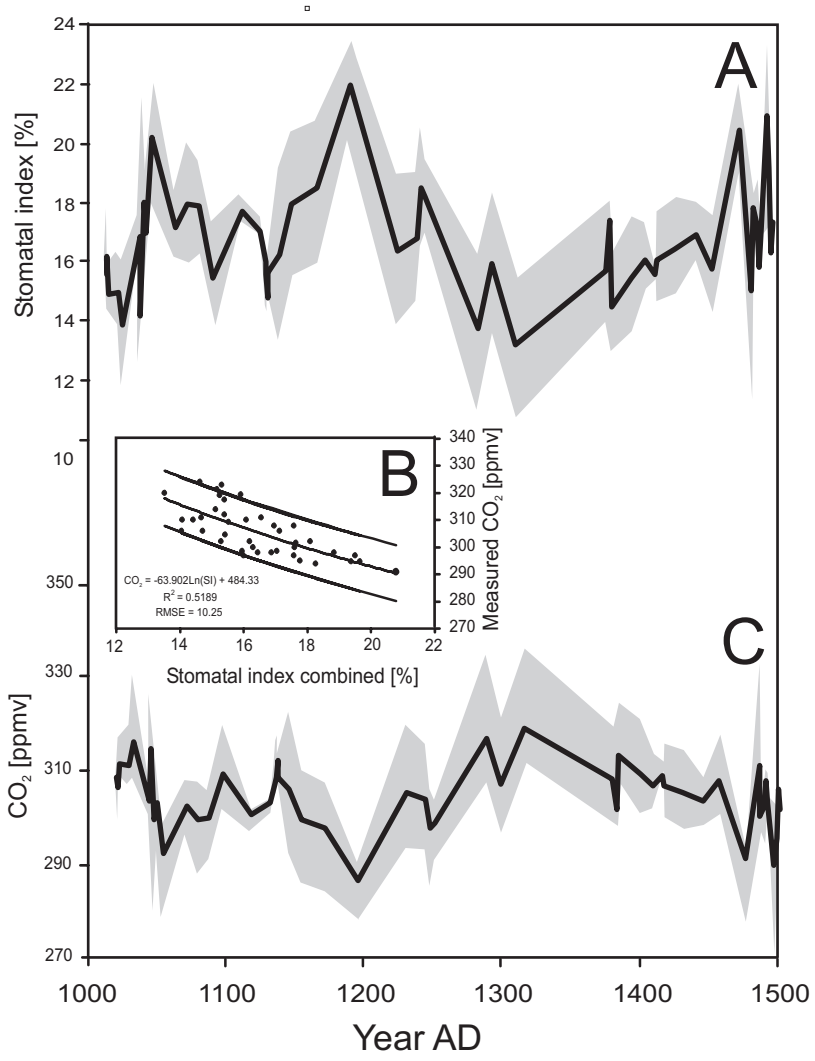

Figure 2.2: A: Stomatal index counts on fossil *Quercus robur* leaves for the time period from 1000 AD to 1500 AD. Black line represents the means of 2-5 leaf fragments per sample. Grey area shows the confidence interval of ± 1 SE (sample specific standard error).

B: Calibration model based on the combination of herbarium as well as sub-fossil leaf litter studies of *Q. robur* and *Q. petraea* (Chapter 1). To reduce uncertainties in the original data-set due to outliers in the data, both SI data and the historical CO_2 values are log-transformed before fitting a linear response curve through the data-set.

C: Atmospheric CO_2 mixing ratios as inferred from the stomatal index counts (Fig. 2.2 A) by applying the calibration model of Chapter 1 (Fig. 2.2 B). Grey area shows the confidence interval of ± 1 SE (sample specific standard error).

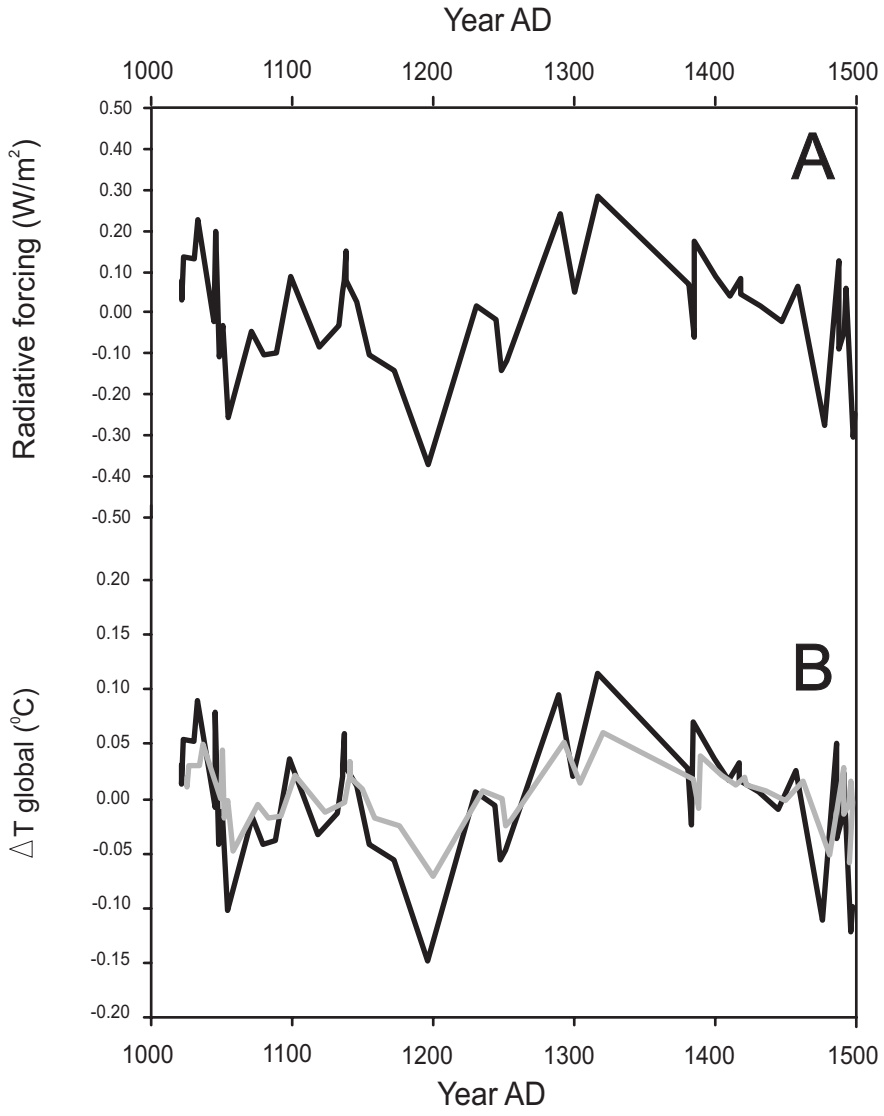

Figure 2.3: A: Radiative forcing calculations of the reconstructed CO_2 fluctuations, **B**: CO_2 global air temperature response as calculated from the radiative forcing (A) by applying ECBILT-CLIO model calculations. Dark line represents high and grey line represents low sensitivity of the model for CO_2.

Comparison with other CO_2 records

In Figure 2.4 the reconstructed CO_2 fluctuations are compared with other published CO_2 records covering the time interval between AD 1000 and 1500 with significant resolution. All CO_2 data are normalized. A stomatal frequency record from Jay Bath, a shallow pond on the flank of Mount Rainier (Washington, USA) is based on buried needles of the conifer *Tsuga heterophylla* (Kouwenberg, 2004). Five AMS ^{14}C datings and one tephra layer at 1481 AD establish the chronology for this reconstruction. Two CO_2 minima are evident, a smaller one around AD 1050 and a more pronounced minimum around AD 1150. Maximum CO_2 levels are registered in the first half of the 14th century AD; these are followed by a steady CO_2 decrease. The trends are similar to those of the present *Quercus robur* record; there are minor timing discrepancies, and the conifer needles suggest higher amplitude CO_2 variations, with a maximum change of 60 ppmv (*vs*. 34 ppmv) during the 13th century AD.

CO_2 trends in the Antarctic ice-core records of South Pole (Siegenthaler et al., 1988) and Law Dome (Barnola et al., 1995) replicate CO_2 minima around AD 1200 and maxima around AD 1300. However, the amplitude of the 13th century AD rise is substantially lower (12 ppmv) in comparison to the stomata-based results.

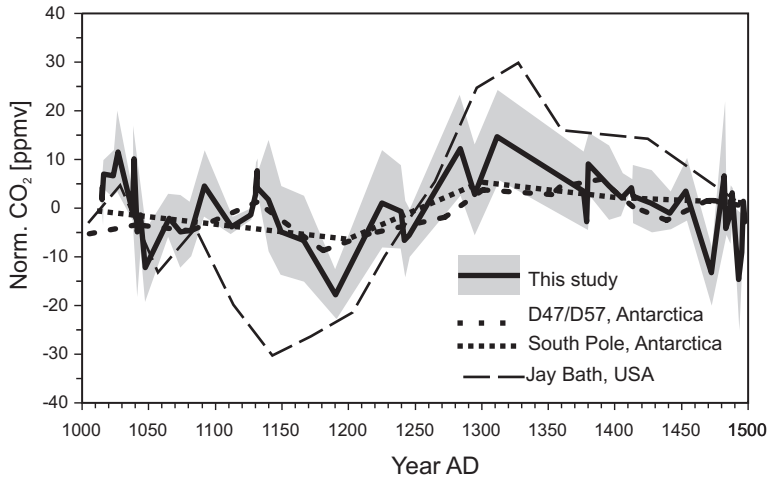

Figure 2.4: Comparison of the normalized CO_2 record of this study with two normalized antarctic ice core CO_2 records (D47/D57, Barnola et al.,1995; South Pole, Siegenthaler et al., 1988) and one normalized stomatal frequency CO_2 record (Jay Bath, Kouwenberg et al., 2004).

Comparison with North Atlantic sea-surface temperatures

Figure 2.5 compares the reconstructed CO_2 fluctuations with a faunal record of sea-surface temperature (SST) variations off West Africa (DeMenocal et al., 2000). SST curves from the Bermuda Rise (Keigwin, 1996), Chesapeake Bay (Cronin et al., 2003) and the Nordic Sea (Andersson et al., 2003) show a similar picture, suggesting that SST trends at the low-latitude African site are representative for the entire North Atlantic realm. The atmospheric CO_2 excursion around AD 1200 is synchronous with a prominent cooling event in the SST record (Fig. 2.5 B). The subsequent CO_2 increase of 34 ppmv corresponds to the warming of North Atlantic surface waters during the 13th century AD.

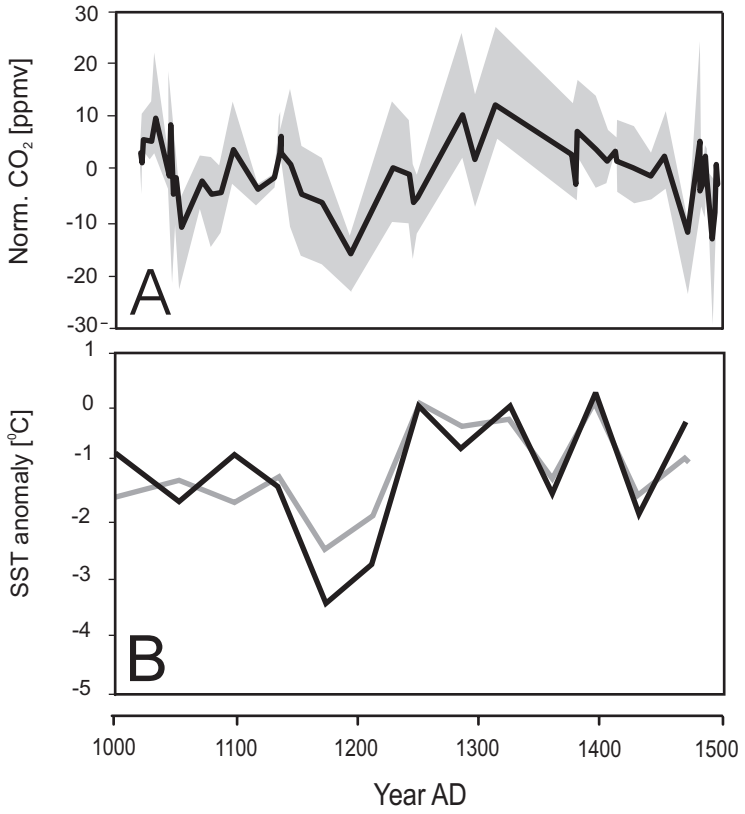

Figure 2.5: **A**: Normalized CO_2 fluctuations (this study), **B**: Sea surface temperature anomalies off-shore West Africa as reconstructed from foraminiferal assemblages (DeMenocal et al., 2000). The Black line are cold season anomalies,whereas the grey line shows the warm season anomalies.

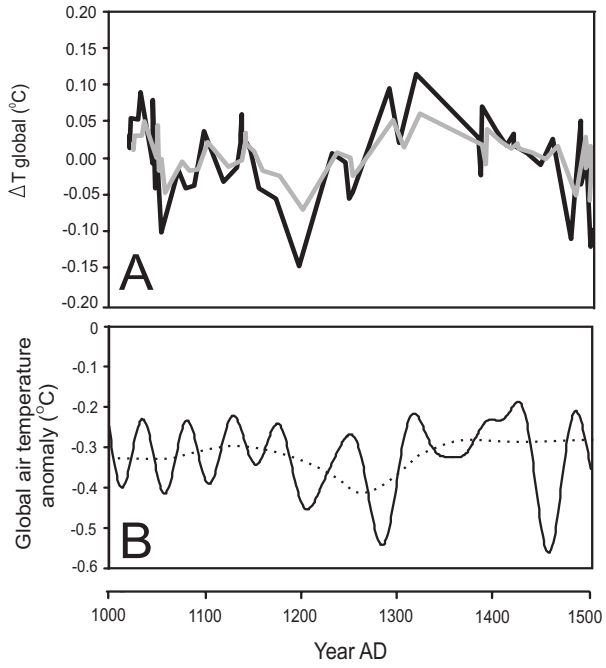

Figure 2.6: **A**: Modeled global air temperature response to the reconstructed CO_2 oscillations. Dark line represents high and grey line represent low sensitivity of the model for CO_2. **B**: Global air temperature anomaly reconstruction (Mann and Jones, 2003). Dotted line represents large scale temperature trend.

Comparison with global air temperatures

Composite proxy records of Northern-Hemisphere and global air temperature for the first half of the last millennium reveal anomalies in the range of 0.2 to 1°C (Mann et al., 1998; Briffa et al., 2000; Esper et al., 2002; Mann and Jones, 2003). It should be noted that the Northern Hemisphere air-temperature history deviates from the global picture, which is mainly the result of differences in landmass distribution on the two hemispheres, as well as limited density of proxy data form the Southern Hemisphere. Yet, because atmospheric CO_2 acts as a greenhouse gas on a global scale, modeled temperature responses to CO_2 fluctuations are compared with a global air-temperature reconstruction (Mann and Jones, 2003; Fig.2.6 B).

A modest cooling trend between AD 1000 and 1250 can be recognized. Superimposed on this trend are a series of multi-decadal temperature fluctuations. Apparently, the amplitude of these higher-order fluctuations increases through the record. A pronounced cooling event around AD 1450 may mark the start of the Little Ice Age *sensu stricto*. However, visual matching of the modeled, CO_2 related, air temperature and the proxy air-temperature record fails to reveal a direct correlation.

The CO_2 regime during the first half of the last millennium

The stomatal frequency records of *Quercus robur* leaves and *Tsuga heterophylla* needles provide independent evidence for CO_2 fluctuations on time-scales varying from decades to centuries (Fig. 2.4). While the timing of the reconstructed trends is in remarkably good agreement, the amplitude of the fluctuations differs significantly. Following the CO_2 minimum around AD 1200, the most prominent CO_2 shift reflected in the *Q. robur* record (34 ppmv) occurred during the 13th century AD. In the *T. heterophylla* record from Jay Bath, the corresponding CO_2 increase reaches 60 ppmv. The different amplitudes may be the result of the conservative nature of the *Quercus* stomatal-response calibration model (Chapter 1). On the other hand, differences may be related to a comparatively lower accuracy of the modern training set for *T. heterophylla* (Kouwenberg, 2004).

Two Antarctic ice-core records (South Pole and D47/D57) also show a small but significant CO_2 increase during the 13th century AD (10 and 12 ppmv, respectively, based on unsmoothed data; Fig. 2.4). The amplitude of the CO_2 shift in the *Q. robur* record is by a factor of 3 larger than in the ice-core records. This difference is likely to be an effect of natural smoothing of the CO_2 signal in ice cores due to diffusion processes that occur in the firn layer before the air is trapped in the ice (Schwander, 1996; Trudinger et al., 2003; Chapter 6).

Coupling between atmospheric CO_2 and North Atlantic SST

Stomatal-frequency based CO_2 reconstructions indicate a temporal association between atmospheric CO_2 levels and North Atlantic SST (Fig. 2.5). This coupling corroborates the role of SST changes, resulting from short-term disturbances of the North-Atlantic thermohaline circulation, o n the production and depletion of atmospheric CO_2 (Wagner et al., 2002; Kouwenberg, 2004).

Following the basic concept of the thermal bipolar seesaw, SST temperature changes on the Northern Hemisphere should be compensated by anti-phase behavior of the Southern Hemisphere (Marotzke, 2000). In this scenario, synchronous effects of opposite SST changes in the Southern Ocean would, at least in part, compensate atmospheric CO_2 fluctuations associated with North-Atlantic SST anomalies. This concept was supported by Antarctic ice-core data that never provided compelling evidence for a distinctive CO_2 response to centennial-scale temperature changes (Raynaud et al., 2000).

The exact phase relationship between the two hemispheres, however, is still difficult to assess due to the incomplete documentation of centennial-scale climate variability on the Southern Hemisphere. Recent model studies focusing on the first half of the last

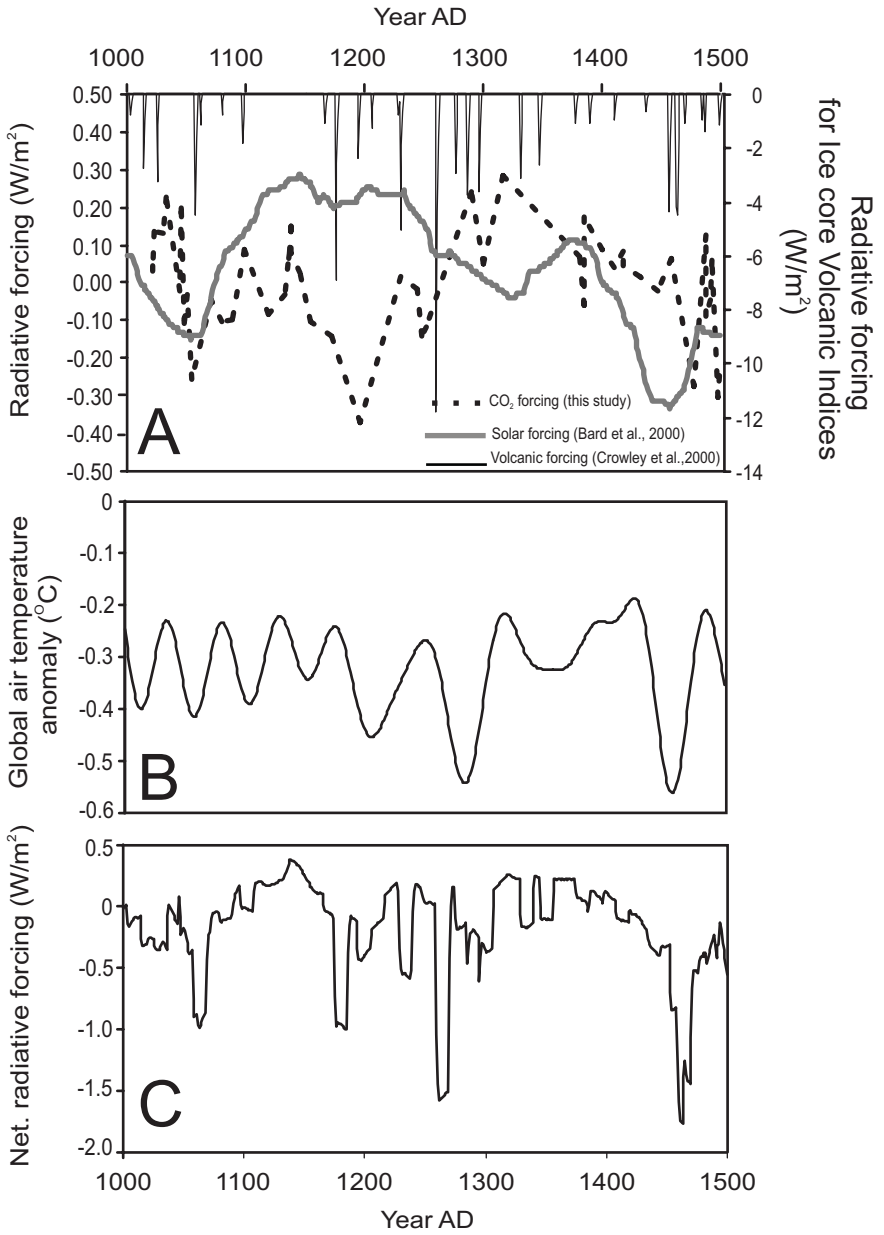

Figure 2.7: A: Three air temperature forcing mechanisms; CO_2 (dotted line, this study), solar irradiance (grey line, Bard et al., 2000) and volcanism (thin black line, Crowley et al., 2000). The left y-axis represent CO_2 and solar radiative forcing while the right y-axis represent volcanic radiative forcing. **B**: Global air temperature anomaly reconstruction (Mann and Jones, 2003). **C**: Cumulative effect of the CO_2, solar and the 11 years smoothed volcanic radiative forcing.

millennium suggest a phase delay of about 150 years between the two hemispheres (Goosse et al., 2004). Time lags of this magnitude could explain, at least in part, the observed relation, where atmospheric CO_2 concentrations closely follow or parallel North Atlantic SST trends.

Role of atmospheric CO_2 as a climatic forcing factor

There is no apparent temporal correlation, in terms of pacing and direction, between multi-decadal CO_2 shifts detected in the *Q. robur* stomatal frequency record and air-temperature. However, since CO_2 acts as a greenhouse gas, these pronounced shifts should account for significant air-temperature fluctuations due to changes in radiative forcing. The calculated air-temperature changes generated by the 13th-century AD CO_2 shift of 34 ppmv, are 0.25ºC on a global scale (Fig. 2.5 B). The amplitude of such CO_2-forced temperature changes would be in excellent agreement with the constrained maximum range of 0.25ºC for reconstructed global air-temperature variability during this period (Fig. 2.6 B). This correspondence emphasizes the potential role of pre-industrial atmospheric CO_2 levels as a forcing factor for climate of the last millennium. On the other hand, the lack of temporal correlation between CO_2 shifts and temperature fluctuations indicates that the global temperature history between AD 1000 and 1500 is not solely the result of CO_2 dynamics.

Previous studies have favored solar radiation and volcanism as the primary climatic forcing factors for the last millennium (Lean et al., 1995; Crowley and Kim; 1996; Overpeck et al., 1997; Mann et al., 1998; Damon and Peristykh, 1999; Free and Robock, 1999; Crowley, 2000). During the time interval studied, the solar radiative forcing variations are in the same order of magnitude as the calculated CO_2 forcing fluctuations (Fig. 2.7 A). But again, there is no clear correlation between changes in solar forcing and global air-temperature fluctuations. Volcanism is likely to be a prominent short-term forcing factor at times of increased eruptive activity, like in AD 1258, when the largest volcanic eruption of the past 7000 years took place (Oppenheimer, 2003).

Intriguingly, the estimated combined radiative effect of CO_2, solar radiation and volcanism allows a much better correlation with global air-temperature history than the individual forcing factors alone (Fig. 2.7). It appears that about 70% of the multi-decadal temperature fluctuations match the netto CO_2-solar-volcanism forcing curve. Particularly the correspondence between AD 1200 and 1500 suggests that the air-temperature history of the first half of the last millennium is substantially the result of combined effects of atmospheric CO_2, solar radiation and volcanism. The correlation indicates that CO_2 forcing may have amplified or reduced periodically the temperature effect significantly.

Conclusions

Stomatal frequency analysis on buried leaf remains of *Quercus robur* provides compelling evidence of a dynamic CO_2 regime during the onset of the Little Ice Age in the period between AD 1000 and 1500. In comparison to coeval changes observed in Antarctic ice-core records, reconstructed atmospheric CO_2 fluctuations are much more pronounced. The CO_2 shifts show a strong correlation with North-Atlantic SST trends. This coupling confirms a causal relationship between disturbances of the North-Atlantic thermohaline circulation, and the production or depletion of atmospheric CO_2.

A coupling between atmospheric CO_2 and air temperature is obscured by the forcing effects of solar radiation and volcanism. Calculated CO_2-induced temperature changes are of the magnitude of short-term fluctuations in the proxy record of global air-temperature history. However, temporal correlation of CO_2 changes and air-temperature changes is only possible by combining the modeled radiative effect of CO_2 fluctuations with coeval effects of changing solar radiation and prominent volcanic eruptions. This exercise falsifies concepts that atmospheric CO_2 represents an insignificant forcing factor for pre-industrial climate in the last millennium.

In general, the results support a much more important role of atmospheric CO_2 than previously suggested. It may therefore be anticipated that combining all forcings (dynamic CO_2, solar, volcanism) in an advanced energy-balance model may result in a better quantification of the global temperature variability of the last millennium, and may, hence reduce the uncertainties with respect to the dynamical response of the ocean-atmosphere system.

Chapter 3

The influence of hydrology on tree ring-width and stomatal frequency of medieval and present-day swamp oaks

The radial growth dynamics of medieval and present-day swamp oaks (*Quercus robur*) were studied in order to evaluate the effects of local environmental conditions such as temperature and precipitation. Climate-growth analysis of a living population at Sint Odiliënberg (the Netherlands) revealed a positive correlation of ring-width to the annual precipitation signal. Unique features in the ring-width series of medieval oak trunks from the same site are prolonged periods of depressed growth. These features may represent recovery periods after root damage caused by anoxia due to growth season flooding. The absence of these growth patterns in the living population at this site is caused by the decrease of river dynamics and intensified drainage activities during the past ~150 years. Similar growth patterns were observed in a living population at a more intensively waterlogged stand in the Netherlands (Oostbroek). To test whether stomatal frequency is affected by water logging, the leaf epidermal anatomy of the *Q. robur* populations at Oostbroek, Sint Odiliënberg and Mariapeel are studied. The results indicate no significant difference in stomatal frequency between the three populations. This suggests that growth-season inundation did not affect the stomatal index proxy used for CO_2 reconstruction.

Introduction

Growth patterns in deciduous trees are closely related to the environmental parameters that determine the specific habitat conditions. Quantifying morphological and / or anatomical adaptations in botanical proxies enables the reconstruction of climate relevant parameters through time. The most successfully applied botanical proxies are tree-ring analyses, indicative for changes in e.g. local temperature and water availability (e.g. Fritts, 1976; Schweingruber, 1993) and stomatal frequency analysis on fossil leaves, which is a proxy for atmospheric CO_2 concentrations (Woodward, 1987; Royer, 2001) and water availability (Bosabalidis and Kofidis, 2003; Woodward et al., 2002). Modern palaeoclimatology increasingly focuses on the synchronous analysis of multiple climate parameters in order to gain information on the linkage of different aspects of our climate system. Combination of different botanical proxies, such as tree ring and stomatal frequency analysis from single data sources would enable such holistic studies. Furthermore, they would provide a unique opportunity to independently validate the applied methods.

A unique site was identified in the vicinity of Sint Odiliënberg (the Netherlands) where channel fill deposits of the river Roer, rich in *Quercus robur* leaf remains, did also contain fossil *Q. robur* tree trunks. The locality makes part of an *Alnus* swamp forest community with year-round high groundwater tables, where hydrology is most likely the dominant factor limiting tree-growth. A palaeo-atmospherical CO_2 reconstruction based on the stomatal index of the *Q. robur* leaves, derived from the AMS ^{14}C wiggle match dated channel fill deposits, revealed a dynamical CO_2 regime during the period from AD 1000 to 1500 (Chapter 2). As stomatal frequency can be affected by local hydrological conditions, the presence of fossil *Q. robur* trunks in these deposits provides the opportunity to compare the local hydrological signature conserved in the tree-ring patterns to the stomatal frequency of the buried leaves.

Detailed analysis of tree-ring patterns in both, modern and fossil *Q. robur* individuals from the same location allows to estimate the influence of hydrological changes on wood anatomy under present day and past growth conditions. In order to ensure the validity of stomatal frequency as a proxy for CO_2 (Chapter 2) it is essential to learn the potentially confounding effects of hydrological changes at this site.

First, the tree-ring patterns of the modern oak population and the medieval oak trunks are compared in terms of mean ring width and (age) trend. Secondly, the relationship between tree-ring widths of the modern oaks and precipitation as well as temperature is assessed. Subsequently, it is evaluated whether the climate-growth relationship of the modern oak population is valid for the medieval oak trunks. To test whether the medieval local hydrological history affected the stomatal frequency of the medieval leaf record, modern leaves from present-day wet oak stands in the Netherlands with diverging

hydrological conditions were compared. Finally, the radial growth dynamics of the medieval trunks are compared to the stomatal index data of the fossil *Q. robur* leaves.

This strategy provides the opportunity to concurrently study the radial growth dynamics of these oaks driven by changes in local environmental conditions, together with micro-morphological adaptations of the leaves to changing atmospheric CO_2 conditions. It further allows to test to which degree local environmental factors contributed to the high levels of intrinsic variability encountered in the stomatal frequency based CO_2 reconstruction.

Material and Methods

Site description

The present-day population of *Quercus robur* is located in an alder swamp forest located near the village of Sint Odiliënberg, The Netherlands, which is classified as a CARICI ELONGATAE-ALNETUM, sub-communities RIBOSETUM NIGRAE and TYPICUM vegetation type (Stortelder et al., 1998) (Fig. 3.1). The soil at the *Q. robur* stand consists of 1 to 2 meters of organic and nutrient rich clays covered in some parts by a thin peat layer. Seepage of groundwater from the terrace border wall provides a year-round high

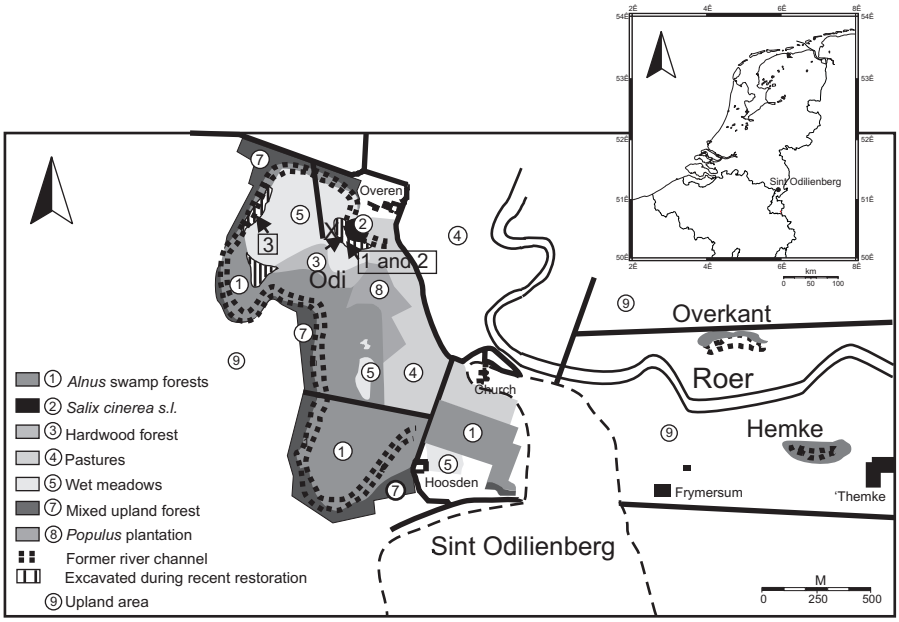

Figure 3.1: Location and vegetation map of the studied site. 1, 2 and 3 (with arrows) represent the sub-fossil trunks. Sub-sites Odi, Hemke and Overkant are indicated, X marks the position of the leaf bearing sediment core

groundwater-table with levels between 30 and 60 cm below surface, which results in the development of shallow root systems of the oaks. Inundation by the river Roer in general takes place during the winter months at extreme high water-levels.

Sampling, *sample preparation and tree-ring measurement*

Twenty-three dominant *Q. robur* trees were sampled by taking one core per tree with an increment corer. The sampled population consists of three sub-sites: (1) Odi, (2) Hemke and (3) Overkant (Tab. 3.1). Sub-site Odi is located nearest to the sediment core site (Fig. 3.1).

The three trunks of *Q. robur* were retrieved from the channel fill deposits near the sediment core location where the *Q. robur* leaf material was obtained (Fig. 3.1). Species specific determination of the trunks was obtained by leaf micro-morphological analysis of leaf material derived from the surrounding sediments. Two trunks were retrieved only a few meters away from the sediment coring site (Roer-1 and 2), while the third (Roer-3) was found 100 meters to the west. Hand-axe cut-marks of the felling of the tree were still present on the base of the trunk of Roer-1. Stem-discs were collected approximately one meter above the root base of the three trees. An additional stem disc was taken from the Roer-1 tree at 210 cm above the stem base.

The increment cores are mounted on wooden holders and the surface is cut with a knife to increase th visibility of the tree-rings. From each stem-disc of the fossil oaks three radial sections are cut, two opposite radials and a third with a 90º angle towards the other two. From the second stem disc of Roer-1, only two radials (90º angle) were analyzed. Tree-ring measurement and data processing was carried out with standard dendrochronological equipment and software (TSAP: Rinn, 1996; COFECHA: Holmes, 1983; Grissino-Mayer, 2001). For both the living as well as the fossil trees early- (EW) and late-wood (LW) width, and the derived ring-width was measured.

Cross-dating and detrending

Cross-dating of the different tree-ring parameters (ring-width, early-wood and late-wood) ensured that measurement errors are detected and each tree-ring measurement was dated to the year when it was formed. Cross-dating was performed visually by comparing the single tree-ring series on the screen (program TSAP) and statistically by calculating running intercorrelation (in 50-year segments) between different radii of the same tree and between tree-ring series of different trees (program COFECHA: Holmes, 1983; Grissino-Mayer, 2001). Statistical characterization of the single tree-ring measurements (e.g. mean tree-ring width, autocorrelation) as well as estimation of tree ages and age trends are summarized in Tab. 3.1. After cross-dating and possible adjustment, the single tree-ring series were combined into different mean curves, so-called chronologies.

Before averaging the single tree-ring series each series was detrended and standardized in order to eliminate tree individual variation and to maximize the common signal in the tree-ring series. The program ARSTAN (www.ltrr.arizona.edu; Grissino-Mayer and Fritts, 1997) was used to detrend the modern oak ring-width series by filtering with a cubic smoothing spline function (Cook et al., 1992) with 30 year stiffness and 50 % cutoff, the tree-ring series of the medieval oak trunks were detrended by using a linear regression in combination wit a 66-year spline (Cook et al., 1992). The resulting index series were subsequently combined into a chronology by using a bi-weight mean (Mosteller and Turkey, 1987), to minimize the influence of extreme values.

Climate-growth analysis

To assess the climate variables that dominantly influences the growth of the modern *Q. robur* population, response function analysis (Fritts, 1976) with bootstrapped confidence intervals was performed (program PRECON: www.ltrr.arizona.edu; Frits, 1999). The climate data were obtained from two weather stations (Maastricht, De Bilt: www.knmi.nl) and checked for homogeneity (program HOM; www.ltrr.arizona.edu). Ultimately, response-function analysis was performed by using the along and homogenous monthly temperature and precipitation records from De Bilt (www.knmi.nl). Response functions are based on a multiple regression whereby monthly temperature and precipitation data (after transformation into principal components) serve as predictors to estimate the tree-ring indices, i.e. the predictants. This model is calibrated for three different time periods: a maximum period from 1905 to 2003, an early period (covering the oldest trees (1905-1960)) and a late period from 1950 to 2003 reflecting the climate-growth relationship during the most recent growth period. As predictors the monthly temperature and precipitation from October of the previous year until October following the actual growing season are included.

Age-assessment of the buried oak trunks

An attempt to date the three fossil tree chronologies by using dendrochronology failed as a comparison with the combined German Dutch bog-oak chronology (Leuschner et al., 2003) as well as with the South German river oak chronology (Spurk et al., 2002) did not yield clear results. Therefore an age-assessment based on AMS ^{14}C analysis was obtained. From Roer-1 and Roer-2 one wood sample was taken from the pith and the four outermost rings, respectively. From Roer-3 three samples were taken, the first was taken at a distance of four rings from the pith, the second sixty-four rings after the first sample and the third fifty-six rings above the second sample. The first sample consists of two rings while the other two include four growth rings. Measurements were performed on the cellulose fraction of the wood samples and were conducted at the AMS facility of the R.J. van der Graaff laboratory (Utrecht University, the Netherlands). Calibration of all samples was performed with the Oxcal 3.9 calibration program (Bronk Ramsey, 2003).

Stomatal frequency analysis

Leaf epidermal characters (Stomatal density (SD [n/mm^2]), epidermal cell density (ED [n/mm^2]) and Stomatal index (SI [%])) of *Quercus robur* leaves were derived from three analogous sites with different hydrological settings (Chapter 1). Between 10 and 15 sun leaves per site were analyzed. Details of the stomatal frequency analysis are presented in Chapter 1. Statistical analysis was performed with the program SPSS 11.5 (2000). Comparability between the three populations was tested with a two-tailed independent variance t-test and are represented by probabilities (p) when no equal variances were assumed.

Results

Present-day population

Results of the dendrochronological analyses of the modern oaks are presented in Table 3.1. Most of the oaks at the investigated locality are ~70 years old, while the oldest living tree reaches an age of 157 years (Tab. 3.1). The mean annual growth varies between 1.83 and 5.95 mm. Individual ring-width series are shown for each sub-site in Fig. 3.2.

The sub-sites represent different generations of oaks established at sub-site 1 (Overkant) around AD 1950, at sub-site 2 (Hemke) around AD 1925 and at sub-site 3 (Odi) around AD1870 and AD 1980. The chronology calculated from the detrended individual tree-ring series of the combined sub-sets is presented in Fig. 3.3. This chronology shows a high frequency signal with recurrent years of depressed growth. The results from the response function analysis indicate an in general positive correlation between precipitation and ring-width during all three studied time intervals of the chronology (1905-2003; 1905-1960; 1960-2003) (Appendix 3.1). The effect of temperature on ring-width showed no clear pattern, although some months indicated a significant correlation (Appendix 3.1). To illustrate the correlation between ring-width and precipitation, the ring-width chronology is plotted together with the October-June precipitation signal in Fig. 3.3. The similarity between both series was tested by calculating the deviation from the average of both series. In 73% of all years the direction of the deviation was the same in both records, indicating a positive correlation between ring-width and precipitation. Around 1920, 1950 and 1980 successive years with a reversed correlation were recorded (Fig. 3.3).

Code	Age at core	Rings	Spint	Wankant	Miss.	Est. age	Av. TRW	Av. Sens.	Autocorr.
OV1	15	38	11	sp2003	10	63	4.68	0.336	0.493
OV2	15	48	11	sp2003	10	73	4.51	0.336	0.613
OV3	15	60	19	sp2003	0	75	1.9	0.25	0.87
OV4	15	50	8	sp2003	3	68	6.03	0.232	0.714
OV5	15	32	10	s2002	15	62	3.83	0.265	0.505
OV6	15	36	9	sp2003	5	56	4.58	0.272	0.5
OD1	15	50	9	s2001	5	70	3.18	0.231	0.693
OD9	15	51	6	s2002	5	71	2.79	0.255	0.685
OD8	15	21	10	sp2003	10	46	4.64	2.82	0.347
OD3	15	132	24	s2001	10	157	1.83	0.277	0.754
OD4	15	124	20	s2001	10	149	2.23	0.279	0.5
OD2	15	39	?	s2001	10	64	5.95	0.243	0.475
OD6	15	21	?	?	15	51	3.79	0.253	0.568
HE2	15	70	14	s2002	5	90	2.22	0.279	0.72
HE8	15	64	14	s2002	10	89	2.35	0.237	0.854
HE7	15	68	15	sp2003	10	93	3.02	0.185	0.815
HE5	15	67	17	sp2003	10	92	2.32	0.257	0.922
HE4	15	70	14	?	5	90	2.23	0.256	1.504
HE6	15	64	14	sp2003	10	89	3.24	0.286	0.634
HE1	15	76	26	sp2003	25	116	2.29	0.198	0.89
OD10	15	125	?	s2003	10	150	2.29	0.26	0.773
OD11	15	124	?	s2003	10	149	1.96	0.251	0.251
OD12	15	131	?	s2003	10	156	2.06	0.25	0.752

Table 3.1.: Tree-ring characteristics for the individual Quercus robur trees of the present-day population at Sint Odiliënberg. Miss.= missing rings, Est. Age = estimated age, Av. TRW = average tree-ring widt and Av. Sens.= average sensitivity. OV, OD and HE indicate the sub-sites; Overkant, Odi and Hemke.

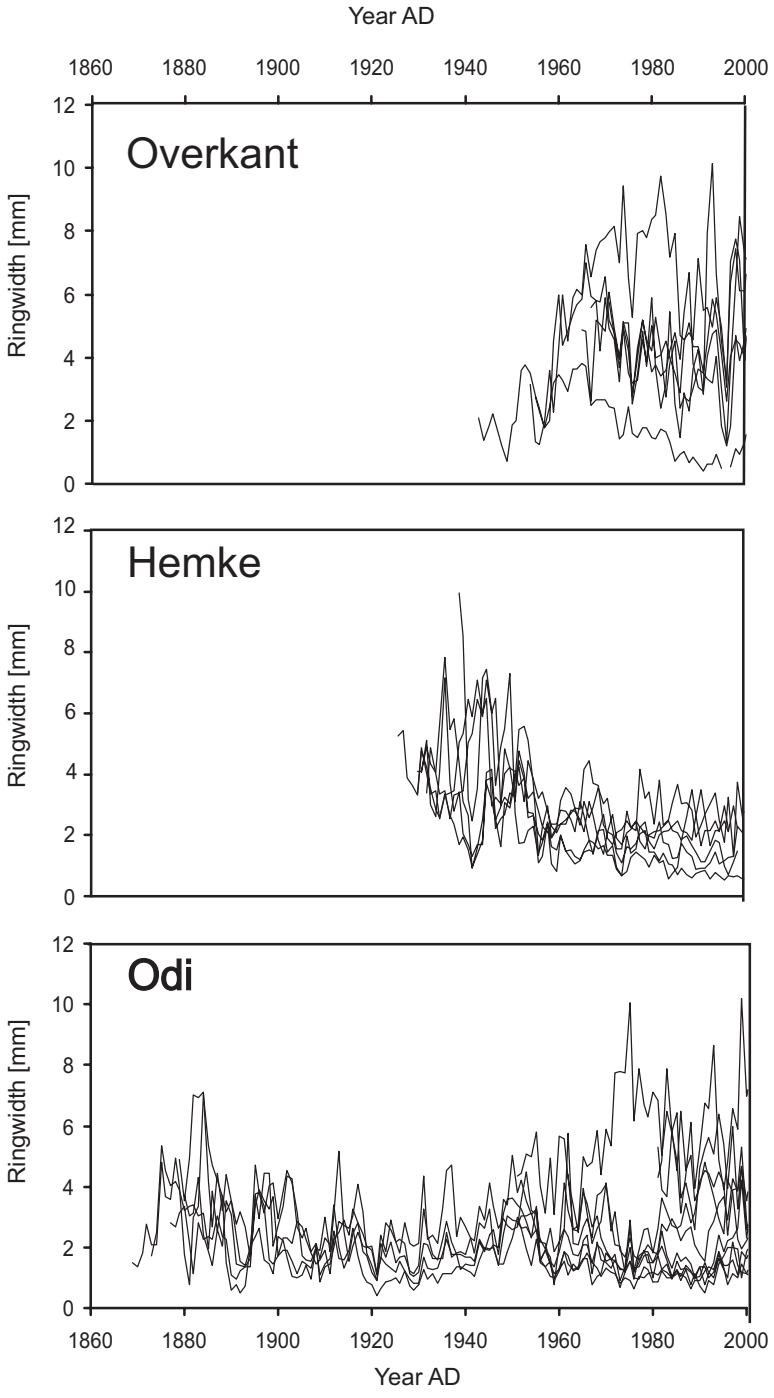

Figure 3.2 : Individual ring-width series of the modern population at Sint Odiliënberg plotted for each sub-site.

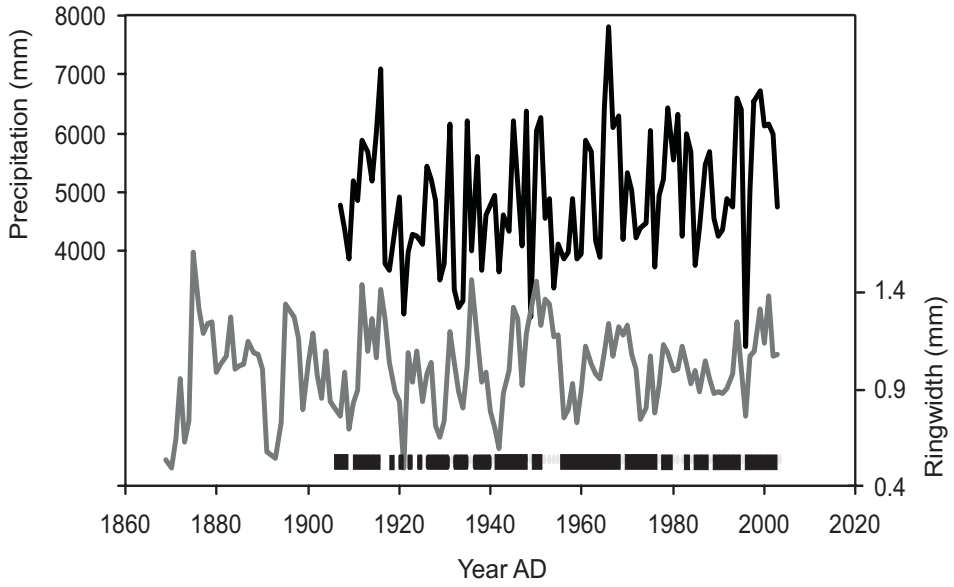

Figure 3.3: Ring width chronology of twenty three living oaks (grey) compared to the sum of precipitation from October through June (station De Bilt) (black). Before the chronology was calculated the single_tree ring series have been detrended using a 30 year spline to remove the age trend. The correspondence of both datasets was tested by calculating the deviation from the average of both series. In 73% of all years the deviation from the average unidirectional (black bars).

Medieval oaks

Fig. 3.4 shows the individual ring-width series of the different radii together with the average ring-width curve for each of the three fossil oaks. Mean annual growth of the fossil trees varied between 1.62 and 4.80 mm/yr, and the length of the averaged tree ring series of Roer-1, Roer-2 and Roer-3 were respectively 120, 86 and 145 years. The exact life-span of the trees could not be determined as the bark was no longer present. In contrast to the modern tree-ring series (Fig. 3.2), all three fossil oaks show extremely wide rings after germination followed by a rapid decrease in ring-width (Fig. 3.4). Another striking feature observed in the averaged ring-width series of the fossil trees is the occurrence of prolonged periods (10 to 20 years) of depressed growth.

Results of the AMS ^{14}C analysis indicated a medieval age of these oaks overlapping the age of the leaf bearing deposits presented in Chapter 2 (AD 1000 - AD 1500) (Tab. 3.2, Fig.3.6). As the trunks Roer-1 and Roer-2 were retrieved from the same leaf bearing channel deposits studied in Chapter 2, they most likely contributed to the accumulated fossil leaf material used for stomatal frequency analysis.

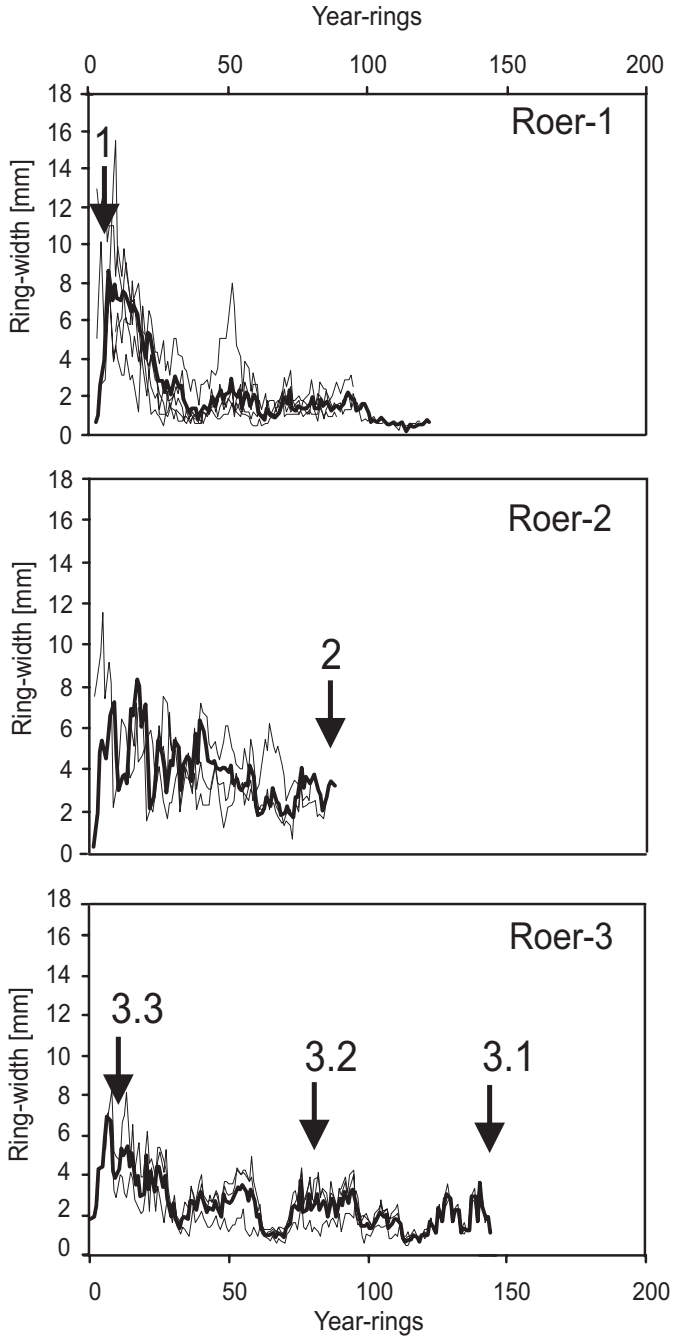

Figure 3.4: Ring-width series of the individual radii measured on the three sub-fossil oaks. Because the outer band of rings (sapwood) was poorly preserved the true life-span of the trees is unknown. Thick black line indicates the average ring-width series for each individual tree. Arrows indicate sample position and code of AMS ^{14}C measurements (Tab.3.2).

		68.2% probability (1-stdev)				95.4% probability (2-stdev)			
Samp.	Uncal BP	max BP	min BP	prob.(%)	mean AD	max BP	min BP	prob. (%)	mean AD
3.3	967±41	940	790	tot range	1058±75	960	760	tot range	1090±100
		940	890	27.3	1035±25				
		870	790	40.9	1120±40				
3.2	980±41	950	790	tot range	1080±80	970	780	tot range	1075±95
		950	900	30.9	1025±25				
		870	790	37.5	1120±40				
3.1	980±50	950	790	tot range	1080±80	980	760	tot range	1080±110
		950	880	34.7	1035±35				
		870	790	33.5	1120±40				
m 3.3	967±41	930	909	68.2	1031±11	970	850	tot range	1040±60
	64 rings								
m 3.2	980±41	866	845	68.2	1095±11	970	850	tot range	1040±60
	56 rings					910	790	91.2	1100±60
						910	820	4.2	1085±45
						910	790	95.4	1100±60
m 3.1	980±50	810	789	68.2	1151±11	850	730	tot range	1160±60
1	536±37	620	515	tot range	1383±53	650	500	tot range	1375±75
		620	605	13.9	1338±8	650	590	28.7	1330±30
		555	515	54.3	14.15±20	570	500	66.7	1415±35
2	485±36	537	508	68.2	1428±15	620	470	tot range	1405±45
						620	610	1.4	1335±5
						560	470	94	1435±45

Table 3.2: AMS ^{14}C results of Tree 1, 2 and 3 calibrated with Oxcal 3.9 (Bronk Ramsey, 1995). Model of tree 3 represents calibration in Oxcal adding restrictions such as sequence and size of the gaps between the samples (64 year-rings between samples 3 and 2, 56 year-rings between samples 2 and 1).

Stomatal frequency

All dendrological analyses show that the present day as well as the fossil populations are sensitive to hydrological changes. While the effect of drought stress on stomatal frequency is generally well known (e.g. Bosabalidis and Kofidis, 2002), the effect of water surplus on the stomatal parameters is less clear. In order to test the sensitivity of stomatal frequency to this hydrological regime, stomatal index (SI) and stomatal density (SD) of *Q. robur* leaves from sites with different hydrological settings were studied. Stomatal index (SI), stomatal density (SD) and epidermis cell density (ED) (Fig.3.5) appear to be slightly higher in the stressed population but statistical analysis proved these differences to be not significant. The stomatal index record established for the site in Sint Odiliënberg is compared to the medieval tree ring series in Fig. 3.6.

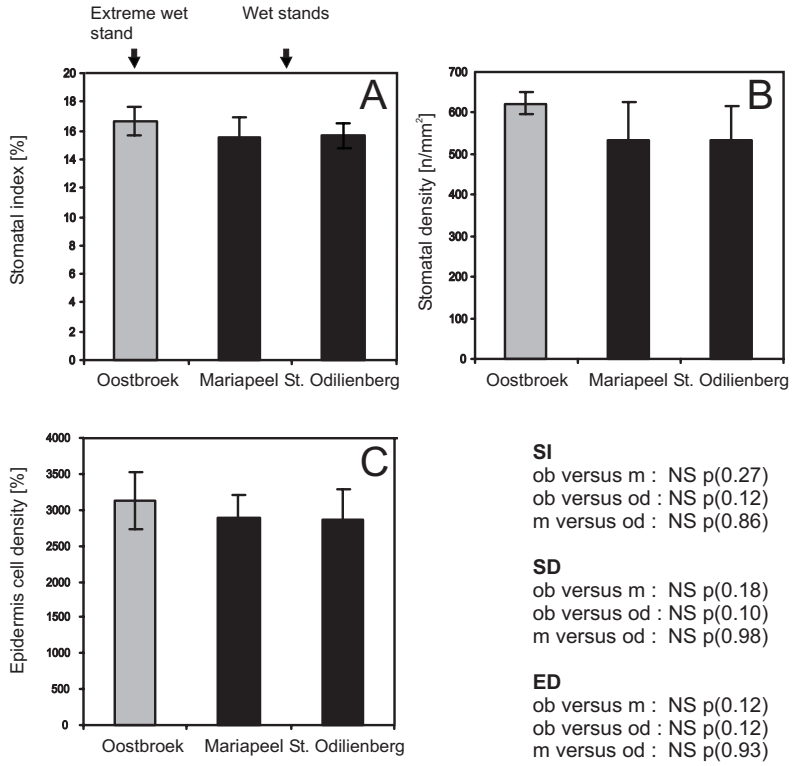

Figure 3.5: Stomatal and epidermal cell measurements of three *Q.robur* populations in the Netherlands. Oostbroek is an alder swamp forest nature reserve east of Utrecht, Mariapeel is a peat-land nature reserve south-east of Eindhoven and the Sint Odiliënberg population forms also part of an alder swamp forest. Sampling size of each population was 10 leaves, counting techniques are described in Chapter 1.Fig 3.5A shows the mean stomatal index [%] of the three populations, B shows the mean stomatal density [n/mm^2] of the three populations, C shows the epidermal cell density [n/mm^2] of the three populations : Error bars represents standard deviations of the mean. The level of similarity between the three populations was tested with a two-tailed independent variance t-test and is represented by probabilities (p) when no equal variances were assumed (ob = Oostbroek, m = Mariapeel, sd = Sint Odiliënberg).

Discussion

The high growth rates of the modern as well as the medieval trees indicate favorable growth conditions for the oaks at the site in Sint Odiliënberg (Tab. 3.1.). The characteristic growth pattern of the medieval oaks (Fig. 3.4) with wide rings in their first years after germination and a rapid decrease in ring-width thereafter is characteristic for an adequate supply of water, nutrients and light during youth followed by an increase in light competition when reaching maturity (Spurk et al., 2002). The modern population at sub-site Odi (Fig. 3.2) has a less-pronounced growth trend indicating a higher level

of competition for light during youth (Spurk et al., 2002). The climate-growth analysis revealed a positive correlation between the year-round precipitation signal (from October previous year to October actual year) and the ring-width, reflecting the high level of adaptation to high groundwater tables of the oaks at this stand (Appendix 3.1.). Due to their shallow root systems, a lowering of the groundwater table due to below average precipitation during the previous winter or early growing season results in stressed growth conditions.

Analysis of the medieval oak trunks revealed different growth patterns of the oaks during medieval times compared to those of today (Fig. 3.3). Next to the diverging growth trends, a striking difference with the modern trees was the occurrence of 10-20 year prolonged periods of depressed growth, observed in all three fossil trees (Fig. 3.4). Reduced oxygen availability due to prolonged inundation of the root system during the growing season is often regarded to be an important factor contributing to prolonged growth depressions in trees from swamp forests (St-George and Nielsen, 2002; Armstrong et al., 1994). Therefore, the prolonged nature of the depressions observed in the fossil trees could very well be caused by seasonal inundation of the stand. Today the river dynamics of the Roer are dampened by the presence of several dams upstream. Therefore growth season inundation of the stand occurs less frequently, explaining the absence of such trends in the present day population. The present day oaks from an extreme waterlogged site (Oostbroek, the Netherlands) have similar prolonged periods of depressed rings width as were observed in the fossil oaks from Sint Odiliënberg. At this site prolonged ring-width depressions (~10-15 yrs.) in the oaks can most likely be related to human induced inundation, and increased groundwater-levels during the past 20 years.

During the periods of depressed ring-width in the medieval oaks, both early- and late-wood width decreased. As early-wood formation and leaf unfolding are closely related processes (Yanosky, 1998) the processes causing the changed early-wood thickness could also have affected the leaf micro-morphological pattern formation, which takes place during the early phase of leaf unfolding (Ticha, 1982). As these fossil trees provided the leaves of the stomatal frequency record used for palaeo-atmospheric CO_2 reconstruction, it could be tested whether extreme wet conditions cause abnormal stomatal frequency patterns. This was achieved by comparing the still extreme waterlogged population of Oostbroek with two normal wet oak stands (Sint Odiliënberg and Mariapeel) (Fig. 3.5).

In Fig. 3.6 the stomatal index record of the medieval oak leaves is plotted together with the ring width series of the medieval oak wood. There is no visual match between the curves evident. Therefore an effect of growth season inundations on the SI record and its inferred CO_2 record is unlikely. This conclusion is supported by the observations in the modern analogue studies discussed above (Fig. 3.5).

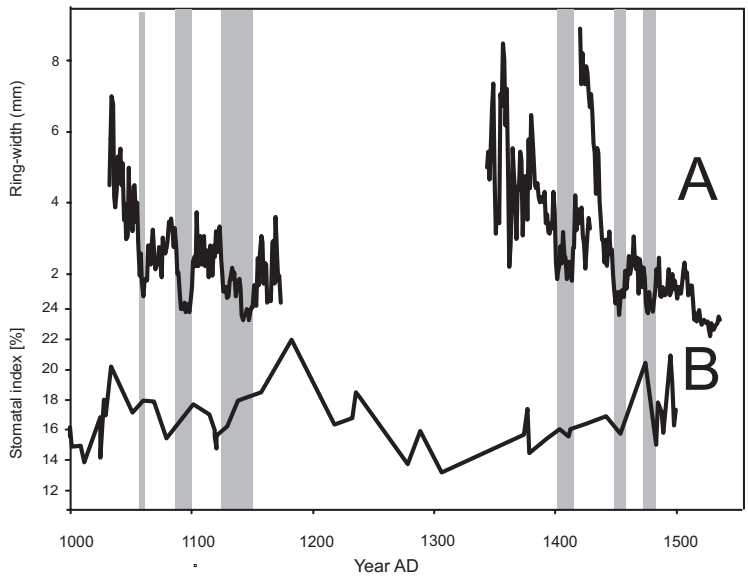

Figure 3.6: **A**: Averaged ring-width measurements of the three medieval oaks (1, 2 and 3). The growth curves consist of mean values of three (1, 2) and five (3) measurements of different trunk samples (Fig. 3.4) **B**: Mean stomatal index values of the *Q. robur* leaf record for the period from AD 1000 to AD 1500 (Chapter 2).

Conclusions

The main local environmental factor determining tree growth in the modern and medieval oaks from the studied swamp forest near Sint Odiliënberg (the Netherlands) is hydrology. The medieval oaks differed from the present-day population by experiencing prolonged periods of depressed growth which was hypothesized to reflect periods of root damage recovery caused by anoxic soil conditions during growth season inundation of the stand. The absence of such growth depressions in the present-day population is explained by drainage activities and dampened river dynamics compared to the medieval situation.

Comparisons of leaf epidermal characters between a present-day severely waterlogged stand, where prolonged periods of ring-width depressions still occur in the oak population, and two normal wet oak stands, revealed no significant differences in the leaf micro-morphological parameters between the studied sites.

It may be concluded from the present study that medieval seasonal inundations in Sint Odiliënberg did not affect the stomatal frequency, and that therefore, the palaeo-atmospheric CO_2 reconstruction based on this leaf record is not confound by changes in local hydrological conditions.

Chapter 4

Carbon sequestration on abandoned medieval farmland after the Black Death pandemic

A well-dated pollen record from an organic-rich infill of an oxbow lake of the river Roer (southeastern Netherlands) provides a high-resolution reconstruction of vegetation and medieval land use for the period between AD 1000 and 1500. Regional effects of the mid-14th century plague pandemic, known as the Black Death, are reflected by a period of significant agricultural regression between AD 1350 and 1440. Concomitant regrowth of forest indicates widespread carbon sequestration on abandoned farmland. Trends in regional forest density of the 13th-15th centuries resemble coeval atmospheric CO_2 trends as reconstructed by means of stomatal frequency analysis of buried leaves. It is conceivable that plague-induced carbon sequestration could have been a contributing factor to atmospheric CO_2 decline during the 14th and 15th centuries.

Chapter 4

Introduction

It was recently hypothesized that anthropogenic greenhouse gas forcing has significantly influenced the global climate since about 8000 years BP, when early agriculture began to extend in previously forested regions of Eurasia (Ruddiman, 2003). Prior to the industrial revolution, progressive forest clearance would have been responsible for the 20–25 ppmv increase of the atmospheric CO_2 mixing ratios detected in Antarctic ice-core records (Etheridge et al., 1996; Indermühle et al., 1999). Superimposed on this long-term trend, recorded negative CO_2 anomalies of 4-10 ppmv during the past 2000 years (Indermühle et al., 1999) would offer evidence of periodic carbon sequestration due to reforestation following pandemics of plague and other diseases, when the human population was decimated in various parts of the world.

CO_2 emission data of the 20th century may confirm that extensive forest regrowth could act as a significant carbon sink. Changes in CO_2 emission were attributed to the reforestation of previously logged mid- and high-latitude terrains (Houghton and Skole, 1990; Dixon et al., 1994; Melillo et al., 1998). Model simulations suggest that a feasible reforestation and afforestation over the next fifty years would result in a decrease of atmospheric CO_2 mixing ratios by 15-30 ppmv (House et al., 2002). Because of the coupling between atmospheric CO_2 and global temperature, Ruddiman's (2003) theory implies that pandemic-driven changes in the terrestrial carbon sink could have played an important role in climate variance of the last millennium. The theory is opposite to the conventional concept that periods of climate deterioration provided appropriate preconditions for pandemic outbreaks (Lamb, 1977).

In order to test whether or not forest regrowth on deserted farmland could sequester sufficient carbon to account for atmospheric CO_2 decline, it is essential to obtain information on the nature, timing and magnitude of land cover changes triggered by massive depopulation events. The largest plague outbreak in European history, the 'Black Death', swept through Europe between AD 1347 and 1350 (e.g. Cartwright, 1972; Taylor, 1983; Bray, 1996; Fagan, 2000; Vasold, 2003a,b). Most historians agree that in various parts of Europe, the Black Death killed 30-45% of the population. There is historical evidence of widespread abandonment of farms and rural villages for decades. Also pollen records reflect changes in the level of agricultural activities during the 14th century. An overall decrease in the frequency of pollen of cultivated plants, notably cereals, has long since been apparent (e.g. Overbeck and Griez, 1954; Philippi, 1965). Traditionally, this decrease has been related to a prolonged agricultural crisis between AD 1300 and 1450 (e.g. Slicher van Bath, 1960), of which the Black Death was only one of the contributing causal factors. At present, however, the reality of persistent agricultural regression in the first half of the 14th century is questioned (e.g. Janssen, 1997; Wiethold, 1998).

It should be noted that the possibilities of accurate correlation of 14th-century palynological land cover changes with well-dated historical events are still limited. This is mainly due to extensive drainage of swamps and cultivation of wetlands resulting in large-scale disappearance or disturbance of peat or lake deposits that could yield AMS ^{14}C-dated pollen records with high temporal resolution for the past millennium. To detect direct effects of the Black Death in pollen diagrams covering the 14th century, a resolution of 10-20 years would be required; to date, such a resolution has never been realized.

In the southeastern part of The Netherlands, fluvio-lacustrine sediments, such as channel deposits of oxbow lakes, show intervals with high sedimentation rates and may therefore be suitable for high-resolution palynological studies. In the vicinity of Sint Odiliënberg (Province of Limburg) we successfully cored an organic-rich infill of an oxbow lake of the river Roer. AMS ^{14}C dating of buried leaf remains indicates that the cores include a continuous sedimentary record for the period between AD 1000 and 1500. In order to estimate the potential of deserted medieval farmland for carbon sequestration, we present a high-resolution palynological analysis of this core section. In combination with ^{14}C wiggle-match dating, palynological data provide insight in the nature and precise timing of effects of the Black Death and its aftermath on regional vegetation and land use.

Study area

The studied site (Fig. 4.1) is an oxbow lake of the river Roer, located in the vicinity of the village of Sint Odiliënberg (Province of Limburg, southeastern Netherlands, 51.08°N 6.00°E). The site is situated within the flooding regime of the Roer; it is repeatedly flooded especially during winter months. This part of the Netherlands belongs to the cover sand area north of the loess district; floodplains are covered by loam, sand and gravel deposits formed by the meandering rivers, while clayey gyttja and peat deposits fill in the oxbow lakes (Berendse, 1997).

The coring site is located close to the church-hill of Sint Odiliënberg, which has a long history of human occupation. Parts of a Roman temple from the 4th or 5th century are still incorporated in the present-day church building (Willemsen, 1889; Coenen, 1922). A monastery was founded in AD 700; this was given to the Chapter of Utrecht in AD 858 as a refuge from Norse invaders, who eventually reached the area in AD 881. Local sources document a civil war that waged in the area around AD 1360 resulting in the looting and burning down of several buildings in Sint Odiliënberg (Coenen, 1922; Timmermans, 1955); in AD 1361 the Chapter of Utrecht left the church-hill. In AD 1480 a new monastery was founded (Willemsen, 1889). South of the site is the Hoosden estate. This estate is first mentioned in historical archives around AD 1537, but its foundation may have been earlier. The continual human settlement during the studied

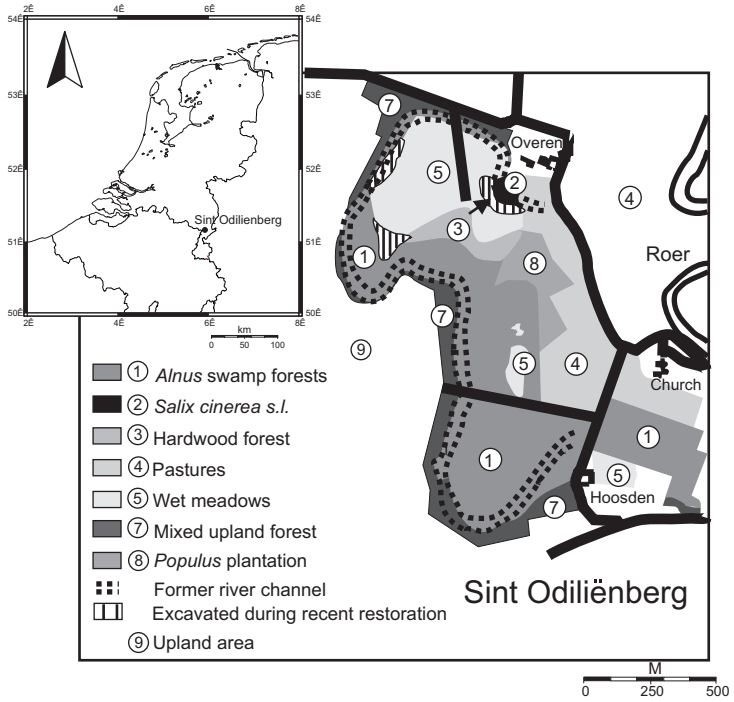

Figure 4.1*:* Location of the studied site and local vegetation.

time interval suggests a high level of human impact on the vegetation composition, which is likely to be reflected in regional and local pollen assemblages.

Natural vegetation

Throughout the past millennium, without impact of humans, the potential natural vegetation of the area would have consisted of deciduous forests. Mixed *Quercus-Fagus* forests with *Carpinus*, *Tilia* and *Corylus* would dominate the uplands. On the driest, nutrient-poorest, sandy soils, *Betula* would play an important role in mixed *Quercus-Betula* forests. Those parts of the floodplains of the meandering Meuse and Roer rivers that are flooded yearly and have a year-round high groundwater table, would be covered with *Alnus-Salix-Populus* woodland (softwood gallery forest). On higher, only briefly inundated parts of the floodplains, ALNO-PADION communities would develop, in which *Alnus*, *Ulmus*, *Quercus* and *Fraxinus* were the potential dominant tree species (hardwood floodplain forests). In the abandoned channels, *Alnus* swamp forest (ALNION community), would replace water-plant and reed communities (after Scaminée et al., 1995, 1996, 1998, 1999; Stortelder et al, 1998).

Present-day vegetation

Present-day vegetation on and around the site consists of *Alnus* swamp forests (Fig. 4.1). The wettest parts of the former oxbow lake (the coring site) are covered by *Salix cinerea s.l.* Pastures and wet meadows occupy the majority of the flood plains. On the flood plain in the vicinity of the coring site, remnants of hardwood forests (dominated by *Quercus*, *Fraxinus* and *Alnus*) and a small *Populus* plantation are present. On the steep slopes at the west bank of the meander, *Quercus* (*Q. rubra, Q. robur, Q. petraea*), *Fagus*, *Carpinus*, *Corylus* and *Betula* are the major constituents of the mixed upland forest. The upland area consists of scattered *Pinus sylvestris* and *Picea abies* plantations and arable fields, replacing larger parts of the former heathland (after Hommel and Hermans, 1994; Hermans and Peters, 1999).

Material and Methods

A sediment core was taken in a former river channel (Fig. 4.1), which is completely filled with organic-rich clayey gyttja deposits and covered at the top by a peat layer. From this locality four meters of partly laminated organic-rich sediments were recovered using a Livingstone piston corer. Sediments contain abundant macrofossil remains of leaves of *Quercus robur*, *Quercus petraea* and *Salix cinerea s.l.* The core was cut into 0.5 cm slices, while a correction for the core compression was applied to calculate the actual depth for each sample.

Total organic matter (LOI) measurements of the core section followed a modification of the procedure described by Dean (1974). A fixed volume of wet material was continuously taken from each core slice (0.5 cm). This volume was put in a pre-weighed ceramic crucible and dried in an oven at 110 °C for one hour, which gives the dry weight of the sample. The dried samples were then put in a muffle furnace for one hour at 550 °C in order to remove all organic carbon. The percentage of weight loss between the dried and the ignited sample therefore represents the percentage of organic carbon that a sample contains.

Eleven samples were used for AMS ^{14}C dating at the AMS facility of the R.J. van de Graaff Laboratory (Utrecht University). All samples (Table 1) consisted of thoroughly cleaned plant macrofossil remains. Conversion of the ^{14}C dates into calendar ages AD with a 1σ-probability has been performed with the calibration programme CALIB 4.4 (Stuiver et al., 1998; Fig. 5.2). In order to lower uncertainty levels, the ^{14}C dates were wiggle-matched to the INTCAL98 ^{14}C calibration curve (Stuiver et al., 1998).

Pollen and spore assemblages were recovered from 0.5 cm samples, following standard palynological peat-processing techniques now in use at the Laboratory of Palaeobotany and Palynology (Utrecht University). Processing included carbonate and

Depth	Composition	^{14}C Age (BP±1sigma)	UTC nr
76.25	*Salix* twigs	351±40	11730
94.54	*Salix* and *Quercus* leaves	355±45	12058
111.25	*Salix* and *Quercus* leaves	369±41	11731
141.25	*Salix* and *Quercus* leaves	454±37	11732
174.84	*Salix* and *Quercus* leaves	713±32	12111
197.25	*Salix* and *Quercus* leaves	544±47	11736
210.79	*Salix* and *Quercus* leaves	783±35	12060
230.13	*Salix* and *Quercus* leaves	861±30	12059
276.4	*Salix* and *Quercus* leaves	1003±39	11733
315.8	*Salix* and *Quercus* leaves	961±36	11734
368.85	*Salix* and *Quercus* leaves	368±85	11735

Table 4.1: Radiocarbon AMS ^{14}C dating results given in years BP (1950) with a 1 sigma confidence interval

silicate removal with HCl and HF, sieving over 7 µm and 120 µm sieving cloth to remove fine and coarse fractions respectively, boiling in KOH to remove organic fractions, and acetolysis for removal of carbohydrates and coloring the pollen. The residue was mounted on microscopic slides using silicon oil. To enable calculation of pollen concentrations, tablets with a known amount of *Lycopodium* spores were added prior to processing.

Results

Lithology and Chronology

LOI values of successive core samples fluctuate between 5% and 80% (Fig. 4.2A). Grey bands in the lithological column mark intervals wherein LOI remains low and relatively stable. The top of the studied core section is characterized by very high LOI values, which correspond to the presence of abundant wood remains. The succeeding decrease at a depth of 75 cm is accompanied by a distinctive sandy interval marking a hiatus in the sedimentary record.

Results of the AMS ^{14}C measurements are presented in Table 5.1 and Figure 5.2B,C. The calibration with CALIB 4.4 provides an age-depth relationship with uncertainty levels of 100-200 yrs. In order to lower these uncertainties, the ^{14}C dates were wiggle-matched to the INTCAL98 ^{14}C calibration curve (Stuiver et al., 1998). Non wiggle-matched dates indicate that sedimentation rates are not constant throughout the core. Therefore the wiggle-match was performed with three different sub-sets, of which each sedimentation rate was assumed to be linear. Results of wiggle-matching are shown in Figure 4.2B. The lower part (368-276 cm) and the upper part (111-76 cm) of the core section show significant higher sedimentation rates (1.17 and 1.04 cm/yr, respec-

tively), compared to the middle part (276-111 cm; 0.29 cm/yr). The wiggle-matched dates provide an age-depth model for the period of AD 1000-1500, which consists of three linear components (Fig. 4.2C).

Separated by a hiatus, the clays and peat deposits of the top 75 cm of the core section were formed after AD 1800 (unpublished palynological and agricultural data).

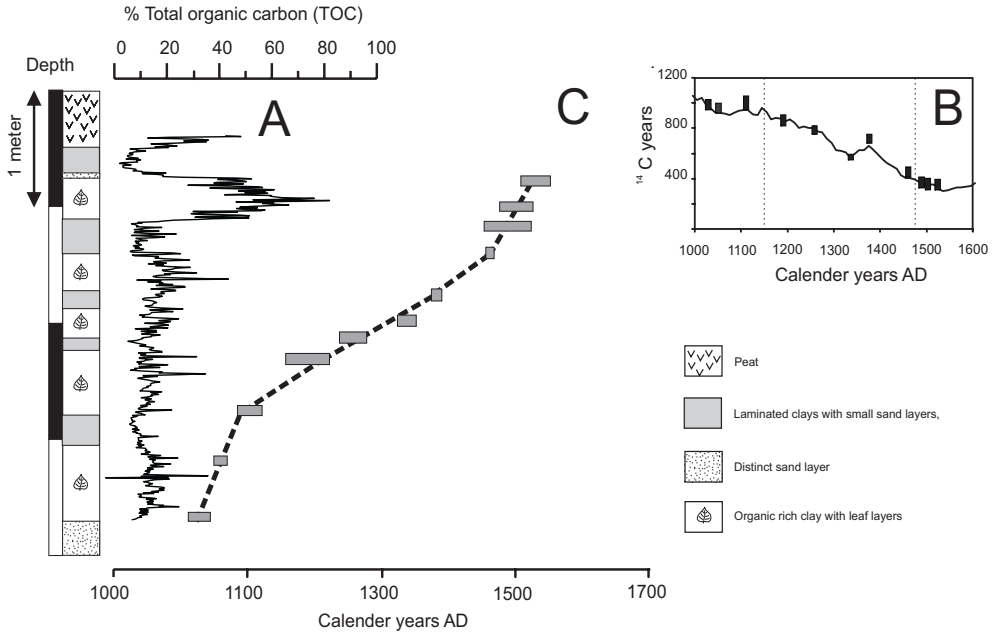

Figure 4.2: **A**: Loss on ignition (LOI) estimates based on loss on ignition. **B**: Radiocarbon versus calender ages of eleven AMS ^{14}C measurements (1 sigma probability) divided in three sub-sets (dotted lines) and wiggle matched to the INTCAL 98 calibration curve of Stuiver et al. (1998). **C**: Age-depth model based on the wiggle matched ^{14}C measurements.

Pollen diagrams

Pollen percentage diagrams are presented in Figures 4.3 and 4.4. Based on the age-depth model of Figure 4.2, diagrams represent the regional and local vegetation development between AD 1000 and 1500. The total pollen assemblage consists of 148 different pollen types, of which 36 regional types and 36 local types selected types have been selected for representation in the diagrams. Concentration diagrams were calculated but not applied because of large-scale fluctuations, probably resulting from the presence of abundant wood debris in the palynological samples.

The pollen sum, the calculation base for both regional and local pollen curves, consists of pollen types from upland plants. In the regional pollen diagram (Fig. 4.3) these are represented by five ecological groups: pollen from (1) trees and shrubs, (2) cultivated plants, (3) ruderals, (4) grassland, and (5) heathland. The cumulative curves of these five pollen groups are displayed in at the left side of the individual regional pollen curves. The pollen record of *Pinus* is presented as an overlay curve.

Pollen of *Alnus* and *Salix* are excluded from the pollen sum because both taxa are locally growing at the coring site. Also oak pollen (*Quercus robur* group) is excluded. The sediments contain numerous macrofossil remains (leaves), and the finding of subfossil *Quercus robur* trunks, 9 m from the coring site, confirms the local presence of fully grown oak trees from AD 1330 to 1550 (Chapter 3). Also the dominance of oak pollen during several intervals, makes it clear that *Quercus* had to be treated as an (extra-)local constituent of the vegetation (*sensu* Janssen, 1973).

The group “cultivated plants” contains pollen of cereals (Cerealia indet., *Secale cereale* and *Fagopyrum esculentum*). The group “ruderals” includes pollen types of arable weeds and plants from other ruderal plant communities. The “grassland” group comprises pollen types of dryer meadows and pastures. Since the *Anthemis* pollen type is produced by plants common in ruderal communities (*Anthemis* spp., *Matricaria* spp., *Tanacetum vulgare*), as well as by grassland plants (*Achillea millefolium*, *Leucanthemum vulgare*), this pollen represents both groups.

Poaceae pollen is excluded from the pollen sum, since *Phragmites* (reed) is present in both the potential and the present vegetation of the coring site. The group “heathland” represents pollen (and spores) of heather communities (*Calluna vulgaris*) and of plants growing on acid, nutrient-poor soils such as *Juniperus* and *Pteridium aquilinum*. Since no discrimination of *Rumex acetosella* (a species indicative for acid sandy soils) and *R. acetosa* (a meadow species) has been attempted, the recognized pollen type *Rumex acetosa*/*acetosella* is regarded to represent both grassland and heathland.

The local pollen diagram (Fig. 4.4) comprises four ecological groups: (1) pollen of

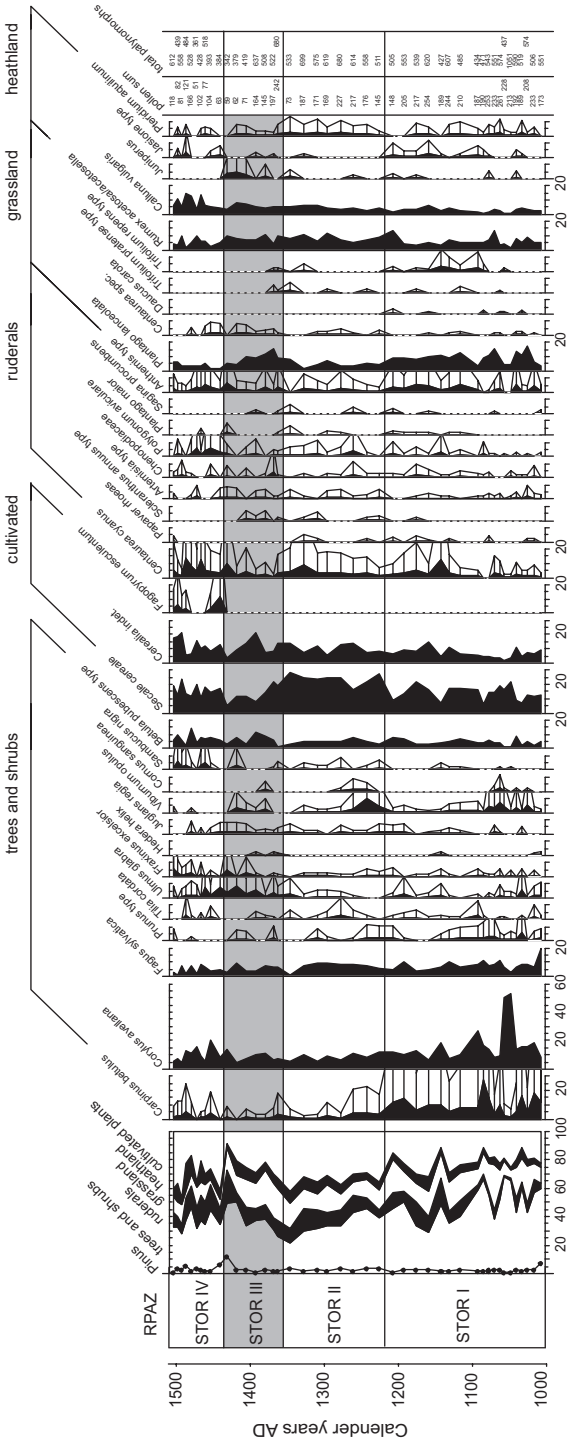

Figure 4.3:
Regional pollen percentage diagram

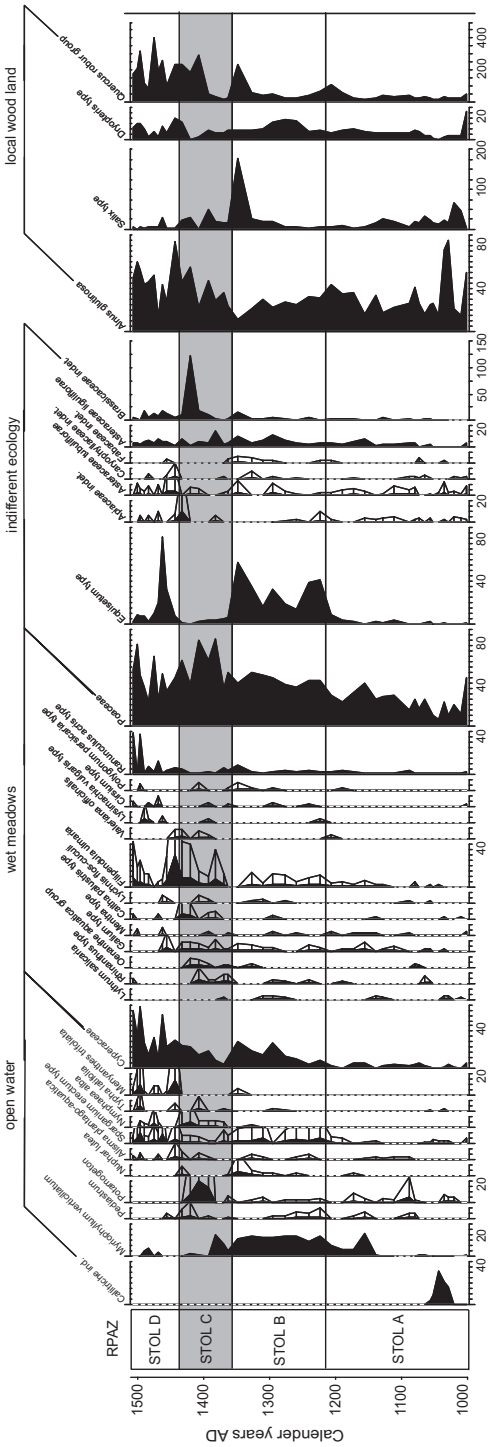

Figure 4.4:
Local pollen percentage diagram

plants from open water, (2) pollen from wet meadows (communities influenced of groundwater), (3) pollen (and spores) of taxa with no distinct ecological preference, such as Poaceae, Asteraceae and *Equisetum*, and pollen of local tree species (*Alnus glutinosa*, *Salix* type, *Quercus robur* group).

Pollen assemblage zones

Distinct changes in the composition of both regional and local pollen assemblages allow the recognition of four regional pollen assemblage zones (STOR I-IV) and four local pollen assemblage zones (STOL A-D):

STOR I – In this zone, pollen of *Carpinus betulus, Corylus avellana* and *Fagus sylvatica* dominates the arboreal pollen (total AP ca. 50%). In addition, pollen from grassland elements and cereals (*Cerealia* indet., *Secale cereale*) plays an important role. The upper zonal boundary (ca. AD 1220) is marked by a distinctive decline of the *Carpinus* curve and by increasing values for cereal pollen, particularly *Secale cereale*.

STOR II - This zone is characterized by a steady increase of non-arboreal pollen (NAP). *Secale cereale* reaches maximum values of 25% towards the top of the zone. Decreasing values for *Secale cereale*, *Centaurea cyanus* and spores of *Pteridium aquilinum* mark the upper boundary the zone (ca. AD 1350).

STOR III - This zone displays a continuing decrease of total NAP pollen. Notably the *Secale cereale* curve shows a distinctive decline, reaching minimum values of 5% at the top of the zone. Values of *Ulmus glabra* type, *Fraxinus excelsior* and *Juniperus* cause a concomitant AP increase. A distinct *Pinus* peak occurs at the top of the zone. Grassland pollen types show high values of *Plantago lanceolata* at the base of the zone. The zonal boundary (ca. AD 1430) is defined by renewed increase of *Secale cereale* and the first occurrence of pollen of *Fagopyrum esculentum*.

STOR IV - This zone is characterized by high NAP values, particularly cereals, and by the presence of *Fagopyrum* pollen. The *Pinus* curve drops back to values <5%, *Juniperus* pollen is absent.

STOL A - The local assemblage is dominated by pollen of *Alnus glutinosa*, Poaceae and, especially in the basal part of the zone, by *Salix* type pollen. The open water plants are represented by a brief increase of *Callitriche*, by *Potamogeton* and, in the upper part of the zone, by pollen of *Myriophyllum verticillatum*. The upper zonal boundary (ca. AD 1210) is placed at the rise of the curves for Cyperaceae, Poaceae and *Filipendula*, a sharp increase of *Equisetum* type spores, and the decline of *Alnus glutinosa* and *Quercus*.

STOL B - This zone is characterized by high values of *Myriophyllum verticillatum*, *Sparganium erectum* type, *Cyperaceae* and *Equisetum* type spores. The curves for *Quercus* and *Salix* show peak values at the top of the zone (>200%), where the *Alnus* curve reaches minimum values (<20%). The upper boundary of the zone (ca. AD 1350) is marked by the drop of *Equisetum*, *Salix* and *Quercus*.

STOL C - In this zone maximum values for *Poaceae*; *Filipendula*, and *Cyperaceae* are reached, while *Alnus* values increase. Relatively high values for *Nymphaea*, *Potamogeton* and *Brassicaceae* indet. are also characteristic for this zone. The upper boundary (ca. AD 1430) is placed at the rise of *Equisetum, Filipendula* and *Menyanthes.*

STOL D - This zone is dominated by pollen of *Alnus*, *Quercus* and *Cyperaceae. Equisetum* type spores rise to maximum values in the lower part of the zone.

Vegetation development and land use AD 1000-1500

The main feature of the analyzed pollen record is a long-term reduction of the arboreal component reflecting regional deforestation in the first half of the last millennium, parallel to the population increase during this period (Slicher van Bath, 1960). The same feature is recorded in pollen diagrams from the adjacent loess area in Germany and southern Limburg (Phase G, H of Bunnik, 1999). For the whole period, the regional diagram (Fig.4.3.) reflects a landscape that is completely altered by intensive agricultural activities. Woodland is exceedingly transformed to arable fields, grassland (pastures and meadows) and heathland.

Cereals, notably *Secale cereale,* were the most prominent crop, even on nutrient-poor soils. The relatively high values for pollen of the accompanying weed *Centaurea cyanus* indicate that cereals were commonly grown as winter cereals. In the agricultural system, heathland was the main production area of sheep and cattle dung. High values of *Calluna vulgaris* underline the increasing importance of heathland in the 15th century. This agrees well with historical records from southern Limburg, where heathland reached its greatest expansion at the end of the medieval period (Hillegers, 1980). The introduction of the low-demanding *Fagopyrum esculentum* (buckwheat) around AD 1450 (Zone STOR IV) can be regarded as an adaptation to the increasing nutrient deficiency of the sandy soils after centuries of agricultural use. Historical records show that buckwheat cultivation in The Netherlands had started already at the end of the 14th century; the low-nutrient demanding crop became increasingly important in the course of the following centuries (Leenders, 1987).

The local vegetation development reflects an infilling and terrestrialization process (Fig. 4.4). In the basal part of Zone STOL A, early successional open-water vegetation of the oxbow is represented by a short-lived peak of *Callitriche*, probably *C. platycarpa*, a

species that is often the only water plant in flowing waters. In the succeeding slow-flowing and stagnant phases, this element was rapidly outcompeted by other open-water plants, such as *Myriophyllum verticillatum*, *Potamogeton*, *Nuphar lutea* and *Nymphaea alba*. Also the curve for *Equisetum* spores may indicate terrestrialization. The species involved is most likely *E. fluviatile*, a pioneer plant in calm shallow waters. In the lateral and succeeding reed vegetation, Cyperaceae and probably also Poaceae (*Phragmites*) played the dominant role, while *Sparganium erectum* and *Typha latifolia* were common elements.

Agricultural crises and associated periods of reforestation

Apart from some earlier short-lived fluctuations, the regional pollen diagram shows a distinctive low in cereal pollen in upper part of Zone STOR I. The anomaly covers a few decades (ca. AD 1180-1215), and may reflect an agricultural crisis caused by consecutive crop failures. This crisis had considerable impact on the landscape. Decline of cereal pollen is accompanied by low values of *Calluna vulgaris* and an increase in tree pollen *(Carpinus*, *Betula*, *Ulmus*, *Quercus*).

In The Netherlands and large parts of northwestern Europe the last quarter of the 12th century and the 13th century AD is characterized by a shift from a relatively stable climate, the so-called Medieval Climatic Optimum (or Medieval Warm Period**)**, to more extreme climate oscillations (Lamb, 1977; Buisman, 1995; Fagan, 2000; Chapter 2). The shift may be regarded as the transition to the Little Ice Age, a lengthy unstable period that lasted until the 19th century AD when the current period of global warming began. Although in northwestern Europe this period started with warm, extremely wet winter conditions that lasted until AD 1430 (Buisman, 1995; Fagan, 2000), the main long-term feature of the Little Ice Age climate oscillations was a declining temperature trend combined with low average-temperature anomalies (Lamb, 1977).

By the end of the 12th century AD, average weather conditions were no longer optimal for agriculture. In various parts of western Europe, historical sources record a famine in AD 1196 caused by several years of crop failure due to wet conditions during harvest season (Buisman, 1995). Also in Cologne, the largest medieval city in the vicinity of the studied area, there was a great shortage of cereals and other food supplies. Reduced tilling resulted in woodland regeneration on previously farmed land. Evidenced by a strong increase of *Secale cereale* pollen, full recovery of agriculture took place after AD 1215 (base Zone STOR II).

Following the period with maximum values for non-arboreal pollen at the top of Zone STOR II, a period of much more prolonged and more pronounced agricultural regression can be identified in the regional pollen record of Zone STOR III (ca. AD 1360-1440). At first, the curves for *Secale cereale* and *Centaurea cyanus* drop sharply. At

the same time, *Plantago lanceolata* reaches high values. Subsequent features are increasing percentages of *Betula* pollen, followed by increasing values for *Ulmus*, *Fraxinus* and *Juniperus,* while the curve for *Plantago lanceolata* drops concomitantly. At the end of the zone, *Pinus* and *Juniperus* reach maximum values.

The pollen record of Zone STOR III can be interpreted as a strong reduction of cereal production. The sharp increase in *Plantago lanceolata*, accompanied by increasing local values for *Poaceae* in Zone STOL C may point to a conversion of cereal fields into grassland, but could also be interpreted as an initial step in a natural vegetation succession on fallow land (Behre, 1992). Subsequent decline of *P. lanceolata*, increasing values of *Ulmus* and *Fraxinus*, together with increasing local values for *Alnus* and *Quercus* in Zone STOL C, indicate growth and expansion of hardwood floodplain forests (ALNO-PADION communities) on rich loamy soils, at the expense of meadows and pastures. High percentages of *Pinus* and *Juniper* pollen in the uppermost part of Zone STOR III are indicative for a reforestation succession on poor sandy soils.

Progressively increasing percentages of *Filipendula ulmaria* in Zone STOL C suggest the reduction of mowing and grazing pressure on wet floodplain meadows in the vicinity of the coring site. Because it is flowering in mid-summer, this grassland species is strongly suppressed by mowing and grazing. When these agricultural activities are discontinued, wet meadows may convert into tall forb communities where *F. ulmaria* finds optimal growing conditions. Cessation of mowing and grazing could well be ascribed to the regional agricultural crisis. An alternative, natural cause for the abandonment of wet meadows could be the excessive 14th-century AD winter precipitation in The Netherlands (Buisman, 1995), resulting in meadows that were too wet for cattle to graze on.

Decreasing trends in the frequency of cereal pollen during the 14th and 15th centuries have long since been recorded in pollen diagrams from various parts of western Europe (Overbeck and Griez, 1954; Philippi, 1965; Riezebos and Slotboom, 1978; Wiethold, 1998; Bunnik, 1999). This long-term decrease has been linked to a prolonged period of agricultural crisis that had started already at the beginning of the 14th century (Sligher van Bath, 1960). Agricultural decline is also evident from historical sources that record large-scale desertion of farms and rural villages in Europe (‘lost villages’ in England; ‘Wüstungen’ in Germany) (Bieleman, 1992). A prolonged late medieval crisis is primarily considered to be a response to the effects of unstable climatic conditions in western Europe. Frequent failure of harvest is held responsible for a gradual weakening of both population and economy. Malnutrition could then have paved the way for epidemic outbreaks of plague and other diseases, culminating in the spread of the Black Death, which decimated the population of large parts of Europe (Slicher van Bath, 1960; Cartwright, 1972; Lamb, 1977; Fagan, 2000). More recent historical research questions the presence of a significant agricultural crisis *before* the spread of the Black

Death (e.g. Janssen, 1997; Wiethold, 1998). Despite occasional famine, in the first half of the 14th century the European population continued to grow, with a concomitant overall increase of agricultural activity.

Also in the study area, there is no evidence of agricultural crisis before AD 1350. With maximum values for *Secale cereale* in the upper part of Zone STOR II, the pollen record demonstrates increasing rather than decreasing agricultural activity. Considering the error margins of the age-depth model, it is obvious that the onset of agricultural regression at the base of Zone STOR III corresponds to regional plague outbreak. The Black Death entered the border region of the southeastern Netherlands and Germany in AD 1349 (Creutz, 1933; Schmitz-Cliever, 1954). In the big cities of the region, like Cologne and Aachen, plague may have killed about one third of the populace in AD 1349-1350.

Similar to the situation in other parts of Europe (e.g. Cartwright, 1972), the impact of the Black Death on agriculture became progressively apparent in the years following the outbreak. Due to high mortality rates among rural peasants, labour had become scarce. Landlords, reluctant to pay higher wages, began to raise more cattle and sheep. Part of the farmland, particularly on nutrient-poor soils, was simply abandoned so that it could turn back into forest. Social unrest and civil war, locally documented for Sint Odiliënberg (Coenen, 1922; Timmermans, 1955), may have reinforced this process of agricultural decline. The agricultural regression lasted for about 80 years. Rapid increase of cereal pollen and the introduction of buckwheat at the transition of Zones STOR III and STOR IV, confirms recovery of agriculture after AD 1440. This date is consistent with the ending of late medieval agricultural crisis recognized elsewhere in Europe (Slicher van Bath, 1960).

A comparable, plague-induced agricultural regression has been identified in detailed pollen records from Schleswig-Holstein, northern Germany (Wiethold, 1998). Unfortunately, however, these records are not constrained by an accurate ^{14}C time-framework. The Black Death is used as the very datum for determining the onset of agricultural decline in these records.

Carbon sequestration on abandoned farmland

The recognition of regional, plague-induced regression of agriculture, as reflected in the pollen spectra of Zone STOR III, is in agreement with the concept of Ruddiman (2003) that abandoned farmland could act as a significant terrestrial carbon sink. Towards the top of the zone, the contribution of cereal pollen in the assemblage is roughly halved (from ca. 40% to ca. 20%).

Forests can reclaim farmland within 50 years. This study only identifies a regional reforestation signal and therefore provides no conclusive information about the exact

size of a supposed Eurasian carbon sink. According to calculations by Ruddiman (2003), 14-27 Gt of terrestrial carbon sequestration would be required to explain CO_2 anomalies in the range of 4-10 ppmv recorded in Antarctic ice cores. At the time of the Black Death and its aftermath, reforestation at a level of 25% to 45% of the total arable area of Europe and Asia could account for this amount. Although quantitative trends in the composition of regional pollen spectra may be influenced by factors other than changes in the size of farmed land, the strongly reduced contribution of cereal pollen of Zone STOR III could well comply with such figures. It is questionable, however, whether the Black Death provided comparable preconditions for reforestation throughout Eurasia. Recent historical research suggests that the geographical spread of the plague in Europe was less extensive than previously thought (Vasold, 2003a,b). Moreover, there is no compelling evidence of widespread coeval plague outbreak in Asia.

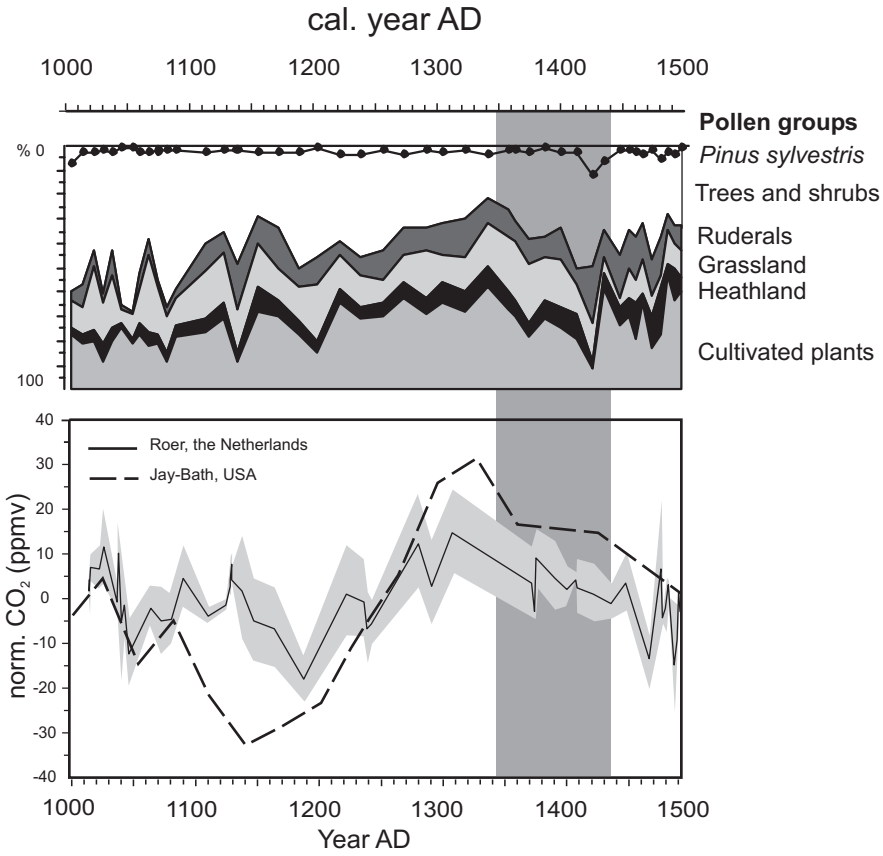

Figure 4.5: Regional vegetational development based on pollen analysis (this study) compared to stomatal frequency based atmospheric CO_2 reconstructions from *Quercus robur* leaves from the oxbow lake of the Roer, the Netherlands (Black line with grey uncertainty envelope; Chapters 2 and 5), and from *Tsuga heterophylla* conifer needles from Jay Bath, USA (Black interrupted line, Kouwenberg, 2000, Chapter 5).

Ruddiman's (2003) proposal that the Black Death and its aftermath could have been responsible for a CO_2 drop of 4-10 ppmv, is based mainly on the presumed CO_2 anomaly measured in the ice cores of Taylor Dome between AD 1300 and 1400 (Indermühle et al., 1999). However, it should be noted that data from different Antarctic coring localities are not in agreement with respect to timing and magnitude of CO_2 changes of the past millennium. The ice-core record from Law Dome suggests that a prominent negative anomaly occurred much later, between AD 1600 and 1800 (Etheridge et al., 1996).

An alternative proxy for detecting and quantifying short-term atmospheric CO_2 fluctuations is provided by stomatal frequency analysis of leaves buried in peat and lake deposits. A wide variety of tree species is capable of sustained adjustment of the number of leaf stomata to changing ambient CO_2 levels (Woodward, 1987; Kürschner et al, 1996; Wagner et al., 1996, Royer, 2001). Calibrated against modern training sets, high-resolution stomatal frequency records from Holocene sections all over the Northern Hemisphere, consistently demonstrate that century-scale CO_2 fluctuations have contributed to a much more dynamic CO_2 evolution than suggested by ice-core measurements (Wagner et al., 1999; Rundgren and Beerling, 1999; McElwain et al., 2002; Wagner et al., 2002; Rundgren and Björck, 2003; Kouwenberg, 2004; Chapter 6).

The rich buried leaf record (*Quercus robur*, *Q. petraea, Salix cinerea s.l.*) from the oxbow lake of the Roer is currently investigated for stomatal frequency signals that could provide insight in the CO_2 evolution during the transition of the Medieval Climatic Optimum to the Little Ice Age in western Europe (Chapter 2). Results for *Quercus robur* are summarized in Figure 4.5, in combination with coeval data obtained from needles of the conifer *Tsuga heterophylla* buried in sediments of a shallow pond on the flank of Mount Rainier, Washington, USA (Kouwenberg, 2004). Both datasets provide evidence for CO_2 fluctuations between AD 1000 and 1500 on time-scales varying from decades to centuries. The *T. heterophylla* record suggests minimum CO_2 in the middle of the 12th century, and maximum CO_2 in the first half of the 14th century AD (Kouwenberg, 2004). This maximum is followed by a steady CO_2 decline during the late 14th and 15th century. Probably because of a more accurate time framework, the reconstructed CO_2 trend based on leaves of *Quercus robur* indicates minimum values around AD 1200. Maxima in the first half of the 14th century AD, as well as the following decrease, are in good agreement with the *T. heterophylla* record.

Since there is no evidence of a pronounced CO_2 minimum between AD 1300 and 1400, stomatal frequency data corroborate the general CO_2 trend registered in the ice cores from Law Dome. This may imply that both methods of atmospheric CO_2 reconstruction do not substantiate Ruddiman's (2003) concept of a specific role of the Black Death. There is a remarkable correspondence between stomata-based CO_2 trends of the 13th-

15th centuries AD and coeval trends in regional forest density as reflected in the pollen record (Fig. 4.5). However, in the aftermath of the Black Death, declining CO_2 trends of the 14th and 15th centuries are not punctuated by effects of maximum reforestation between AD 1400 and 1440. Despite some decadal oscillations, CO_2 decrease of the 15th century is not reversed at the time when the agricultural crisis ended around AD 1440.

Conclusions

The present palynological study allows, for the first time, a relatively clear reconstruction of the nature and precise timing of regional effects of the mid-14th century Black Death on late medieval agriculture. The pollen record reflects significant agricultural regression at the time of the Black Death and its aftermath (AD 1350-1440). Results do not corroborate the concept of a more prolonged, great medieval agricultural crisis (AD 1300-1450) that has been deduced from documentary sources (Slicher van Bath, 1960).

The palynological data confirm that plague-induced reforestation of abandoned farmland could promote significant carbon sequestration. It remains questionable, however, whether this regional picture of forest regrowth can be scaled up geographically to account for negative CO_2 anomalies in the range of 4-10 ppmv recorded in Antarctic ice cores (Ruddiman, 2003).

The precise timing of pre-industrial CO_2 anomalies needs reconsideration. Atmospheric CO_2 reconstructions based on stomatal frequency analysis of buried leaves do not support the presence of a pronounced CO_2 minimum between AD 1350 and 1450 that correlates with the Black Death and its aftermath (Ruddiman, 2003). However, considering the apparent correspondence between forest density changes and CO_2 trends of the 13th-15th centuries, plague-induced carbon sequestration in Europe could have contributed to a longer-term process of CO_2 decline that had already started before the spread of Black Death. As long as the volume of this, probably modest, contribution cannot be specified, it would be premature to hold the Black Death directly responsible for a cooler climate.

Chapter 5

Reproducibility of Holocene atmospheric CO_2 records based on stomatal frequency analysis

The majority of the stomatal frequency based CO_2 estimates for the Holocene do not support the widely accepted concept of comparably stable CO_2 mixing ratios throughout the past 11,500 years. To address the critique that these stomatal frequency variations result from local environmental change or methodological insufficiencies, multiple stomatal frequency records were compared for three climatic key periods during the Holocene, namely the Preboreal oscillation, the 8.2 kyr cooling event and the Little Ice Age. The highly comparable fluctuations in the paleo-atmospheric CO_2 records, which were obtained from different continents and plant species (deciduous angiosperms as well as conifers) using varying calibration approaches, provide strong evidence for the integrity of leaf-based CO_2 quantification.

Introduction

A variety of land plants is capable of sustained adjustment of the number of leaf stomata to changing atmospheric CO_2 mixing ratios. Measured on fossil leaves and calibrated against modern training sets, stomatal frequency data are increasingly applied as a proxy for palaeo-atmospheric CO_2 reconstructions. The quality and quantity of fossil leaf remains preserved in lake and peat deposits of Holocene age allows the generation of stomatal frequency records from sites worldwide.

The majority of the stomatal frequency based CO_2 estimates for the Holocene do not support the widely accepted concept of comparably stable CO_2 mixing ratios throughout the past 11,500 years (Indermühle et al., 1999). The available high resolution CO_2 reconstructions based on plant fossils suggest that century-scale CO_2 fluctuations contributed to Holocene climate evolution (Wagner et al., 1999a; Rundgren and Beerling., 1999; McElwain et al., 2002; Wagner et al., 2002; Rundgren and Björck, 2003; Kouwenberg, 2004).

Within the ongoing discussion on the alternative concept of a dynamic CO_2 regime, the approach of translating observed shifts in stomatal frequencies in terms of atmospheric CO_2 changes has often been questioned. It has been suggested that these shifts are a consequence of environmental factors other than CO_2 or an artifact of improper assembling and calibration of the modern training sets (Birks et al., 1999; Indermühle et al., 1999b). These comments emphasise the necessity to examine the amplitude and duration of reconstructed CO_2 fluctuations by comparing stomatal frequency records based on taxonomically and ecologically contrasting plant species. The global nature of the CO_2 signal should be revealed by records originating from a wide geographical range.

In the present review, we discuss the reliability of stomatal frequency derived CO_2 records by comparing available data from three different time slices in the Holocene which are known to be phases of major climatic change on the Northern Hemisphere. The first in a series of century scale Holocene climate deteriorations evident in marine, terrestrial and ice core derived climate reconstructions is the so-called Preboreal oscillation, a short-lived cool pulse recorded at ~ 11.2 kyrs BP, soon after the end of the Younger Dryas (Björck et al., 1997; INTIMATE, 1998). The most prominent and best documented cooling in the Holocene is centred around 8.2 kyrs BP (Alley et al., 1997; Barber et al., 1999), where fresh water pulses from the melt-down of the Laurentian ice-sheet are thought to have reduced the thermo-haline circulation in the North Atlantic for approximately 300 years. Well known from historical records and direct instrumental measurements is the pre-industrial cooling trend of the last millennium, commonly addressed as the Little Ice Age. Interrupted by periods of relative warmth, cool pulses occurred at different times in different parts of the world. In many Northern Hemisphere

regions, the Little Ice Age culminated in a series of cool pulses between the 14th and early 19th century AD.

For all of these three events multiple stomatal frequency records are available. By directly comparing the results from the contrasting studies, we illustrate that the harmonious variation in stomatal frequency responses cannot be a result of local environmental changes or methodological insufficiencies, but do have their origin in a common, at least hemispherically acting forcing factor, namely atmospheric CO_2 dynamics throughout the Holocene.

Modern calibration data sets

The most critical issue in calculating atmospheric CO_2 mixing ratios from fossil stomatal frequency data is the accuracy of the modern calibrations data sets. These training sets enable quantification of the response rates of individual species to atmospheric CO_2 changes and, therefore, serve as reference data for CO_2 estimates from fossil leaves. An unique opportunity to study the leaf morphological adaptation of plants to changing ambient CO_2 is provided by the well documented continuous CO_2 increase from pre-industrial values of approximately 280 ppmv to 375 ppmv present day level. Analysis of herbarium specimens of known age allows to tie up known historical CO_2 and corresponding stomatal frequencies. Uncertainties in the herbarium data sets due to varying sample localities can be reduced by adding data from continuous, but often less well dated, leaf sequences accumulated in e.g. young peat deposits (Wagner et al., 1996).

Fossil and herbarium leaves grown during the industrial CO_2 rise, however, do not cover CO_2 levels below 280 ppmv, which hampers the statistical modelling of the stomatal response to lower CO_2 mixing ratios. To obtain data from the lower CO_2 range, the plants' response to CO_2 partial pressure (in Pa) rather than CO_2 mixing ratio (in ppmv) can be utilized (Woodward and Bazzaz, 1988). Because partial pressure decreases with elevation due to the reduced air pressure, inclusion of leaf material grown at higher altitudes allows extension of the historical training set to CO_2 levels below 28 Pa (equivalent to 280 ppmv at sea level). If the leaf material in the modern training set as well as the fossil assemblages originate from localities at the same elevation, expression of CO_2 levels in either partial pressure or mixing ratio will be of no consequence. However, if leaves from different altitudes are in included in the training set or fossil stomatal frequency data, CO_2 levels must be calculated as partial pressure for stomatal frequency calibration (Fig. 5.1 B). The estimated local barometric pressure at the site where the fossil material was derived from, can then be used to reconvert the reconstructed CO_2 partial pressure to mixing ratio, to enable quantitative comparison with other CO_2- reconstructions.

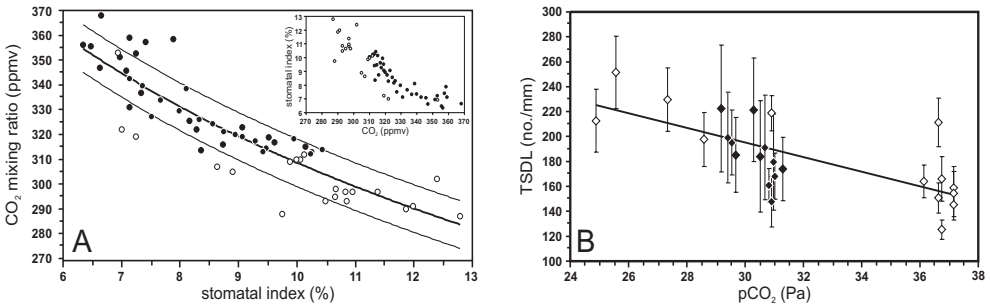

Figure 5.1: Modelled relation between atmospheric CO_2 concentration and stomatal frequency in training sets consisting of leaves from herbaria and subfossil deposits calibrated against historical CO_2 concentrations. CO_2 mixing ratios of 290–315 ppmv were derived from shallow Antarctic ice cores (http://cdiac.esd.ornl.gov/trends/co2/siple.htm; Neftel et al., 1985), mixing ratios of 315–368 ppmv are annual means from instrumental measurements at Mauna Loa (http://cdiac.esd.ornl.gov/ndps/ndp001.html).

A: Thick black line: Model for CO_2 estimates based on linear regression of log-transformed stomatal index (SI) data for Betula pendula/pubescens ($CO_2 = 10^{2.802 - [0.313 + \log(SI_f)]}$; $r^2 = 0.79$); thin lines indicate ± 1 RMSE (= 9.6 ppmv). Inset: historical response of SI to global atmospheric CO_2. Training set includes leaf remains from modern peats (black circles) and herbarium specimens (open circles).

B: Response of number of stomata per mm needle lenght (TSDL) of Tsuga heterophylla to a p CO_2 increase from 24 to 38 Pa. CO_2 partial pressure was calculated by multiplying the CO_2 mixing ratio by local barometric pressure PB (Pa), estimated according to Jones (1992): $P_B = 101.325/e^{[(z/29.3)/T]}$ where z is altitude above sea level and T air temperature in K (estimated from mean annual temperature at the closest weather station, corrected by a temperature lapse rate appropriate for the region in case of significant altitudinal difference between site and station). Black diamonds represent subfossil and modern needles from Jay Bath (Mount Rainier, WA), open diamonds modern and herbarium needles from other localities. Error bars indicate ± 1 SE. Solid line indicates best fit in classical regression analysis. TSDL: true stomatal density per mm needle length (TSDL = $-5.8581 \times$ p $CO_2 + 371.14$; $r^2 = 0.5124$; RMSE = 42.8 ppmv).

In this manner significant changes in stomatal frequency under changing atmospheric CO_2 have been demonstrated for many woody angiosperms, of which deciduous trees such as *Betula*, *Quercus* and *Ginkgo,* as well as common high latitude shrubs like *Salix* and *Dryas,* show the most pronounced responses. Conifers exhibiting a prominent decrease in stomatal frequency with increasing historical CO_2 include *Tsuga*, *Picea*, *Larix*, and *Metasequoia* (see Royer, 2001; Kouwenberg et al*.,* 2003). Although desirable, a general model for fossil CO_2 estimates embracing multiple genera can not be generated, due to the highly individual responses of the various genera (Kürschner et al*.*, 1997; Rundgren and Björck, 2003).

For broad-leaved plant species the ratio between stomata and the total amount of epidermal cells on the leaf surface (the stomatal index) has been proven to be the most sensitive parameter to quantify their response to CO_2 changes. By applying the cell ratio rather than the pure number of stomata, undesirable effects of lateral epidermal cell expansion due to contrasting light regimes, leaf age or temporary hydrological conditions are circumvented (Poole and Kürschner, 1999). Because of the specific stomatal patterning in the narrow-leaved conifers, the number of stomata per mm needle length rather than the stomatal index responds to atmospheric CO_2 levels. Although this parameter is density-based, leaf age and environmental conditions do not mask the adjustment to CO_2 levels (Kouwenberg et al*.*, 2003; Kouwenberg, 2004).

While the conifer species studied show a linear decrease in stomatal frequency under present day atmospheric CO_2, the majority of broad-leaved species currently used for CO_2 reconstructions indicate a decrease in CO_2 sensitivity at values above approximately 320 ppmv (Kürschner et al*.*, 1997). The response patterns on species or genus level determined in the modern training sets require the application of taxon-specific statistical treatments for the individual plant categories to guarantee the best fit of the models for palaeo- CO_2 estimations. Two contrasting examples of models for inferring palaeo-CO_2 based on modern training sets of broad-leaved trees and conifers, both incorporating herbarium material as well as sub-fossil leaves from peat sequences, are presented in Figure 5.1.

Analysis of modern *Betula pendula* and *Betula pubescens* leaves has demonstrated a distinct reduction of the stomatal index over the post-industrial CO_2 increase from 290 ppmv to 370 ppmv, with a levelling off in the CO_2 response at values higher than 350 ppmv (Fig. 5.1 A). The good correspondence of the stomatal index response revealed for the two closely related species allows treatment of *B. pendula* and *B. pubescens* as one single group in the model (Fig. 5.1 A, Wagner et al*.*, 2000). In order to accommodate the partial non-linearity of the data while maintaining the best fit, the model for CO_2 estimations from fossil material is based on a log transformation of both SI and CO_2 values in the training set (Fig. 5.1 A).

The stomatal frequency response of *Tsuga heterophylla* in contrast is best described using a linear rather than a non-linear model. The linearity of the response over the entire CO_2 regime from 25 to 37 Pa allows the fossil CO_2 estimation by using a classical linear regression, the most conservative statistical approach (Fig. 5.1 B).

All *Tsuga* and *Betula* data presented hereafter are calibrated according to the models above. As a consequence of the adjusted model for *Betula*, the CO_2 reconstructions based on this genus may differ slightly from initial publications (Wagner et al., 1999a; Wagner et al., 2002).

Palaeoatmospheric CO_2 reconstructions

Based on the well defined response rates of *Betula* and *Tsuga*, palaeoatmospheric CO_2 records have been established for three key periods of climate change during the Holocene (Wagner et al., 1999a; Wagner et al., 2002; Kouwenberg, *2004*). Additional CO_2 records from other species are available for the Preboreal oscillation (McElwain et al, 2002; Rundgren and Björck, 2003), the 8.2 kyrs cool pulse (Rundgren and Beerling, 1999), and the Little Ice Age (Chapter 2). The present study focusses on the comparability of independent stomatal frequency records in terms of trends in atmospheric CO_2 and the temporal synchroneity of the records. In order to emphasize the amplitude of reconstructed atmospheric CO_2 changes associated with the three Holocene cool pulses, all available records are given in normalized CO_2 mixing ratios (ppmv); whereas all ages are given in calibrated calendar years BP.

The Preboreal oscillation (Fig. 5.2 A, D)

The Preboreal stage of the Holocene is represented in three different stomatal frequency records. *B. pubescens* and *B. pendula* leaf remains were obtained from a peat section temporarily exposed at the Borchert archaeological excavation site in Denekamp, The Netherlands (52°23'N, 7°00'E; 30 m a.s.l., Fig. 5.2 A). The section spans the period from 11,620 cal BP to 10,920 cal BP, with a high-resolution age assessment based on wiggle matching of 18 ^{14}C datings over the 35 cm peat section (Van der Plicht et al., 2004). The stomatal index values from this record are calibrated according to the model in Fig. 5.1 A and provide evidence for a short-term CO_2 decrease between 11,250 cal BP and 11,080 cal BP with a CO_2 minimum at 11,120 cal BP (Fig. 5.2 D).

This distinct minimum is supported by stomatal frequency analysis of *Larix laricina* needles preserved in a lake in New Brunswick, Canada (Fig. 5.2 A, D, Splan Pond, 45°14'N, 67°06'W, 106 m a.s.l., age assessment based on two AMS ^{14}C datings for this interval; McElwain et al., 2002). The timing of the CO_2 decrease documented in both records, parallels the Preboreal oscillation sensu Björck et al. (1997) which is equivalent to the GH 11.2 temperature decline documented in Greenland ice cores (INTIMATE, 1998).

Further evidence for a CO_2 decrease during this time is provided by a stomatal frequency record based on *Salix herbacea*, *Salix polaris*, and *Betula nana* leaves from Lake Madtjärn in southwestern Sweden (58°35'N, 12°10'E; 135 m a.s.l.; Rundgren and Björck, 2003). The age assessment for this record is based on the age depth model for the entire Madtjärn profile, in which the early Preboreal is covered by six AMS ^{14}C datings. A slight temporal offset of 100 calendar years between this record and the two records above might be an artifact of the selected age-depth model for the earliest Holocene (see Rundgren and Björck, 2003 for original data).

Consistent in all records, the shifts in stomatal frequency indicate a change in the atmospheric CO_2 mixing ratio of 20 - 30 ppmv associated with the Preboreal oscillation.

The 8.2 kyrs BP cooling event (Fig. 5.2 B, E)

For the time slice of the 8.2 kyrs cool pulse, two stomatal frequency based CO_2 reconstructions are available (Fig. 5.2 E). The first record (Wagner et al., 2002) is based on the stomatal index values from European tree birch leaves derived from organic rich gyttja deposits from Lille Gribso, a small kettle hole lake North of Copenhagen, Denmark (55°58'N, 12°18'E; 45 m a.s.l., Fig. 5.2 B). Well preserved *B. pubescens* and *B. pendula* leaf remains occur continuously through an interval corresponding to the period between 8700 cal BP and 6800 cal BP. Chronological control is provided by a series of six AMS ^{14}C dates measured on single birch leaves (Wagner et al., 2002).

The second record is based on *S. herbacea* leaf material from 10 horizons accumulated in a small lake close to Abisko, Northern Sweden (Lake Njulla, 68°22'N, 18°42'E; 999 m a.s.l.; Rundgren and Beerling, 1999, Fig. 5.2 B). For the time interval of interest three ^{14}C datings are available. The two data sets consistently reveal a century-scale interval of 30 ppmv CO_2 mixing ratio changes with lowest CO_2 levels centred around 8.2 kyrs BP.

The last millennium (Little Ice Age) (Fig. 5.2 C, F)

For the period between 1000 and 1500 AD, covering part of the Little Ice Age, two independent stomatal frequency reconstructions are shown in Fig.5.2 F.

Tsuga heterophylla needle assemblages were obtained from a 91 cm sediment core drilled in Jay Bath, a shallow pond on the southern flank of Mount Rainier (Washington, USA; 46°46' N 121°46' W; Fig. 5.2 C). The age assessment for this site is established on five AMS ^{14}C datings and one tephra layer at 1481 AD (Kouwenberg, 2004). The *T. heterophylla* stomatal frequency results in this study are calibrated according to the

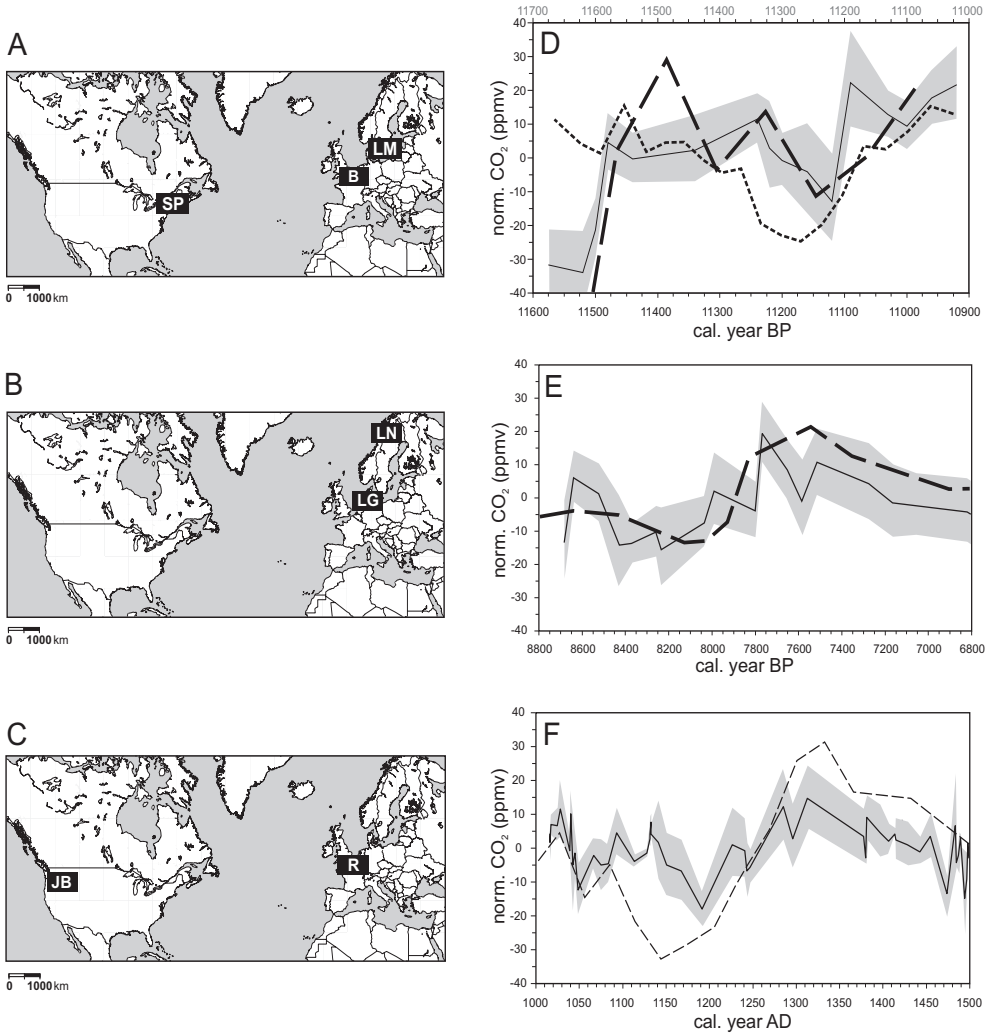
A
LM
B
SP
0 1000 km
B
LN
LG
0 1000 km
C
JB
R
0 1000 km
D
norm. CO2 (ppmv)
cal. year BP
E
norm. CO2 (ppmv)
cal. year BP
F
norm. CO2 (ppmv)
cal. year AD

Figure 5.2

Figure 5.2: Localities of the fossil assemblages (A, B, C) used for stomatal frequency records (D, E, F).
A: SP = Splan Pond (Canada), **B** = Borchert (Netherlands) and LM = Lake Madtjärn (Sweden). **B**: LG = Lille Gribsø (Denmark) and LN = Lake Njulla (Sweden).
C: JB = Jay Bath (Washington, USA) and R = Roer river (Netherlands).
D: Reconstructed normalized CO_2 mixing ratios from three stomatal records (deviations from the long term average in each record) centred around the time of the Preboreal Oscillation. The black line represents unsmoothed normalized mixing ratios based on stomatal index measurements of Betula pubescens leaves from the Borchert section (Wagner et al., 1999). The black dashed line represents unsmoothed normalized mixing ratios based on stomatal number per mm needle length of Larix laricina from Splan Pond (McElwain et al., 2002). The dotted line represents a locally weighted average of normalized mixing ratios based on stomatal indices of *Salix herbacea, Salix polaris* and *Betula nana* from Lake Madtjärn (Rundgren and Björck, 2003). The time scale at the bottom of the figure is based on the age-assessment of the Borchert and Splan Pond records. The original time-scale of the Lake Madtjärn record is shown at the top of the figure and has been shifted by 100 years (within one ^{14}C standard deviation) to facilitate comparison. The grey confidence interval represents ± 1 SE (standard error of the samples per depth) in the Borchert record.
E: Reconstructed normalized CO_2 mixing ratios based on two different stomatal frequency records (deviations from the long term average in each record) around the 8.2 kyr cooling event. The black line represents unsmoothed normalized mixing ratios based on stomatal index of *Betula pendula/pubescens* from Lille Gribsø (Wagner et al., 2002). The dashed line represents a five point moving average of normalized mixing ratios based on stomatal index of *Salix herbacea* from Lake Njulla (Rundgren and Beerling, 1999). The stomatal index of the training set was calibrated against CO_2 partial pressure and also expressed in Pa in the original study. Here, the reconstructed partial pressures were converted to mixing ratios using the estimated local barometric air pressure at the site (Fig. 5.1; Jones, 1992) to allow comparison with the other records. Both records are plotted on a common time scale and the confidence interval represents ± 1 SE (standard error of the samples per depth) in the Lille Gribsø record.
F: Reconstructed normalized mixing ratios based on two different stomatal frequency records around the onset of the Little Ice Age. The black line represents the unsmoothed normalized mixing ratios based on stomatal index of *Quercus robur* leaves from the Roer river area (Chapter 2). The dashed line represents a three point moving average of normalized mixing ratios based on stomatal numbers per mm needle length (TSDL) of *Tsuga heterophylla* needles from Jay Bath (Kouwenberg, 2004). The TSDL of the modern training set was calibrated against CO_2 partial pressure and the reconstructed partial pressures were converted to mixing ratios using the estimated local barometric air pressure (Fig. 5.1; Jones, 1992). The grey confidence interval represents ± 1 SE (standard error of the samples per depth) in the Roer record.

modern training set shown in Fig. 5.1 B. Two CO_2 minima are evident in the record, a smaller one around 1050 AD and a very pronounced minimum centred around 1150 AD (Fig. 5.2 F). Maximum CO_2 levels are registered during the 14th century, followed by a steady CO_2 decrease.

These initial results are confirmed in a high resolution record of fossil *Quercus robur* leaves from an oxbow lake of the river Roer, near Sint Odiliënberg, The Netherlands (51°08'N, 6°00'E; 25 m a.s.l., Fig. 5.2 C; Chapter 3). Wiggle match dating of eleven AMS ^{14}C datings provides a precise age assessment of the 60 leaf-rich layers in this section, covering the period from 1000 AD to 1500 AD. The CO_2 reconstruction based on *Q. robur* leaves reproduces and substantiates in detail the short-term CO_2 decrease around 1050 AD. The second minimum in this high resolution record is assigned to the late 12th to early 13th century. In good agreement with the *T. heterophylla* record, the *Q. robur* data indicate decreasing CO_2 mixing ratios during the late 14th and 15th century. Both records provide independent evidence for rapid CO_2 fluctuations on time-scales varying from decades to centuries. While the estimated amplitudes of 20 ppmv to 30 ppmv in the *Q. robur* record are in good agreement with the fluctuations documented for the Preboreal oscillation and the 8.2 kyrs event, the maximum change up to 60 ppmv estimated in the *T. heterophylla* record exceeds the other records. The difference, however, is within or close to the standard error of the *Q. robur* record and may be caused by the comparably lower accuracy of the modern training set for *T. heterophylla* (Fig. 5.1 B).

Temperature reconstructions for the period of the Little Ice Age based on marine and terrestrial evidence show a series of short, moderately cool pulses rather than the very pronounced single century-scale coolings of the Preboreal oscillation and the 8.2 kyrs event. This pattern is also evident in the stomatal frequency based CO_2 reconstructions.

Discussion

The compilation and detailed comparison of the seven records provides an indirect but powerful assessment of the reliability of stomatal frequency analysis as a proxy for paleoatmospheric CO_2 mixing ratios. So far, the validation of stomatal frequency as a sensitive parameter to changing CO_2 mixing ratios has basically been performed for individual species (see Royer, 2001 for review). Potential influences of environmental factors other than CO_2, e.g. light, water availability and temperature, have frequently been tested in experiments under controlled growth conditions. The results obtained in a controlled and artificial environment in growth experiments, however, can not unambiguously be transferred to responses under the natural growth conditions in the field. Field studies, on the other hand, provide insight in the intrinsic variability under natural growth conditions but observed variations are often a response to a combination of environmental parameters.

By directly comparing the generated CO_2 estimations based on independent stomatal frequency records, species-specific uncertainties may be minimized, which permits testing of the overall quality of the CO_2 reconstructions.

Taking into account the wide geographical area the investigated leaf material originates from, the difference in photoperiod over the covered latitudinal range from 45°N to 68°N could potentially affect the stomatal frequency records. Light intensity and photoperiod have been long known to strongly affect stomatal frequency (Schürmann, 1959; Kürschner et al., 1996; Poole et al., 1996, Wagner et al., 2000). While light intensity primarily regulates epidermal cell expansion and, therefore, influences stomatal densities, prolonged photoperiods lead to enhanced stomatal initiation rates quantified in the stomatal index (Schürmann, 1959; Wagner et al., 2000). The dependency on photoperiod may consequently cause erroneous data when stomatal index values from contrasting latitudes are compared to data from a restricted latitudinal range (Wagner et al., 1999b).

CO_2 estimates from high and mid-latitudes are combined in the second case study, the 8.2 kyrs event, where stomatal index data of *Betula* leaves from Denmark and *Salix herbacea* data from northern Sweden are available. The calibration data for *Betula* (Fig. 5.1 A) are based solely on leaf material from Denmark and the Netherlands, since field studies have demonstrated the high sensitivity of birch to changes in photoperiod (Wagner et al., 2000). No such dependency is known for *Salix*, and calibration data are derived from a wide latitudinal range (Rundgren and Beerling, 1999). Independent of the different approaches, the good correspondence of paleo-CO_2 estimates from the high and mid- latitude records strongly suggests that latitudinal differences in photoperiod did not bias these data sets.

Only very sparse information is available so far on the potential influence of temperature on stomatal frequency. Controlled environment experiments with *B. pendula* under (extremely) different growth temperatures provide evidence for a positive correlation between the stomatal index and temperature for this particular species (Wagner et al., 1998). No interaction between stomatal frequency and temperature was observed in experiments with cotton (Reddy et al., 1998). Comparison of spring and annual temperatures near Jay Bath with the stomatal frequency of the subfossil *T. heterophylla* needles during the last ninety years showed no correlation (Kouwenberg et al., 2003). Although the available data are not unequivocal, they suggest that the temperature changes are unlikely to have caused the observed changes in the individual stomatal frequency records. The three periods discussed here are generally referred to as cool pulses, but the regional temperature changes have not been uniform over the Northern Hemisphere. The good agreement of stomatal frequency records from sites located at

different altitude, latitude, and longitude with their individual temperature ranges minimizes the possibility of temperature changes as the responsible factor for the observed parallel changes in the record.

Effects of water availability on epidermal morphology are well known. Drought stress for instance leads to the development of distinct xeromorphic features during leaf development (Bosabalidis and Kofidis, 2003; Li and Wang, 2003). One of the most common and pronounced effect observed in growth experiments, is the reduced lateral epidermal cell expansion under drought conditions (Bosabalidis and Kofidis, 2003; Li and Wang, 2003). The stomatal index, however, is not influenced by water shortage in these performed experiments. Under natural growth conditions, the comparison of actual precipitation data for the last seventy years and the stomatal frequency of *T. heterophylla* shows no correlation (Kouwenberg et al., 2003).

This observational evidence for the independence of the stomatal frequency parameters from precipitation is corroborated by the good agreement between the CO_2 records in spite of the highly regional precipitation surpluses or deficits associated with the periods of climate change studied. Again, as with temperature, the broad geographical distribution of the sites studied provides evidence for the independence of the CO_2 records from precipitation changes associated with the Preboral oscillation, the 8.2 kyrs event and the Little Ice Age.

Besides the potential impact of environmental factors other than CO_2 mixing ratios, genetic variations within individual plant species or hybridization of related species could be a potential cause for the changing stomatal frequency patterns. Studies on genetically controlled leaf material from *B. pendula* and *B. pubescens*, however, have shown that at least for these two species the influence of genetic difference can be neglected (Wagner, 2000; Fig. 5.1 A). In cases where the species specific stomatal frequency response does not allow a grouping, single site CO_2 reconstructions based on multiple species can be derived by developing separate calibration data sets as demonstrated for *S. polaris* and *S. herbacea* (Rundgren and Björck, 2003). The approach of combining CO_2 estimates including a wide range of taxonomically contrasting plant types in this study a priori excludes any influence of taxonomic or genetic nature as shown by the consistency of CO_2 reconstructions derived from broad-leaved trees, herbaceous shrubs, and conifers, or a combination of those.

Conclusions

The successful replication of stomatal frequency records in terms of timing and duration in the seven compared records provides strong evidence for the integrity of the leaf-based proxy for atmospheric CO_2 mixing ratios. The general coherence of the reconstructed amplitudes of atmospheric CO_2 fluctuations corroborates the assumption that a wide range of terrestrial plants show a common response to this environmental factor independent of geographical setting, habitat conditions or taxonomy.

The agreement between stomatal frequency records from the Atlantic realm and sites located in the Pacific Northwest of the USA indicates that the observed stomatal parameter shifts are not restricted to the circum North Atlantic sector, but are at least northern hemispheric in nature. The demonstrated ability of stomatal frequency analysis to generate independent but highly comparable proxy records clearly meets the requirements for a paleo-proxy in the field of global atmospheric CO_2 dynamics.

Chapter 6

Atmospheric CO_2 during the 13th century AD

a case study based on ice core measurements and stomatal frequency analysis

Atmospheric CO_2 reconstructions are currently available from direct measurements of air enclosures in Antarctic ice and, alternatively, from stomatal frequency analysis performed on fossil leaves. A period where both methods consistently provide evidence for natural CO_2 changes is during the 13th century. The results of the two independent methods differ significantly in the amplitude of the estimated CO_2 changes (10 ppmv Ice versus 34 ppmv stomatal frequency). Here, we compare the stomatal frequency and ice core results by using a firn diffusion model in order to assess the potential influence of smoothing during enclosure on the temporal resolution as well as the amplitude of the CO_2 changes values. The seemingly large discrepancies between the amplitudes estimated by the contrasting methods diminish when effects of natural smoothing of the ice-core record is simulated for the raw data of the stomatal frequency record. Results indicate that the differences derived by the two methods are less significant than previously thought.

Introduction

Analysis of gas enclosures in polar ice is the most established and widely accepted source of information on atmospheric CO_2 dynamics during the late Quartenary. While glacial - interglacial cycles are generally characterized by large shifts in atmospheric CO_2 levels, Antarctic ice core records document only small natural variations of maximal 15 ppmv during the warm stages (Indermühle et al., 1999; Monin et al., 2001; Barnola et al., 1995; Etheridge et al., 1996).

Alternatively, atmospheric CO_2 proxy records can be generated by studying the genetically controlled leaf morphological adaptation of selected C3 plants, in which the amount of stomata (gas exchange pores) on the leaf is directly determined by the ambient CO_2 mixing ratio during the growth period (Wagner et al., 1996; Lake et al., 2001). The high abundance of leaf fossils in Quaternary lake and peat deposits increasingly focuses interest on this time interval. Numerous stomatal frequency based CO_2 records, especially for the Holocene, are already available (Beerling et al., 1995; Wagner et al., 1999; Rundgren and Beerling, 1999; Wagner et al., 2002; McElwain et al., 2002; Rundgren and Björck, 2003; Kouwenberg et al., 2004). A common pattern to all these records is a significant variability of atmospheric CO_2 levels throughout the Holocene, showing repeated short-lived CO_2 shifts of 20 - 30 ppmv (Chapter 5), that clearly exceed the fluctuations documented in polar ice.

The major differences between the results of the two techniques are: A) the different CO_2 average base levels for the Holocene; B) the pacing of CO_2 variations; and C) the amplitude of the detected shifts. These factors need considerable attention for understanding natural, short-term climate dynamics. Whether the apparent discrepancies are real, however, or just a result of cumulated inaccuracies introduced by the technique-inherent uncertainties, is difficult to assess.

It is well known, that diffusion processes within the firn layer and the gradual enclosure of the air in the lock-in-zone of the ice lead to a reduced signal of the original atmospheric variability and may obscure high frequency variations (e.g. Trudinger et al., 2003).
In stomatal frequency analysis, the intrinsic variability of plants, resulting from environmental factors other than CO_2, often affects the precision of CO_2 inference models and commonly leads to relatively high standard deviations of the mean CO_2 prediction values (Wagner et al., in press). To explore the accuracy of the atmospheric CO_2 reconstructions based on the different methods, the results need to be directly compared. Here, we make a contribution to the comparison of stomatal frequencies and ice core results by using a firn diffusion model. A period where both methods consistently provide evidence for natural CO_2 changes is the 13th century AD. A significant CO_2 increase with a range of 12 ppmv at this time is measured in at least two Antarctic ice cores, namely South Pole and D47 (Siegenthaler et al.,1988, Barnola

et al., 1995) while a stomatal frequency reconstruction from the Netherlands show a range of 34 ppmv change during the same period (Chapter 2).

In the present study we try to answer the question whether the amplitude differences of fast shifts in CO_2, detected by the two methods for the early part of the last millennium, are caused by overestimation of CO_2 mixing ratios in stomatal frequency records or result from alteration of CO_2 content by diagenetic processes involved during trapping of the air in the firn and ice.

In order to assess the influence of smoothing during enclosure on the temporal resolution, as well as on the amplitude of the CO_2 changes, we apply a one-dimensional numerical firn air diffusion model (Kaspers et al., 2004a) on the high resolution stomatal frequency based CO_2 record. In this way the stomatal frequency record can be directly compared with the ice core results. It simulates how the stomatal frequency record would be observed in a synthetic ice core. The firn air diffusion model is forced with the meteorological conditions characterizing the ice core drilling site at D47. The smoothed output is subsequently compared to the actual CO_2 measurements from core D47 (Barnola et al., 1995). This procedure makes the two independent data sets compatible and allows to comment on the likeliness of the higher amplitude CO_2 changes observed in the stomatal frequency record during this particular time interval.

Material and Methods

The stomatal frequency CO_2 reconstruction (Fig. 6.1 A; hereafter CO_2 [SI]) is based on stomatal index measurements of buried oak leaves (*Quercus robur*) derived from channel deposits of the river Roer (Sint Odiliënberg, the Netherlands, 51.08^{0}N, 6.00^{0}E; Chapter 2). A detailed chronology for the CO_2 [SI] reconstruction is provided by eleven AMS ^{14}C dates wiggle-matched to the INTCAL98 calibration curve (Stuiver et al. 1998) and supplemented with a high resolution palynological based biostratigraphy of the channel deposits (Chapters 2 and 4). The leaf bearing part of the deposits is restricted to the time period from AD 1000 to1500, of which 60 horizons were sampled for stomatal frequency analysis, thereby obtaining a decadal resolution of the record (Chapter 2). CO_2 [SI] estimates were obtained by using the inverse relationship between SI and CO_2 of this species as was monitored and modelled during the post-industrial atmospheric CO_2 increase of the last two centuries (Chapter 1).

A suitable CO_2 profile based on gas enclosure analysis (hereafter CO_2 [ice]) that covers the same time slice is available from the D47 ice core (67^{o}23'S,154^{o}03'E) (Barnola et al., 1995). The D47 record provides the highest data density of the available ice cores covering the last Millennium and shows a distinct 13th century AD CO_2 shift (Barnola et al., 1995).

The first step towards comparison of stomatal frequency and and ice core data was to transform the atmospheric CO_2 [SI] record into a yearly resolved CO_2 record by means of linear interpolation. The interpolated CO_2 [SI] record was subsequently used as input data for a firn air diffusion model (Schwander et al., 1993; Spahni et al., 2003, Kaspers et al., 2004a) which was forced with the present-day characteristic site conditions of the D47 core drilling site. The meteorological quantities used in the diffusion model (e.g. annual mean temperature (at 10m depth; 247.2 K) and the accumulation rate for site D47 (26.8 cm w.e.a^{-1}) are derived from the initial study of the D47 ice core (Barnola et al.,1995). While the values for annual mean surface pressure (780 hPa) and wind speed at 10m (7 m/s) are derived from a Regional Atmospheric Climate Model for Antarctica (RACMO-ANT, van Lipzig et al., 2002). From the meteorological quantities site specific parameters were obtained: surface snow density (407 kg/m^3), the density at pore close off (818 kg/m^3), pore close off depth (56 m) and the tortuosity (4.1). The site specific parameters were derived from the parameterisations described in Kaspers et al., (2004b). This parameterisation is based on a compilation of all existing firn air measurements to date. The firn air diffusion model is applied over the entire period from 1000 AD to 2001 AD with a resolution of approximately 1m between 350m depth and 56m depth, the pore close off depth for D47. Sensitivity tests have been performed for changes in temperature and accumulation, but have shown to be a negligible effect on the results.

For the direct comparison of the modelled CO_2 [SI] with the D47 CO_2 [ice] measurements, only the interval between 190 and 310 metre depth of the model output is used, as this represents the stomatal frequency based part of the input data.

Results

The model output of CO_2 [SI] versus CO_2 [ice] D47 is presented in Fig. 6.1 B. Model output data are shown as a function of depth, and accordingly, plotted on CO_2 [ice] depth scale.The CO_2 [SI] model output has a maximum amplitude of 25 ppmv, with a CO_2 minimum at 260 m and a maximum at 215 m. Of selected data-points that resemble the actual sample depths of the CO_2 [ice] measurements of the D47 core, methodological errors (6 ppmv) of the CO_2 [SI] are shown. CO_2 [ice] measurements show a maximum amplitude of 12 ppmv with a CO_2 minimum at 265 m and a maximum at 210 m (Fig. 6.1 B; Barnola et al., 1995). The grey band represents the 3 ppmv methodological error of the D47 record (Barnola et al., 1995).

Discussion

The effect of the synthetic smoothing of CO_2 [SI] leads to a 25% reduction of the amplitude from 34 ppmv in the raw data to maximal 25 ppmv according to the model output. Furthermore, the numerous single high-resolution data point shifts that characterize the CO_2 [SI] record are eliminated due to the diffusion. The output sequence

follows in great detail the CO_2 [ice] mixing ratio data measured in D47. The resulting profiles are not significantly different. By applying the firn air densification model to the raw stomatal frequency CO_2 data, a hypothetical profile is generated, where the main processes acting on atmospheric CO_2 in air bubbles trapped in ice are simulated. During enclosure, the trapped air is subjected to processes that alter the CO_2 mixing ratio ultimately preserved in the ice (Anklin et al., 1995; Schwander, 1996; Trudinger et al., 2003). Diffusion through the firn layer or gradual enclosure in the bubbles leads to smoothing of the record and, thus, underestimation of the amplitude of the CO_2 changes (Trudinger et al., 2003). In the present study, we assume the highly variable stomatal frequency CO_2 record to represent the actual ambient atmosphere. The applied smoothing during firn densification should then reduce the information to a level on which it would be preserved in the air measured from the specific ice core, in this case D47. If the trends in stomatal frequency data do correctly reflect past CO_2 changes, the match between CO_2 [SI] and CO_2 [ice] should be perfect. The observed firm correspondence between the CO_2 [SI] and CO_2 [ice] data indeed confirm that the observed amplitude differences between the raw stomatal frequency record and the ice core data can be explained by the smoothing of CO_2 during ice formation.

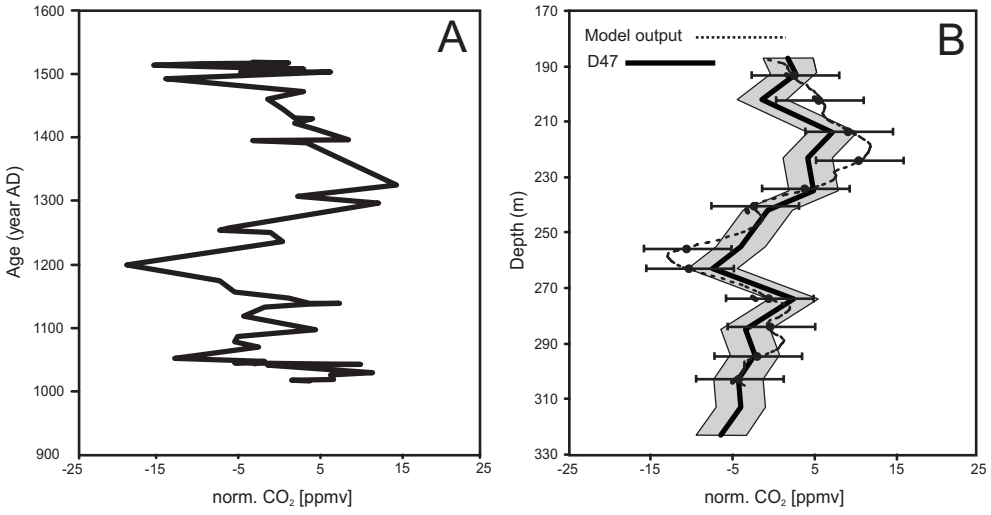

Figure 6.1: A: Raw data: Normalized stomatal frequency based CO_2 mixing ratios as calculated from stomatal index (stomatal index (SI) [%] = stomatal density (SD) [n/mm^2] / epidermal cell density (ED) [n/mm^2]) of fossil *Q. robur* (oak) leaves derived from channel deposits of the river Roer (the Netherlands) (Chapter 3). The chronology of the stomatal frequency record is based on wiggle match dating of eleven AMS ^{14}C measurements (Chapters 2 and 4). **B** : Dotted black line; CO_2 [SI]: Output after application of the firn densification model (Kaspers et al., 2004a). Of selected data-points that resemble the actual sample depths of the CO_2 [ice] measurements of the D47 core, methodological errors (6 ppmv) of the CO_2 [SI] are shown. Black line: Normalized CO_2 mixing ratios (CO_2 [ice]) of the D47 ice core with the grey area representing the methodological error (3 ppmv) (Barnola et al, 1995).

The remaining discrepancies between CO_2 [SI] and CO_2 [ice] may very well be an artifact of the uncertainties in the CO_2 inference model used for CO_2 estimates from stomatal index values of oak leaves. For atmospheric CO_2 reconstructions, the adaptation of oak to the industrial CO_2 increase from 280 ppmv to 370 ppmv serves as modern training set from which response rates are determined. The response of oaks to changing CO_2 mixing ratios, however, is a sigmoidal function, since the number of stomata on the leaf surface can neither become zero, nor infinite (Kürschner et al., 1997). For calibration purposes only the linear phase of the resulting sigmoidal response curve is interpreted in the CO_2 inference model, since secure quantification of the asymptotes is hampered by the lack of response data under pre-industrial CO_2 mixing ratios below 280 ppmv. The model is thus conservative in reconstructing past CO_2 mixing ratios outside the monitored response range, which introduces inaccuracies in the CO_2 range where the linear model diverges from the sigmoidal response (Chapter 1).

The most prominent feature in both profiles is the distinct CO_2 oscillation between 1150 AD and 1350 AD. Both data sets show an initial decrease of 10 ppmv, reaching minimum levels at 1200 AD followed by a CO_2 increase of 12 ppmv in CO_2 [ice] and 15 ppmv in CO_2 [SI] during the 14th century. The timing as well as the rates of change are in excellent agreement in the CO_2 [SI] model output and the CO_2 [ice] record. A CO_2 increase associated with the 13th century was originally measured in the South Pole ice core, were a maximum of 10 ppmv increase was calculated by deconvolving the raw data (Siegenthaler et al., 1988). The exact temporal pattern of this fluctuation, however, is difficult to assess, due to the weakly confined age width of the ice samples (Barnola et al., 1995). More recent cores like Law Dome (Etheridge et al., 1996) or Taylor Dome (Indermühle et al., 1996) that cover the last millennium also indicate fluctuating CO_2 levels, but the interpretation of these records is severely hampered due to low sample resolution and / or age uncertainties (Etheridge et al., 1996; Indermühle et al., 1996). So far, no conclusive temporal delineation of the CO_2 variation during the early part of the last millennium has been achieved.

Although an indirect proxy measure, stomatal frequency analysis has the major advantage of providing real-time data. The leaf morphological CO_2 signal is permanently fixed at the moment of growth, and remains resistant to diagenetic processes acting on the leaf material during fossilization. For actual reconstructions this implies that the potential temporal resolution is high, often on (sub-) decadal scale (Chapter 5).

The detailed ^{14}C wiggle-match dating (WMD) age assessment of the stomatal frequency record allows to give an accurate age range with a maximum uncertainty of 30 years. The reconstructed CO_2 oscillation started at 1150 AD, with a CO_2 minimum at 1200 AD and maximum levels at 1320 AD.

Conclusions

A significant CO_2 change during the 13th century is evident from direct measurements of CO_2 in gas enclosures in Antarctic ice core D47 as well as from stomatal frequency analysis of fossil oak leaves. The independent detection of this CO_2 shift, and the good agreement between the different records, provides persuasive evidence for the actuality of this event.

The seemingly large discrepancies between the amplitude of the CO_2 oscillation estimated by the contrasting methods, diminish when effects of natural smoothing of the ice-core record is simulated for the raw data of the stomatal frequency record. The results show that the differences derived by the two methods may be less significant than previously thought. Consequently, cross testing of the additional CO_2 fluctuation observed in stomatal frequency records with the relevant properties of ice records may help to improve our knowledge on Holocene CO_2 dynamics.

References

References

Alley, R.B., P.A. Mayewski, T. Sowers, M. Stuiver, K.C. Taylor and P.U. Clark 1997. Holocene climatic instability: A prominent, widespread event 8200 yr ago. Geology. 25:483-486.

Anklin, R.B., J.-M. Barnola, J. Schwander, B. Stauffer and D. Raynaud 1995. Processes affecting the CO_2 concentrations measured in Greenland ice. Tellus. 47:461-470.

Armstrong, W., R. Brändle and M.B. Jackson 1994. Mechanisms of flood tolerance in plants. Acta Botanica Neerlandica. 43:301-358.

Astrade, L. and Y. Bégin 1997. Tree-ring response of *Populus tremula* L. and *Quercus robur* L. to recent spring floods of the Saône river, France. Ecoscience. 4:232-239.

Atkinson, C.J., J.M. Taylor, D. Wilkins and R.T. Besford 1997. Effects of elevated CO_2 on chloroplast components, gas exchange and growth of oak and cherry. Tree Physiology. 17:319-325.

Barber, D.C., A. Dyke, C. Hillaire-Marcel, A.E. Jennings, J.T. Andrews, M.W. Kerwin, G. Bilodeau, R. McNeely, J. Southon, M.D. Morehead and J.-M. Gagnon 1999. Forcing of the cold event of 8,200 years ago by catastrophic drainage of Laurentide lakes. Nature. 400:344-348.

Barnola, J.M., M. Anklin, J. Porcheron, D. Raynaud, J. Schwander and B. Stauffer 1995. CO_2 evolution during the last millenium as recorded by Antarctic and Greenland ice. Tellus. 47:264-272.

Bauer, E., M. Claussen and V. Brovkin 2003. Assessing climate forcings of the Earth system for the past millennium. Geophysical Research Letters. 30:1-4.

Beerling, D.J., H.H. Birks and F.I. Woodward 1995. Rapid late-glacial atmospheric CO_2 changes reconstructed from the leaf stomatal density of fossil leaves. Journal of Quaternary Science. 10:379-384.

Beerling, D.J. and W.G. Chaloner 1993. The impact of atmospheric CO_2 and temperature change on stomatal density: observations from *Quercus robur* lammas leaves. Annals of Botany. 71:231-235.

Beerling, D.J. and D.L. Royer 2002. Reading a CO_2 signal from fossil stomata. New Phytologist. 153:387-397.

Behre, K.E. 1981. The interpretation of anthropogenic indicators in pollen diagrams. Pollen Spores. 23:225-245.

Bieleman, J. 1992. Geschiedenis van de landbouw in Nederland 1500-1950. Boom Meppel, Amsterdam.

Birks, H.J.B., W. Eide and H.J.B. Birks 1999. Early Holocene atmospheric CO_2 concentrations. Science. 286:1815.

Björck, S., M. Rundgren, O. Ingólfsson and S. Funder 1997. The Preboreal Oscillation around the Nordic Seas: terrestrial and lacustrine responses. Journal of Quaternary Science. 12:455-465.

Björck, S., M.J.C. Walker, L.C. Cwynar, S.J. Johnsen, K.L. Knudsen, J.J. Lowe, B. Wohlfarth and I. Members 1998. An event stratigraphy for the Last Termination in the North Atlantic regionbased on Greenland Ice Core record: a proposal by the INTIMATE group. Journal of Quaternary Science. 13:283-292.

Bosabalidis, A.M. and G. Kofidis 2002. Comparative effects of drought stress on leaf anatomy of two olive cultivars. Plant Science. 163:375-379.

Bray, R.S. 1996. Armies of Pestilence. The Lutterworth press, Cambridge.

Bronk Ramsey, C. 1995. Radiocarbon calibration and analysis of stratigraphy: the OxCal program. Radiocarbon. 37:425-430.

Buisman, J. 1995. Duizend jaar weer, wind en water in de lage landen Ed. A.F.V.v. Engelen. van Wijnen, Franeker.

Bunnik, F.P.M. 1999. Vegetationsgeschichte der Lößbörden zwischen Rhein und Maas- von der Bronzezeit bis in die frühe Neuzeit. Laboratory of Palaeobotany and Palynology. Utrecht University. Utrecht. pp. 1-149.

Cartwright, F.F. 1972. Disease and History. Northumberland Press Limited, Gateshead.

Coenen, J. 1922. De drie munsters der Maasgouw, Aldeneyck, Susteren, St.-Odiliënberg. *In* Publications de la Société Historique et Archéologique dans le limburg.

Cook, E. and K. Briffa 1990. Data Analysis. *In* Methods of Dendrochronology Eds. E.R. Cook and L.A. Kairiukstis. Kluwer, Dordrecht.

Creutz, R. 1933. Pest und Pestabwehr im alten Köln. Jahrbuch des Kölner Geschichtsvereins. 15.

Dean, W.E. 1974. Determination of carbonate and organic matter in calcareous sediments and sedimentary rocks by loss on ignition: a comparison with other methods. Journal of Sedimentary Petrology. 44:249-253.

Dixon, R.K., S. Brown, R.A. Houghton, A.M. Solomon, M.C. Trexler and I. Wisniewski 1994. Carbon pools and flux of global forest ecosystems. Science. 263:185-190.

Etheridge, D.M., L.P. Steele, R.L. Langenfels, R.J. Francey, J.M. Barnola and V.I. Morgan 1996. Natural and anthropogenic changes in atmospheric CO_2 over the last 1000 years from air in Antarctic ice and firn. Journal of Geophysical Research. 101:4115-4128.

Fagan, B. 2000. The Little Ice Age: how climate made history. Basic Books, New York.

Fritts, H.C. 1976. Tree Rings and Climate. Academic Press, London.

Fritts, H.C. 1999. PRECON. University of Arizona, Tucson.

George, S. and E. Nielsen 2002. Flood ring evidence and its application to paleoflood hydrology of the red river and assiniboine river in Manitoba. Géographie physique et Quartenaire. 56:1-10.

Goosse, H., V. Masson-Delmotte, H. Renssen, D. M, T. Fichefet, V. Morgan, T. van Ommen, K.B. Kim and B, Stenni 2004. A late medieval warm period in the Southern Ocean as a delayed response to external forcing. Geophysical Research Letters. 31

References

Grissino-Mayer, H.D. 2001. Evaluating crossdating accuracy: a manual and tutorial for the computer program COFECHA. Tree-ring research. 57:205-221.

Grissino-Mayer, H.D. and H.C. Fritts 1997. The International Tree-Ring Data Bank: An enhanced global database serving the global scientific community. The Holocene. 7:235-238.

Grove, J.M. 1988. The Little Ice Age. Routledge, London.

Hermans, J.T. and G.M.T. Peters 1999. Flora en vegetatie van landgoed Hoosden. Stichting de Lierelei.

Holmes, R.L. 1983. Computer-assisted quality control in tree-ring dating and measurement. Tree-ring Bulletin. 43.

Hommel, P.W.F.M. and J.T. Hermans 1996. Het Landgoed Hoosden en de Turfkoelen. *In* Excursieverslagen van de plantensociologische kring Nederland, *Eds*. P.W.F.M. Hommel and M.A.P. Horsthuis.

Houghton, R.A. and D.L. Skole 1990. Carbon. *In* The Earth as transformed by human action Eds. B.L. Turner, W.C. Clark, R.W. Kates, J.F. Richards, J.T. Mathews and W.B. Meyer. Cambridge University Press, Cambridge.

Houghton, J.T.,Y. Ding, D.J. Griggs, M. Noguer, P.J. van der Linden, D. Xiaosu 2001. Climate Change 2001: The Scientific Basis Contribution of working Group 1 to the Third Assessment Report of the Intergovernmental Panel on Climate Change (IPCC). Cambridge University Press, Cambridge.

House, J.I., C. Prentice and C. LeQuere 2002. Maximum impacts of future reforestation or deforestation on atmospheric CO_2. Global Change Biology. 8:1047-1052.

Indermühle, A., B. Stauffer, T.F. Stocker, D. Raynaud and J.-M. Barnola 1999a. Early Holocene Atmospheric CO_2 Concentrations. Science. 286:1815a.

Indermühle, A., T.F. Stocker, F. Joos, H. Fischer, H.J. Smith, M. Wahlen, B. Deck, D. Mastroianni, J. Tschumi, T. Blunier, R. Meyer and B. Stauffer 1999b. Holocene carbon-cycle dynamics based on CO_2 trapped in ice at Taylor Dome, Antarctica. Nature. 398:121-126.

Janssen, C.R. 1973. Local and regional pollen deposition. *In* Quartenary Plant Ecology, 14th Symposium of the British Ecological Society Eds. H.J.B. Birks and R.G. West, pp. 31-42.

Janssen, W. 1997. Kleine Rheinische Geschichte. Patmos Verlag, Düsseldorf.

Jones, H.G. 1992. Plants and microclimate. University Press, Cambridge.

Kaspers, K.A., R.S.W.v.d. Wal, M.R.v.d. Broeke, J. Schwander, N.P.M.v. Lipzig and C.A.M. Brenninkmeijer 2004a. Model calculations of the age of firn air across the Antarctic continent. Atmosphere Chemistry Physics. 4:1-37.

Kaspers, K.A., R.S.W.v.d. Wal, J.A.d. Gouw, C.M. Hofstede, M.R.v.d. Broeke, C.v.d. Veen, R.E.M. Neubert, H.A.J. Meijer, C.A.M. Brenninkmeijer, L. Karlöf and J.G. Winther 2004b. Analyses of firn gas samples from Dronning Maud Land, Antarctica: Study of nonmethane hydrocarbons and methyl chlorine. Journal of Geophysical Research. 109

Keeling, C.D. and T.P. Whorf 2002. http://cdiac.esd..ornl.gov/ndps/ndp001.html

Kouwenberg, L.L.R. 2004. Application of conifer needles in the reconstruction of Holocene CO_2 levels. LPP Contribution Series 16. Utrecht University, Utrecht.

Kouwenberg, L.L.R., J.C. McElwain, W.M. Kürschner, F. Wagner, D.J. Beerling, F.E. Mayle and H. Visscher 2003. Stomatal frequency adjustment of four conifer species to historical changes in atmospheric CO_2. American Journal of Botany. 90:610-619.

Kürschner, W.M. 1996. Leaf stomata as biosensors of palaeoatmospheric CO_2 levels. LPP Contribution Series 5. Utrecht University, Utrecht, p. 143.

Kürschner, W.M., I. Stulen, F. Wagner and P.J.C. Kuiper 1998. Palaeobotanical observations with experimental data on the leaf anatomy of Durmast Oak[*Quercus petraea* (Fagaceae)] in response to environmental change. Annals of Botany. 81:557-664.

Kürschner, W.M., J. Van der Burgh, H. Visscher and D.L. Dilcher 1996. Oak leaves as biosensors of late Neogene and early Pleistocene paleoatmospheric CO_2 concentrations. *In* Pliocene climates Eds. R. Poore and L.C. Sloan, pp. 299-312.

Lake, J.A., W.P. Quick, D.J. Beerling and F.I. Woodward 2001. Signals from mature to new leaves. Nature. 411:154.

Lamb, H.H. 1977. Climatic History and the future. *In* Climate : present, past and future. Methuen & co Ltd, London. 835 p.

Leenders, K.A.H.W. 1987. De boekweitkultuur in historisch perspectief. Geologisch Tijdschrift. 21:213-227.

Li, C. and K. Wang 2003. Differences in drought response of three contrasting *Eucalyptus microtheca* F. Mueli populations. Forest Ecology and Management. 179:377-385.

Lipzig, N.P.M.v., E.v. Meijgaard and J. Oerlemans 2002. The spatial and temporal variability of the surface mass balance in Antarctica: results from a regional climate model. International Journal of Climatology. 22:1197-1217.

McElwain, J.C., F.E. Mayle and D.J. Beerling 2002. Stomatal evidence for a decline in the atmospheric CO_2 concentration during the Younger Dryas stadial: a comparison with Antarctic ice core records. Journal of Quaternary Sciences. 17:21-29.

Monnin, E., A. Indermühle, A. Dällenbach, J. Flückinger, B. Stauffer, T.F. Stocker, D. Raynaud and J.-M. Barnola 2001. Atmospheric CO_2 concentrations over the Last Glacial Termination. Science. 291:112-114.

Neftel, A., E. Moor, H. Oeschger and B. Stauffer 1985. Evidence from polar ice cores for the increase in atmospheric CO_2 in the past two centuries. Nature. 315:45-47.

Oppenheimer, C. 2003. Ice core and palaeoclimatic evidence for the timing and nature of the great mid-13th century volcanic eruption. International Journal of Climatology. 23:417-426.

References

Poole, I. and W.M. Kürschner 1999. Stomatal density and index: the practice. *In* Fossil plant and spores: modern techniques Eds. T.P. Jones and N.P. Rowe. The Geological Society. London, pp. 257-260.

Poole, I., J.D.B. Weyers, T. Lawson and J.A. Raven 1996. Variations in stomatal density and index: implications for paleoclimatic reconstructions. Plant, Cell and Environment. 19:705-712.

Reddy, K.R., R.R. Robana, H.F. Hodges, X.J. Liu and J.M. McKinion 1998. Interactions of CO_2 enrichment and temperature on cotton growth and leaf characteristics. Environmental and Experimental Botany. 39:117-129.

Rinn, F. 1996. TSAP, Heidelberg.

Royer, D.L. 2001. Stomatal density and stomatal index as indicators of paleoatmospheric CO_2 concentration. Review of Palaeobotany and Palynology. 114:1-28.

Royer, D.L., S.L. Wing, D.J. Beerling, D.W. Jolley, P.L. Koch, L.J. Hickey and R.A. Berner 2001. Paleobotanical evidence for near present-day levels of atmospheric CO_2 during part of the Tertiary. Science. 292:2310-2313.

Rundgren, M. and D. Beerling 1999. A Holocene CO_2 record from the stomatal index of subfossil *Salix herbacea* L. leaves from northern Sweden. The Holocene. 9:509-513.

Rundgren, M. and S. Björck 2003. Late-glacial and early Holocene variations in atmosperic CO_2 concentration indicated by high-resolution stomatal index data. Earth and Planetary Science Letters. 213:191-204.

Scahaminée, J.H.J., E.J. Weeda and V. Westhof 1998. De vegetatie van Nederland. Opulus press. Leiden.

Schmitz-Cliever, E. 1954. Pest und pestilenzische Krankheit in der Geschichte der Reichsstadt Aachen. Zeitschrift des Aachener Geschichtsvereins. 66/67.

Schürmann, B. 1959. Über den Einfluß der Hydratur und des Lichtes auf die Ausbildung der Stomata-Initialien. Flora. 147:471-520.

Schwander, J. 1996. Gas diffusion in firn. *In* Chemical exchange between the atmosphere and polar snow Eds. E.W. Wolff and R.C. Bales. Springer Verlag, Berlin Heidelberg, pp. 527-539.

Schwander, J., J.M. Barnola, C. Andrié, M. Leuenberger, A. Ludin, D. Raynaud and B. Stauffer 1993. The age of the air in the firn and ice at Summit, Greenland. Journal of Geophysical Research. 98:2831-2838.

Schweingruber, F.H. 1993. Jahrringe und Umwelt-Dendroökologie. Eidgenössische Forschungsanstalt für Wald, Schnee und Landschaft, Birmensdorf. 474 p.

Shi, G. 1992. Radiative forcing and Greenhouse-effect due to atmospheric trace gases. Science in China series B - Chemistry. 35:217-229.

Siegenthaler, U., H. Friedli, H. Lötscher, A. Moor, A. Neftel, H. Oeschger and B. Stauffer 1988. Stable-isotope ratio and concentration of CO_2 in air from polar ice core. Annals of Glaciology. 10:151-156.

Slicher-van-Bath, B. 1962. De agrarische geschiedenis van west-Europa (500-1850). Het Spectrum. Utrecht.

Soon, W. and S. Baliunas 2003. Proxy climatic and environmental changes of the past 1000 years. Climate Research. 23:89-110.

Spahni, R., J. Schwander, J. Flückiger, B. Stauffer, J. Chappellaz and D. Raynaud 2003. The attenuation of fast atmospheric CH_4 variations recorded in polar ice cores. Geophysical Research Letters. 30:1571, doi:10.129/2003GL017093.

Stauffer, B., G. Fischer, A. Neftel and H. Oeschger 1985. Increase of atmospheric methane recorded in Antarctic ice cores. Science. 229:1386-1388.

Stortelder, A.H.F., P.W.F.M. Hommel and R.W.d. Waal 1998. Broekbossen. *In* Bosecosystemen van Nederland KNNV Utrecht.

Stuiver, M., P.J. Reimer, E. Bard, J.W. Beck, G.S. Burr, K.A. Hughen, B. Kromer, G. McCormac, J. van der Plicht and M. Spurk 1998. INTCAL98 radiocarbon age calibration, 24.000-0 cal. BP. Radiocarbon. 40:1041-1084.

Taylor, L. 1983. Everyday Life: The Seventeenth Century. Silver Burdett Company. Morristown.

Tichá, I. 1982. Photosynthetic characteristics during ontogenesis of leaves: 7. Stomata density and sizes. Photosynthetica. 16:375-471.

Timmermans, H. 1955. St. Odiliënberg, Historische schets over het oudste pelgrimsoord van midden-Limburg, Roermond.

Trudinger, C.M., P.J. Rayner, I.G. Enting, M. Heimann and M. Scholze 2003. Implications of ice core smoothing for inferring CO_2 flux variability. Journal of Geophysical Research. 108:4492.

Van der Burgh, J., H. Visscher, D.L. Dilcher and W.M. Kürschner 1993. Paleoatmospheric signatures in Neogene fossil leaves. Science. 260:1788-1790.

van der Plicht, J., B. van Geel, S.J.P. Bohncke, J.A.A. Bos, M. Blaauw, A.O.M. Speranza, R. Muscheler and S. Björck 2004. Early Holocene solar forcing of climate change in Europe. Journal of Quaternary Science. 19:263-269.

Vasold, M., 2003 Die Ausbreitung des Schwarzen Todes in Deutschland nach 1348: Zugleich ein Beitrag zur deutschen Bevölkerungsgechichte. Historische Zeitschrift 277(2), 281-308.

Vasold, M., 2003 Die Pest. Ende eines Mythos. Theiss Verlag, Stuttgart.

Wagner, F. 1998. The influence of environment on the stomatal frequency in *Betula*. LPP Contributions Series 9. LPP Foundation, Utrecht.

Wagner, F., B. Aaby and H. Visscher 2002. Rapid atmospheric CO_2 changes associated with the 8.200-years-B.P. cooling event. Proceedings of the National Academy of Sciences. 99:12011-12014.

Wagner, F., R. Below, P. De Klerk, D.L. Dilcher, H.J.H. Joosten, W.M. Kürschner and H. Visscher 1996. A natural experiment on plant acclimation: Lifetime stomatal frequency response of an individual tree to annual atmospheric CO_2 increase. Proceedings of the National Academy of Sciences USA. 93:11705-11708.

References

Wagner, F., S.J.P. Bohnke, D.L. Dilcher, W.M. Kürschner, B. van Geel and H. Visscher 1999a. Century-Scale Shifts in Early Holocene Atmospheric CO_2 Concentration. Science. 284:1971-1973.

Wagner, F., S.J.P. Bohnke, D.L. Dilcher, W.M. Kürschner, B. van Geel and H. Visscher 1999b. Response to technical comments by Indemühle et al. and Birks et al. on "Century-scale shifts in early Holocene atmospheric CO_2 concentration". Science. 286:1815a.

Wagner, F., D.L. Dilcher and H. Visscher in press. Stomatal frequency responses in a hardwood swamp vegetation from Florida during 60 years continuous CO_2 increase. American Journal of Botany.

Wagner, F., L.L.R. Kouwenberg, T.B.v. Hoof and H. Visscher 2004. Reproducibility of Holocene atmospheric CO_2 records based on stomatal frequency. Quaternary Science Reviews. 23:1947-1954.

Wagner, F., S. Neuvonen, W.M. Kürschner and H. Visscher 2000. The influence of hybridization on epidermal properties of birch species and the consequences for palaeoclimatic interpretation. Plant Ecology. 148:61-69.

Wiethold, J. 1998. Studien zur jüngeren postglazialen Vegetations- und Siedlungsgeschichte im östlichen Schleswig-Holstein. *In* Institut für Ur- und Frühgeschichte. Universität Kiel. Kiel.

Willemsen, M.A.H. 1889. Oorkonden en bescheiden aangaande de kerk en het kapittel van Sint Odiliënberg. Heemkunde vereniging Roerstreek, Sint Odiliënberg.

Woodward, F.I. 1987. Stomatal numbers are sensitive to increases in CO_2 concentration from the pre-industrial levels. Nature. 327:617-618.

Woodward, F.I. and F.A. Bazzaz 1988. The response of stomatal density to CO_2 partial pressure. Journal of Experimental Botany. 39:1771-1781.

Woodward, F.I., J.A. Lake and W.P. Quick 2002. Stomatal develoment and CO_2: ecological consequences. New Phytologist. 153:477-484.

Appendix

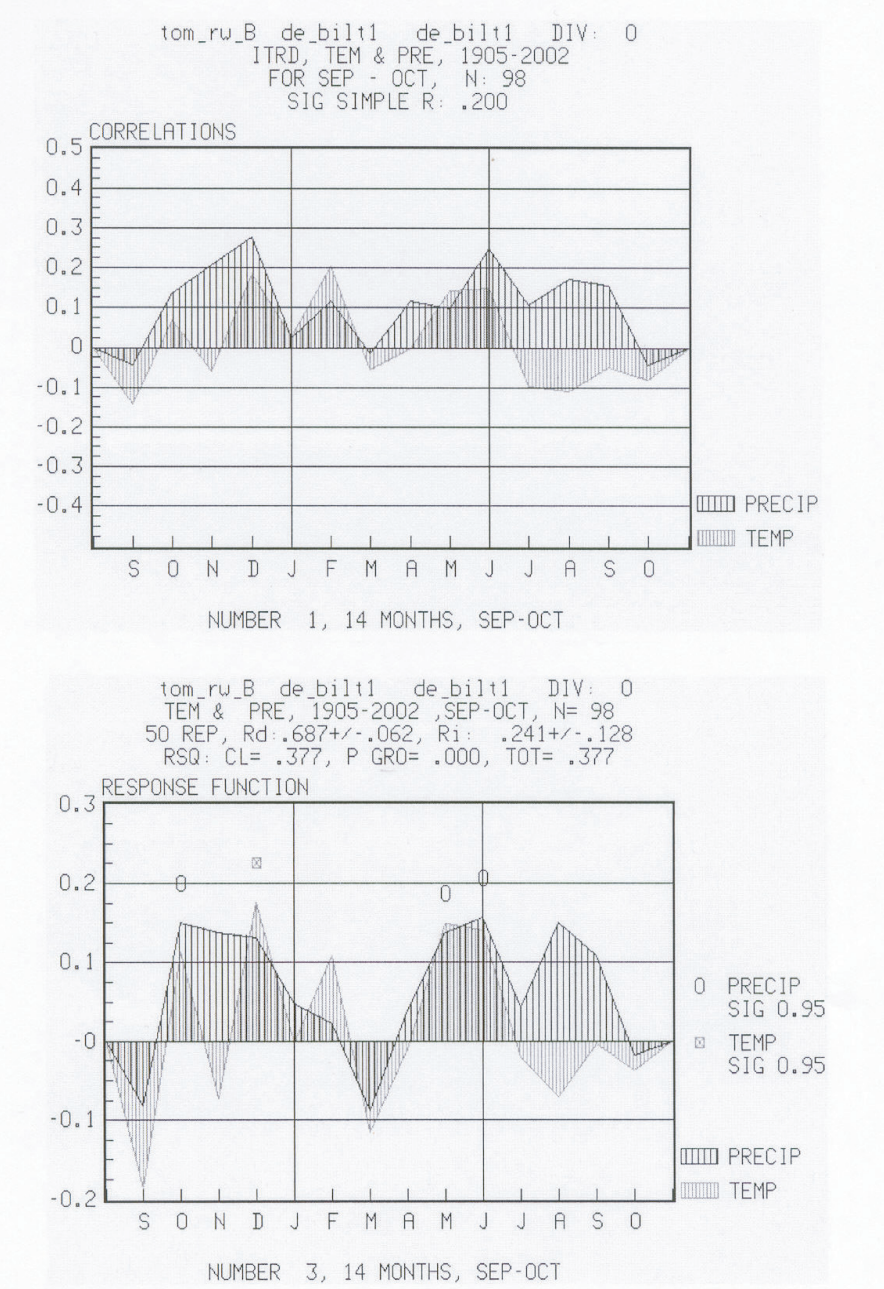

A: Correlation and response function analysis of the present day ring-width chronology to the monthly temperature and precipitation recorded at the De Bilt meteorological station for the time-interval from AD 1905 to 2000 (output of PRECON, Fritts, 1999).

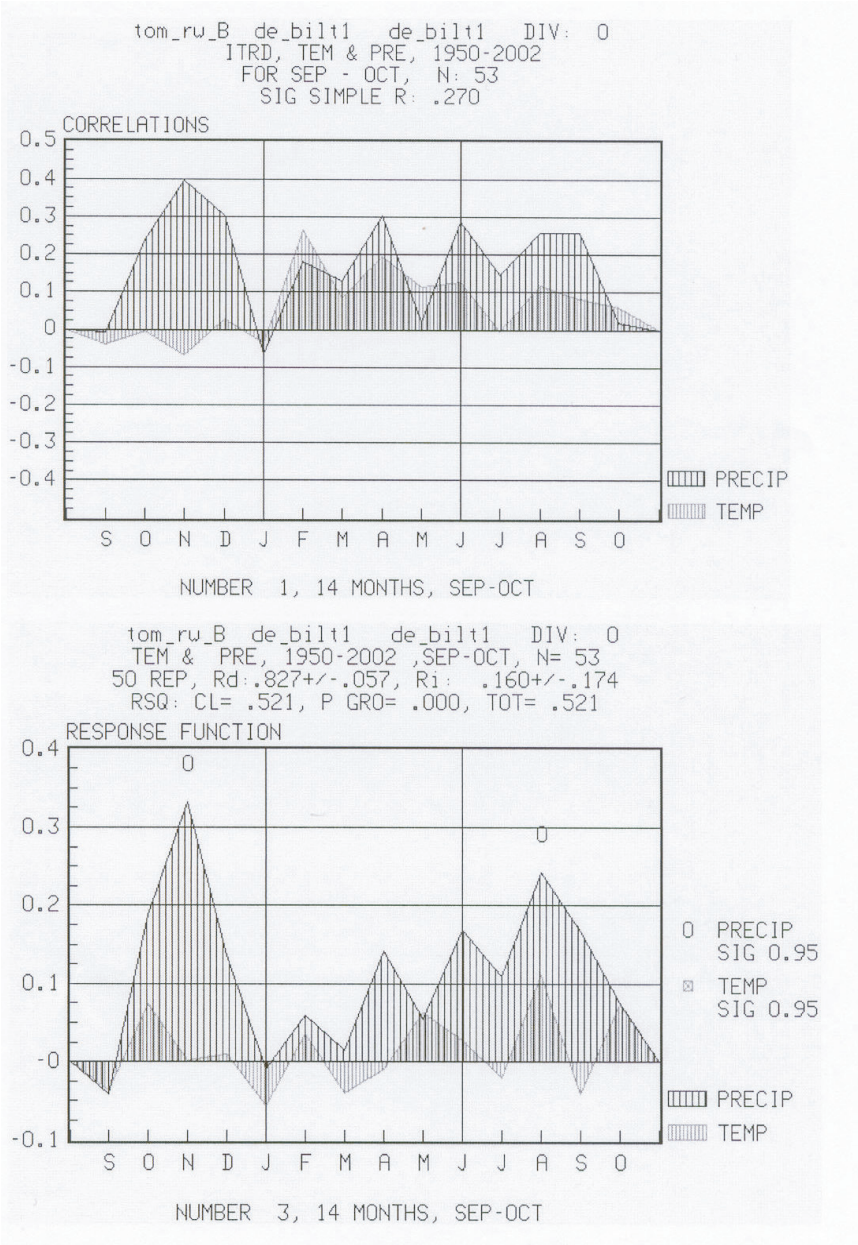

B: Correlation and response function analysis of the present day ring-width chronology to the monthly temperature and precipitation recorded at the De Bilt meteorological station for the time-interval from AD 1905 to 1950 (output of PRECON, Fritts, 1999).

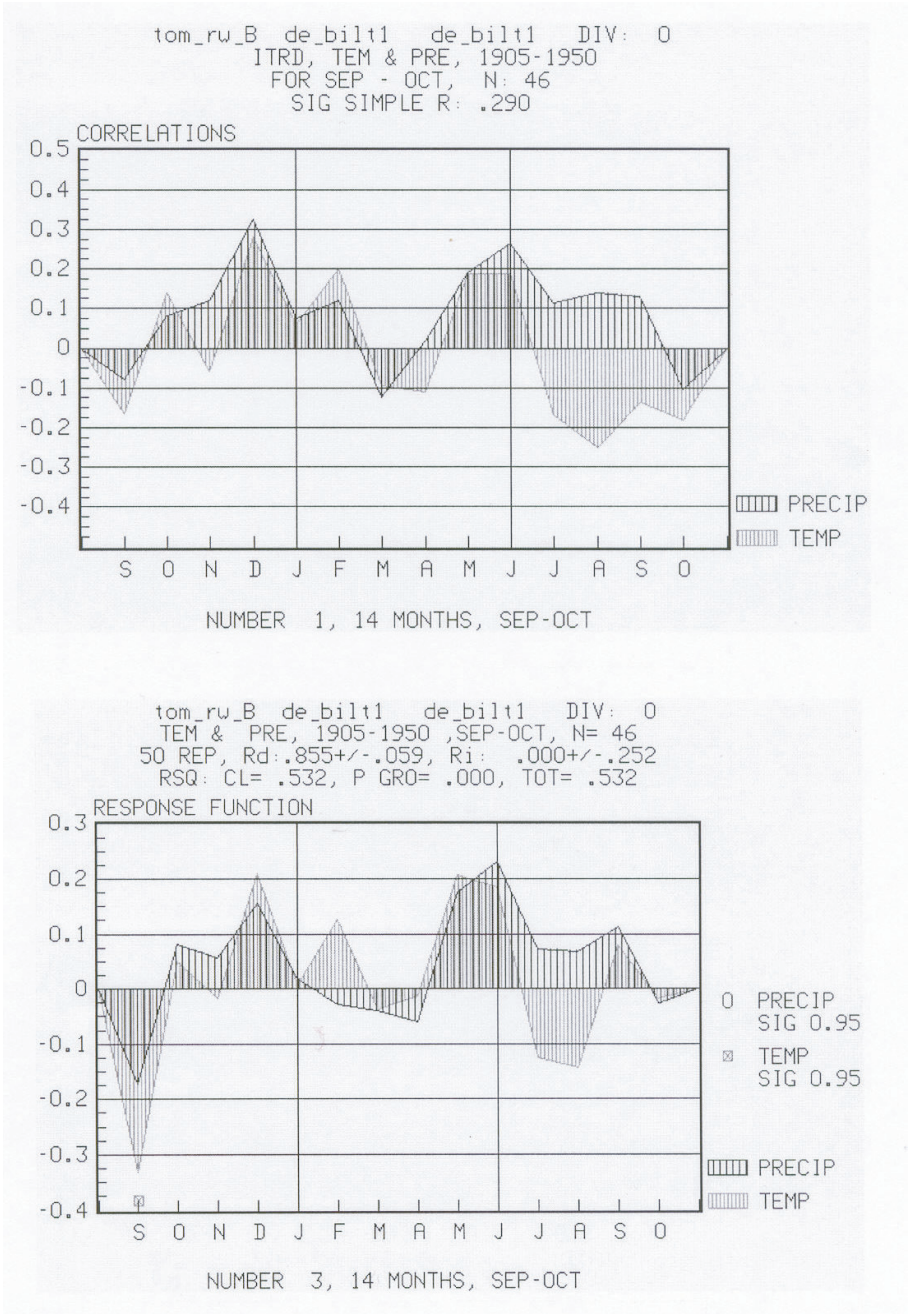

C: Correlation and response function analysis of the present day ring-width chronology to the monthly temperature and precipitation recorded at the De Bilt meteorological station for the time-interval from AD 1950 to 2000 (output of PRECON, Fritts, 1999).

Acknowledgements

First of all I want to thank my promotor and co-promotor, Henk Visscher and Wolfram Kürschner, for providing me with the opportunity to do a PhD at the Laboratory of Palaeobotany and Palynology. You two have been a great help, especially during the last few months. I immediately also want to thank Rike Wagner, my inofficial second co-promotor, for supervising me throughout the past four years.

I also want to thank everybody I worked together with: Frans Bunnik and Jean Waucomont (for the palynology and the wonderful fieldwork), Ute Sass-Klaassen (for introducing me into the world of wood) and Karsten Kaspers and Roderik van de Wal (for their contributions to Chapter 6). Hans Renssen and Hughes Goosse are thanked for their help with the radiative forcing and temperature calculations and Andy Lotter and David Dilcher are sincerely thanked for useful comments on the manuscript.

Timme, sharing a room with you was big time fun !, (*meej un mooi pakkie an !*). All the other (ex-) LPP/StratPal people; Lenny, Henk B, Aap, Jeroen, Merlijn, Welmoed, Alice, Holger, Oliver, Johan, Han, Marjolein, Jan, Natasja, Leonard, Zwier, Roel, Cindy, Ivo, Marloes,Frank, Erwin: Thanks! I especially want to thank Ton van Druten for being irreplaceable during fieldworks.

The best part of science (next to fieldtrips to exotic places like Sint Odiliënberg) is that you meet a wide variety of people and develop some international friendships. I want to thank the Danish/Swedish connection: Catherine, Mats Rundgren, Bent Aaby, Bent Odgaard and Morton Fischer Mortensen (*the sieving viking !*), and the Spanish (*future holiday*) connection; Nacho thanks for learning me La Bamba... *¿una poca de gracia?*

Even terug naar Sint Odilienberg, ik wil hierbij Antoon Verbeek speciaal bedanken voor de toestemming om in zijn natuurgebied te mogen werken. Vooral het regelen van de staalkabels en bulldozers waarmee we geprobeerd hebben een van de middeleeuwse moeraseiken uit de blubber te trekken is iets wat ik niet snel zal vergeten. Verder, wil ik hierbij ook de familie Waucomont bedanken voor de limburgse gastvrijheid en de heerlijke vlaai.

Naast wetenschap is er natuurlijk ook nog een ander leven (toch?!?), en wil ik natuurlijk mijn familie bedanken voor hun steun, Pa, Ma, Oma, Lydia, Jan, Annelieke en Boris, bedankt!. En natuurlijk de rest van de families Hagenaars en van Hoof (teveel om op te noemen). Verder zijn er natuurlijk ook nog mijn vrienden (en vage...kennissen); Siep, Fausto en Rob, Jozef, Jeroen, Ollekebolleke en Marlous. Ook wil ik de families Janssen en Verhagen en iedereen die ik verder nog vergeten ben bedanken !

Dan is er natuurlijk nog een speciaal iemand zonder wie het er in mijn leven de afgelopen jaren er een stuk minder zonnig zou hebben uitgezien...**Marijke**, bedankt voor je liefde...

Curriculum vitae

Thomas Bastiaan van Hoof werd geboren op 10 juni 1976 te Oosterhout. In 1994 behaalde hij het VWO diploma aan het Mgr. Frencken College te Oosterhout. In datzelfde jaar begon hij aan zijn studie Biologie aan de Universiteit Utrecht. Hij koos voor de afstudeerrichting palaeo-ecologie en tijdens de doctoraalfase verrichtte hij twee afstudeeronderzoeken. Het eerste onderzoek werd onder begeleiding van Dr. Henk Brinkhuis uitgevoerd op het Laboratorium voor Palaeobotanie en Palynologie, en betrof een studie naar de palaeo-ecologie en stratigrafie van dinoflagellatencysten over de Krijt-Tertiair grens in Texas (USA). Ook deed hij tijdens deze periode drie maanden geologisch veldwerk in de Dolomieten (Italië), met als doel het onder-Trias van de Werfen formatie van de Cattinaccio te karteren. Zijn tweede onderzoek werd deels uitgevoerd onder begeleiding van Prof. Dr. David Dilcher aan het Florida Museum of Natural History te Gainesville (Florida, USA) en betrof een anatomische studie naar de verschillen in bladanatomie tussen zonne- en schaduwbladeren van de Loblolly bay (*Gordonia lasianthus*). Het uitwerken van dit onderzoek gebeurde op het Laboratorium voor Palaeobotanie en Palynologie onder begeleiding van Dr. Wolfram Kürschner. In 2000 behaalde hij het doctoraal diploma in de Biologie waarna hij aansluitend in dienst trad bij de leerstoelgroep Palaeoecologie (voorheen Palaeobotanie en Palynologie) van de faculteit Biologie (Universiteit Utrecht). Hier begon hij in mei 2000 als Assistent in Opleiding aan het in dit proefschrift beschreven onderzoek. Dit onderzoek is een bijdrage aan het nederlandse CLIVARNET programma (gefinancieerd door ALW-NWO), wat deel uitmaakte van het wereldwijd onderzoeksprogramma naar klimaatsvariabiliteit, CLIVAR.